2019-04-09

A Geochemical Description of Shark Bay's Hamelin Pool, WA

Sean Peter Ahearn
University of Miami, sean_ahearn@outlook.com

UNIVERSITY OF MIAMI

A GEOCHEMICAL DESCRIPTION OF SHARK BAY'S HAMELIN POOL, WA

By

Sean Peter Ahearn

A THESIS

Submitted to the Faculty
of the University of Miami
in partial fulfillment of the requirements for
the degree of Master of Science

Coral Gables, Florida

May 2019

UNIVERSITY OF MIAMI

A thesis submitted in partial fulfillment of
the requirements for the degree of
Master of Science

A GEOCHEMICAL DESCRIPTION OF SHARK BAY'S HAMELIN POOL, WA

Sean Peter Ahearn

Approved:

Peter K Swart, Ph.D. Professor of Marine Geosciences	R. Pamela Reid, Ph.D. Professor of Marine Geosciences
Gregor P. Eberli, Ph.D. Professor of Marine Geosciences	Guillermo Prado, Ph.D. Dean of the Graduate School

AHEARN, SEAN PETER (M.S., Marine Geology and Geophysics)
A Geochemical Description of (May 2019)
Shark Bay's Hamelin Pool, WA

Abstract of a thesis at the University of Miami.

Thesis supervised by Professor Peter K. Swart.
No. of pages in text. (131)

Hamelin Pool, the eastern embayment in Western Australia's Shark Bay, hosts the world's largest assemblage of actively growing marine stromatolites. In 1996, UNESCO named Shark Bay a World Heritage site. Consequently, Hamelin Pool is strictly protected and only limited research has been approved in the area. In this thesis, I have investigated some of the stable isotopic and geochemical signatures of Hamelin Pool basinal waters and sediments collected during 2013 and 2014. Prior investigations show the pool is hypersaline, with salinity values in the southern waters measuring nearly double that of sea water. Hamelin Pool's salinity distribution is partially mixed, with increasing values from north to south. Similar to the salinity distribution, Hamelin Pool's average $\delta^{18}O$ value measured enriched at +3.95‰, with maximum value of +5.27‰ at the southern end of and minimum value of +3.16‰ at the northern end. The mean $\delta^{2}H$ values measured +22.9‰ with maxima at +26.73‰ and minima of +14.32‰, again increasing from north to south. Sill growth and restriction directly impacts the water chemistry. Modeling results show that nearly 50% of the basinal water evaporated each year for ~700 yrs to reach its current $\delta^{18}O$ and $\delta^{2}H$ values. Modeling suggests impacts from Sea Level Rise within a 70yr time period. The Sr, Mg, Ca and Cl ratios indicate that Hamelin Pool basinal waters are evolved seawater. Heightened Sr/Ca ratios in basinal waters suggest calcite precipitation reactions occur in Shark Bay prior to reaching Hamelin Pool. The distribution of Sr/Ca ratios mirror the salinity and stable isotopic values, which implies a

high residence time of water in the southern end of the pool. Sediment minerology is predominantly (96%) aragonite with residual amounts of High-Mg Calcite. To complement the water samples, basinal sediments were also analyzed for their inorganic $\delta^{13}C$ and $\delta^{18}O$ values. The $\delta^{13}C$ values ranged +6.18 to +2.83‰, and the $\delta^{18}O$ values ranged +4.07 to +2.17‰. The values increase from north to south, further supporting high residence times in the southern end of Hamelin Pool. Finally, organic matter present in the sediments was also analyzed for its $\delta^{15}N$, $\delta^{13}C$ values and C:N ratios. The organic $\delta^{15}N$ mean value measured +0.77‰ with maxima at +9.06‰ and minima of -4.28‰. The organic $\delta^{13}C$ mean value measured -15.38‰ with maxima at -8.95 and minima of -21.58‰. The atomic C:N ratios of the organic matter ranged from a 1.5:0.35 to 0.43:0.02 with an average of 10.1. The organic matter appeared to be sourced from a mixture of seagrass & microbial mat decay, with an enriched source of ^{13}C. This enrichment can be explained by high residence times of the restricted water body. The geochemical properties measured create a baseline for Hamelin Pool basinal water chemistry to be evaluated over time. The predictions made in this thesis may help in the understanding of the magnitude and pace of chemical changes in the modern environment, which may stress the growth of marine stromatolites.

For Corinna Rae Lallier

In the vastness of space and immensity of time,
it is my joy to share
a planet and an epoch with Corinna Rae.

Acknowledgments

My immense gratitude to my advisors Peter Swart, Pam Reid, and Gregor Eberli your insights, guidance and patience with me and this project have been remarkable, thank you.

This thesis and several other projects from Hamelin Pool would not have been possible without the contributions from our sponsors at British Petroleum (BP), Chevron Corporation, Shell Oil Company & Repsol S.A--thank you.

The University of Miami Libraries for supporting me on this journey and allowing me to grow as a scientist and a person: Anna Stoute, thank you.

The Western Australia Geological Survey and Philip Playford – Playford's discovery opened the doors for scientist to explore the unique wilderness of Shark Bay and Hamelin Pool--thank you.

Stable Isotope Laboratory at the University of Miami Rosenstiel School, this project would never have been possible without the assistance of Amel Saied, Christopher Kiaser, Sharm Giri--thank you.

The Hamelin Pool 2014 Spring field group, Brooke Vitek, Gray Milano (skipper), Blanch (the snake wrangler), and Erica Parke-Suosaari. Erica after so many field seasons your passion and drive to understand Hamelin Pool is unwavering and contagious; I hope you find peace of mind in knowing you will always be an inspiration to scientists and proof that hard work will pay off--thank you.

The Brazilian summer interns Isabela Coimbra, Erik Dari, and Itassu Porto, your assistance in sieving and cataloging sediments was critical your hard work is appreciated--thank you.

Table of Contents

List of Figures

List of Tables

List of Abbreviations

Abbreviation	Description
Arag	Aragonite
BBGG	Baas Becking Geobiological Group
BW	Bore Water
CW	continuous wave
D	the distribution coefficients
DIC	Dissolved Inorganic Carbon
DOM	Dissolved Organic Matter
FIU	Florida International University
GISP	Greenland Ice Sheet Precipitation
GMWL	Global Meteoric Water Line
GSWA	Geologic Survey of Western Australia
GW	Ground Water
HCl	Hydrochloric Acid
HMC	High Mg Calcite
HP	Hamelin Pool
IAPSO	International Assoc. for the Physical Sciences of the Oceans
ICP-OES	Inductively Coupled Plasma Optical Emission Spectroscopy
IR	The insoluble residue
LMC	Low Mg Calcite
MW	Meteoric Water
NTP	Normal Temperature and Pressure
ODP	Ocean Drilling Program
Q	Flux (dv/dt)
SB	Shark Bay
SI	Saturation Index
SLAP	Standard Light Antarctic Precipitation
SLR	how Sea Level Rise
SSW	Standard Sea Water
TOC	Total Organic Carbon
TON	Total Organic Nitrogen
UNESCO	United Nations Educational, Scientific and Cultural Org.
VPDB	Vienna Pee Dee Belemnite
VSMOW	using Vienna Standard Mean Ocean Water scale
WA, BOM	Western Australia Bureau of Meteorology
XRD	X-Ray powder Diffraction

Chapter 1: **Background**

1.1 ***Overview***

Shark Bay and Hamelin Pool, situated approximately 800km North of Perth (Figure 1-1), have been of interest since the area was described in the mid 1950's by West Australian Petroleum Pty Ltd (Cockbain, 1976). These marine environments are home to a unique range of wild endangered marine species like the *Dugong dugon* (Manatee) and *Rhincond typus* (Whale Shark) and within Hamelin Pool living fossils known as, stromatolites. The following sections will provide a background to Hamelin Pool, the geological and geochemical research that has already been completed, as well as the motivations for this research.

1.2 ***UNESCO World Heritage Site***

Shark Bay, located on the west coast of Western Australia, describes water bounded by a 'W'-shaped double peninsula (Figure 1-1) and is home to over 300 marine species. The lower eastern side of Shark Bay, as a result of partial isolation imposed by the formation of the Faure Sill (FS) has formed a hyper saline embayment, Hamelin Pool. Within Hamelin Pool (HP) is a vast accumulation of modern living stromatolites. The unique wilderness of Shark Bay has been deemed a World Heritage Site and is heavily protected by both national and international agencies (UNESCO, 2014). Although several organizations such as University of Western Australia (UWA), Geological Survey of Western Australia (GSWA), Baas Becking Geobiological Group (BBGG), Florida International University (FIU), and the University of Miami (RSMAS) have studied Shark Bay, Hamelin Pool is a heavily protected area, many key questions about this environment remain unanswered.

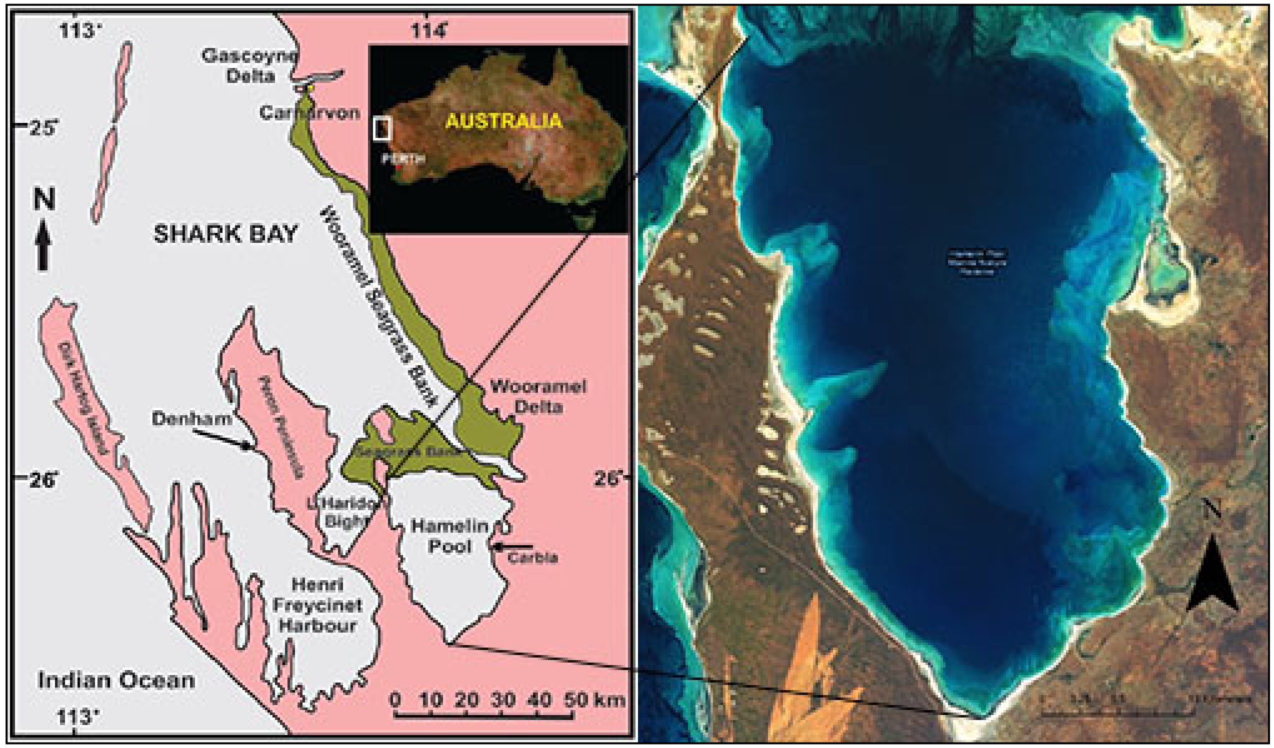

Figure 1-1. Left is the study area Shark Bay, which is located on the west coast of Western Australia. Right is Hamelin Pool, the eastern embayment in Shark Bay.

1.3 *Geology of Shark Bay*

Composed of Pleistocene and Holocene Dune deposits accumulated over Tertiary anticlinal limestone ridges, Shark Bay (SB) is shallow marine embayment of about 5,000 square miles (Playford, 1990). This shallow area of sea in the southern Carnarvon Basin is bounded to the west by Dirk Hartog, Dorre and Bernier Islands, and Edel land Peninsula. Shark Bay is further divided into two arms by the Peron Peninsula (Figure 1-2). The gross modern morphology is controlled by underlying folds. Facies exposed in Shark Bay consist of Cretaceous, Tertiary, Pleistocene and Holocene units (Playford, 1990).

The late Cretaceous *Toolonga Calcilutite* is the oldest genetic unit found along the Eastern margin of SB, and is composed of white chalk, lime mudstone with calcrete exposure surface, and contains ample chert nodules. Over lying the *Toolonga Calcilutite* are Tertiary *Giralia Calcarenites* and *Lamont Sandstones* (Playford, 1990).

To the west of the *Toolonga Calcilutite* is the Pleistocene *Peron Sandstone* which is exposed primarily at the Peron Peninsula (Figure 1-2). This is a unit of red eolian sandstone that is overlain and interlocked with *Tamala Limestone*. The Tamala formation was accumulated as large dunes on the western shoreline of the area during glacial periods of the Pleistocene, when the area was subject to extremely strong southerly winds. The linear unit along the Zuytdorp Cliffs is described as a Quaternary fault (Playford, 1990). The *Dampier Limestone* is the oldest Pleistocene marine deposit in SB; it consists of shelly limestone laid down under waters of normal marine salinity. The

Carbla Oolite member is found associated within the Dampier Limestone on the shores of Hamelin Pool. The *Bibra Limestone* consists largely of beach-ridge deposits with some tidal-flat and coralline deposits and contains open marine fauna. This unit is found around shores of Hamelin Pool, suggesting that at the time (~120 kA), Hamelin Pool was not restricted. Evaporite deposits, formed by trapped and evaporated sea water in Solar Ponds also appear throughout these Pleistocene units (Playford, 1990).

Holocene sedimentation is composed primarily of Hamelin Coquina, a beach-ridge deposit laid down on the shores of hypersaline waters of Hamelin Pool and Lharidon Bight, with calcrete and beach deposit inclusions. Hamelin Coquina is composed almost entirely of the small bivalve *Fragum erugatum*, which thrives under hypersaline conditions. Finally, there are the Hamelin Pool stromatolites which are pervasive along the coastline's intertidal and shallow subtidal zones, and appear as both fossil and actively growing forms (Playford, 1990)

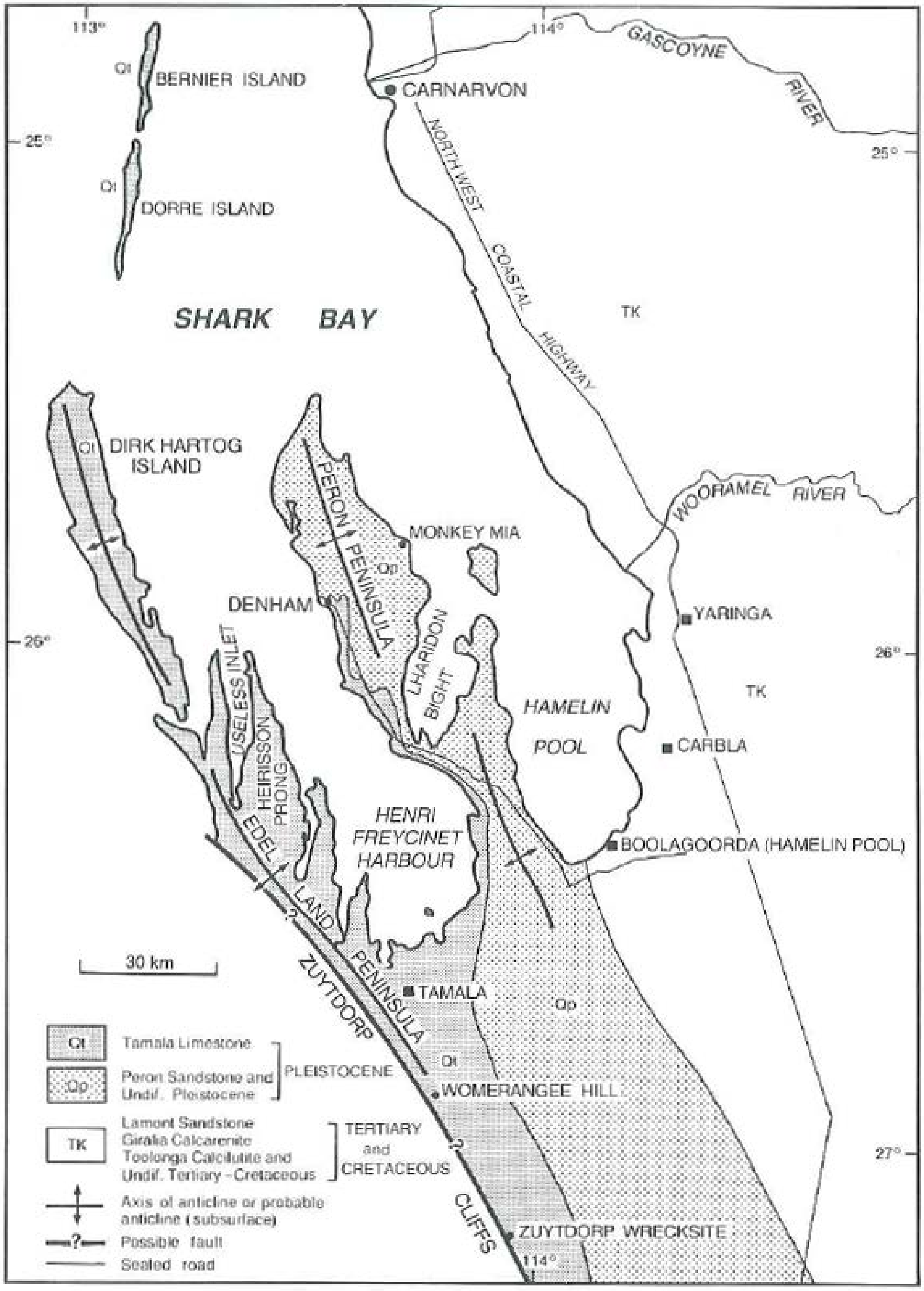

Figure 1-2 From Playford, 1990. A generalization of the dominate facies observed at Shark Bay

1.4 ***Stromatolites***

Stromatolites are macroscopically layered, lithified sedimentary structures formed by the interaction of microbes and sediment (Awramik et al., 1976), Figure 1-3. Stromatolites are found throughout ~85% of the geologic record, and as such, the presence of modern stromatolites in Hamelin Pool suggests that this area may be an analog for ancient environments (Awramik, 1992). Hamelin Pool is home to the most diverse and abundant examples of living marine stromatolites the world (Jahnert and Collins, 2012; Suosaari et al., 2016a). In Hamelin Pool, a variety of environmental pressures, including hypersalinity and wide ranges of temperature and water level, lower competition and predation allowing the stromatolites to thrive (Suosaari et al., 2016b). Stromatolites discovered on the margins of Exuma Sound, Bahamas in the 1980's were the first example of stromatolites growing in open marine conditions (Dravis, 1983); (Dill et al., 1986). Stromatolite growth in the Exuma Cays is associated with physical stress due to burial by oolitic sand, which also minimizes predation (Dill et al., 1986) and competition (Steneck et al., 1998). The differing environments of Hamelin Pool and Bahamas, which both produce similar structures, are an indication that a variety of environmental factors can be associated with microbialite growth. However, both examples require a preexisting substrate; exposed bedrock or submarine hardground to provide a hard substrate required for colonization (Jahnert and Collins, 2013). The variety of microbial types and morphologies found in Hamelin Pool has led to several investigations by Logan et al (1974), Playford (1990), Reid et al (2003), Janhert &Collins (2011) and Suosaari et al 2016a,b. Many morphologies of stromatolites, including smooth, pustular, colloform, cerebroid, pavement microbial types, have been identified and mapped across the pool using a variety of techniques (i.e. GIS, aerial photo mapping, submarine video transects, multi-beam survey's as well as traditional petrology and microscopic techniques) (Jahnert and Collins, 2012; Suosaari et al., 2016a). The existence of morphologically complex structures with characteristic microstructures within Hamelin Pool (Hagan, 2015) and associated with distinct geographic areas within Hamelin Pool (Suosaari et al., 2016a), points to the possibility of temporal and spatial variation in chemical and physical environmental factors (Awramik, 1992). Some of these factors are directly related to, or can be highly influenced by water chemistry variability.

Figure 1-3 Taken from *Stromatolites* (Clary and Wandersee, 2013) – An example of a lithified stromatolite, found in the Pilbara Craton in Australia, which has been dated to be between 3.6 billion to 3.2 billion years old.

1.5 *Hamelin Pool Climate*

Hamelin Pool is subtropical environment with an annual temperature maximum of ~29˚C and minimum of 15˚C. The annual rainfall is about ~ 210mm and average relative humidity is about 75% as reported by the Australian Bureau of Meteorology (ABOM).

1.6 *Hamelin Pool Hydrologic Environment*

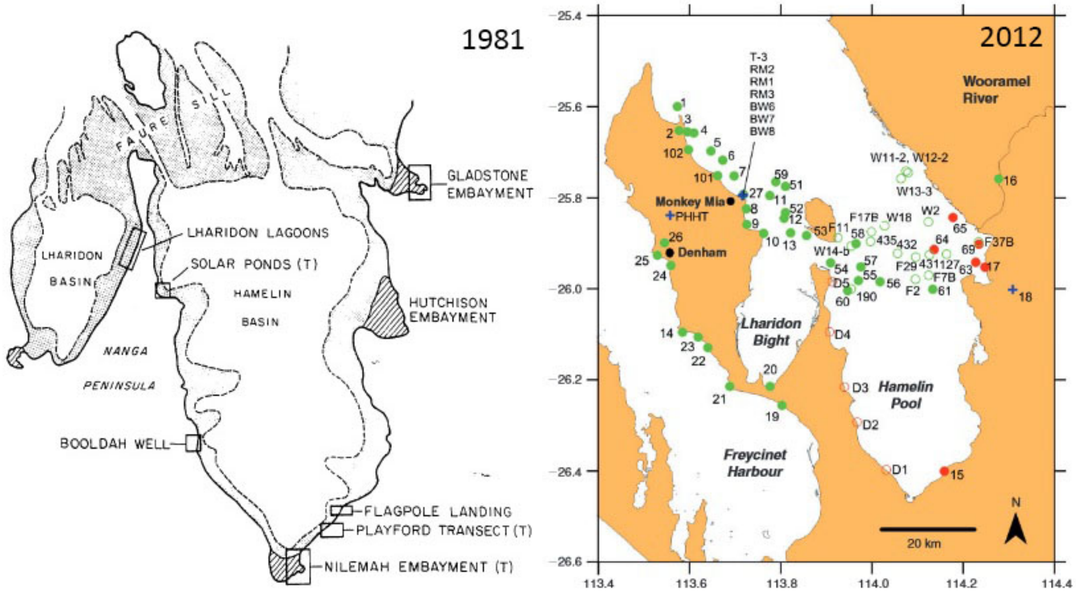

Figure 1-4 Right, is modified from the 1981 Baas Becking report, rectangular areas denote where water samples were collected, 'T' represent where transects were investigated. Left, taken from Price et al 2012 where each filled circles represents a surface water sample, Bore waters (BW) were also collected. Note that in both studies the basinal waters within Hamelin Pool where not investigated.

Hamelin Pool (volume =7.05km^3- area=1400km^2), the southeastern portion of Shark Bay (Figure 1-4), is partially isolated by the Faure Sill (FS). In the 1970's, Logan et al. (1970) found that runoff influx is negligible and that the combined physical barriers of banks and sills, as well as, an evaporation rate that exceeds precipitation have resulted in a salinity gradient. Shark Bay was subsequently divided based on its salinity, into oceanic (36-40), metahaline (40-56) and hypersaline (56+) (Logan and Cebulski, 1970). Hamelin Pool waters are partially mixed vertically creating isohalines, or lines of equal salinity, which can be drawn to show increasing salinity from the north to south. (Logan and Cebulski, 1970).

From 1980 to 1987 the Baas Becking Geobiological Laboratory launched a research initiative to better understand the processes by which the formation of particular types of oil accumulations and metal deposits occur. While none of these accumulations or deposits occur in Hamelin Pool, the processes by which they form are active (i.e. the accumulation of organic matter in sediments) and can be studied. This investigation led to the measuring of meteoric and groundwater chemistry on the coast of Hamelin Pool along selected transects. Burne et al., 1990 (The Baas Becking report) was unable to produce any clear differentiation of either continental or marine ground waters but was able to use the Nilemah transect geochemical data to create 4 distinctive zones (Figure 1-5), all of which are characteristic of mixing and are most related to topography. The first zone lies under the Holocene beach ridges, has a low salinity, and appears to have little marine influence but rather evaporated continental water mixing with marine salt. Zone II waters resemble marine water with stable isotopic values of $\delta^{18}O$ and $\delta^{2}H$ close to 0.00‰, the four samples measured suggested a continental brine and seawater mix. Sulphate values of 20.5‰ in Zone II also suggest marine origin. Zone III is beneath the lithified carbonate crust at the intertidal area. Zone III stable isotopic values also appear to be a mixing zone between evaporated marine brine and strongly evaporated continental water. Zone IV contains the intertidal sediments with gypsum precipitates; the water chemistry is also a mixing zone with values being midway between seawater and continental water beneath the beach ridges. Mixing is so pervasive that the tidal flats appeared to be homogenous, suggesting tidal mixing (Burne et al., 1990).

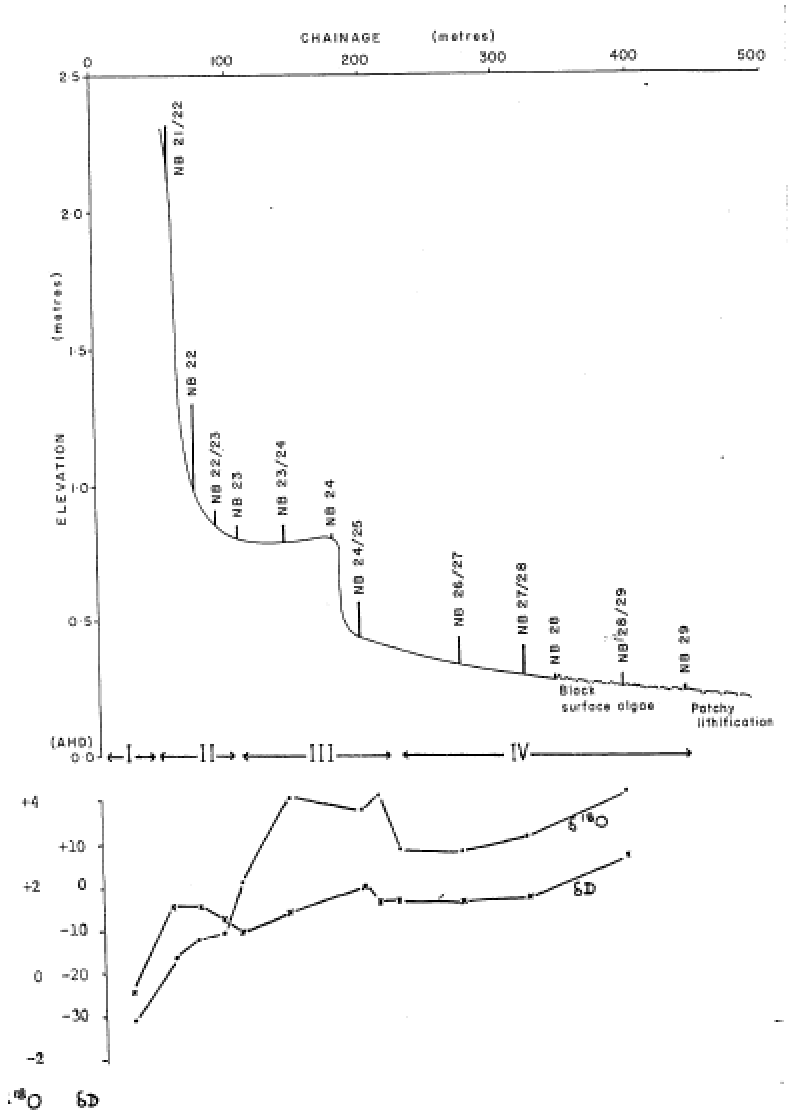

Figure 1-5 Reprinted from Bass Becking report 1990, the chemically defines zones within the Nilemah transect.

1.7 *Hamelin Pool Sedimentary Environment*

Figure 1-6 Top, an example of the shallow Hamelin environment with bivalve dominated sedimentation. Bottom, Penicillus algae roots attached to debris with living benthic foraminifera.

Hamelin Pool is dominated by carbonate sediments with a salinity gradient controlling the distribution of facies. The restrictions imposed on the biota by increases in salinities create a distinctive assemblage of organisms which that can tolerate salinity ranges from 56-70 (Logan and Cebulski, 1970).

An example of salinity restriction on fauna can be seen from an examination of the foraminiferal population within Hamelin Pool which contains only three common species: *Miliolinella circularis* var. cribostoma, *Peneroplis planatus*, and *Spirolina hamelini* (Logan and Cebulski, 1970). The molluscan population is also affected by salinity, limited to only small bivalves and small gastropods. The small bivalve *Fragum eragatum* is present in vast numbers dominating the sublittoral platform of Hamelin Pool and is the most typical sediment found, both articulated and inarticulate (Figure 1-6). The halo-tolerant floral population consists of cyanobacteria which produces both coherent (stromatolitic) and incoherent (mats) layers throughout the area, most extensive at or near the coasts. The algal population also includes green macro algae *Penicillus* sp., *Acetabularia peniculus* and *A.*

calyculus which tend to grow in shallow waters and attach themselves to shells and rock debris(Figure 1-6) (Logan et al., 1970).

1.8 ***Motivation***

Although there have been some important studies on Hamelin Pool, there has previously been an absence of information on the chemistry of the waters and sediments. This thesis will provide a basis from which to evaluate this environment in its current, modern, context to better understand how Hamelin Pool has evolved in the past and how it may evolve in the future. The present study uses geochemical measurements to better understand, the water budget, chemical equilibrium, and origin of sediment within the water body.

(i)Water Budget

A water budget was constructed using a mass balance model that combines the stable isotopic values ($\delta^{2}H$ & $\delta^{18}O$) and salinity. Results from analyses of water collected within Hamelin Pool basin, combined with previous data collected outside of Hamelin Pool, were used to create a realistic water budget with major and minor sources of input and output. This model was then used to make a predictive model that can be interpreted to predict the evolution of Hamelin Pool water.

(ii)Chemical Equilibrium

Measurements of Ca, Sr, Mg, Cl and alkalinity were used to calculate the Saturation State (Ω) of Hamelin Pool waters and hence determine which areas are more likely to precipitate carbonate minerals.

(iii)Sedimentary Origins

Descriptions by size fraction (Dunham Classification), mineralogy (XRD) and both organic and inorganic stable isotopes ($\delta^{13}C$, $\delta^{15}N$, $\delta^{18}O$) values of sediments were used interpret the sediment source and organic matter origin.

Chapter 2: **Salinity, Stable Isotopes and Modeling of Hamelin Pool Waters**

2.1 ***Introduction to Salinity and Stable Isotopes***

Salinity, measured as conductivity, is a fundamental property of water that can indicate water type (fresh, brackish, marine). Meteoric waters have a low amount of dissolved solids and consequently a salinity value close to 0 (conductivity close to 0 microsiemens (μS)). In contrast, marine waters have a higher salinity measuring approximately 35 (conductivity of about 55,000μS) (Kendall and McDonnell, 1998). Isotope geochemistry analyzes various elements for the natural variation of the relative abundance of isotopes. The ratios can fingerprint physical processes and give insight into environmental conditions such as temperature, source tracking, nutrient cycling, and other applications (Kendall and McDonnell, 1998). Water is composed of hydrogen and oxygen; both elements contain more than one stable isotope. The stable isotopic composition of water can provide information on water history and source. In this chapter I review the measurements of salinity and stable isotopes in Hamelin Pool and discuss the relationship between the two. In addition, a water budget for Hamelin Pool has been created with salinity and isotopic (O and H) data. This model has been used to predict past and future water balances within Hamelin Pool.

Stable isotope geochemistry: Stable isotope geochemistry uses the ratio of rare to common stable isotopes of a given element. The stable isotopic ratio of an element is represented below as 'R'.

For element 'X' with a rare isotope of 'n' and common isotope of 'm':

$$R = \frac{^{n(rare)}X}{^{m(common)}X} \qquad \text{Eqt 2.1}$$

Oxygen for example has a naturally occurring distribution of ^{16}O at 99.76% and ^{18}O at 0.201%. In this case R would be equal to ^{18}O divided by ^{16}O expressed as:

$$R = \frac{^{18}O}{^{16}O} \qquad \text{Eqt 2.2}$$

The 'R' ratio is then compared the 'R' of a reference standard with a known isotopic composition.

$$\delta^{n}X = \left(\frac{R_{sample}}{R_{reference}} - 1\right) * 1000 \qquad \text{Eqt 2.3}$$

The standard for oxygen in waters is Vienna Standard Mean Ocean Water (VSMOW) which is about zero, in this example the isotopic value of oxygen in water would be expressed as Eqt 2.4.

$$\delta^{18}O = \left(\frac{\frac{^{18}O}{^{16}O}_{sample}}{\frac{^{18}O}{^{16}O}_{vsmow}} - 1\right) * 1000 \qquad \text{Eqt 2.4}$$

The resultant δ^nX value, expressed as δ^nX‰, is equal to the difference in the $^{18}O/^{16}O$ of the sample water ratio compared to that of the standard. The same is true for Hydrogen, Carbon, and any other element being analyzed for its stable isotopic ratios. These values are useful because chemical reactions and phase changes cause these values to shift; such a process is called fractionation.

Isotope fractionation: Isotope fractionation describes the processes that affect the relative abundance of isotopes. Mass independent fractionation occurs when proportions of isotopes are separated regardless of their masses.

There are two main types of mass dependent fractionation; equilibrium, and kinetic. Equilibrium fractionation occurs during chemical equilibrium. For example, within a sealed glass of water there is an exchange of H_2O between the liquid and vapor phase in the headspace of the container. This fractionation is due to bond forces and vibrational energy. At normal temperature (20˚C) and pressure (1atm) (NTP) the bond force of the heavier isotope is stronger than that of the bond force of the lighter isotope. This reduction in vibrational energy results in the heavier isotopes staying in the liquid phase as the lighter isotope enters the vapor phase. Therefore, the liquid tends to be more enriched in ^{18}O than the vapor. Equilibrium fractionation rates are temperature dependent, leading to $^{18}O/^{16}O$ being widely applied as a paleoclimate proxy for temperature. Kinetic fractionation is a manner by which isotopes are separated in a one directional process. Biological utilization of carbon dioxide by photosynthesis is an example of kinetic fractionation. Plants will utilize the CO_2 molecules with lighter masses of carbon and oxygen at a greater rate than the molecules with heavier masses. This process gives plant matter more negative $\delta^{13}C$ values than the atmosphere.

The amount of change is measured by the fractionation factor (α) (equations Eqt2.5 and Eqt2.6). This fractionation fraction is in turn related to the isotopic difference between two compounds (Ɛ) which have experience isotopic exchange or been produced as a result of a chemical reaction (equations 2.7 and 2.8)

$$\alpha_{A-B} = \frac{1000+\delta_A}{1000+\delta_B} \quad \text{Eqt 2.5}$$

$$\alpha = \frac{1}{\alpha} = \alpha_{A-B} = \frac{R_A}{R_B} \quad \text{Eqt 2.6}$$

Ɛ is used for small values to express the fractionation between two substances.

$$\varepsilon_{AB} = (\alpha_{A-B} - 1)*1000 \quad \text{Eqt 2.7}$$

$$\varepsilon_{AB} = (\alpha_{A-B} - 1)*1000 \quad \text{Eqt 2.8}$$

2.2 ***Objectives***

This portion of the thesis uses salinity and stable isotopic data to model water sources in Hamelin Pool. During the 2014 field season, 134 water samples were collected (Figure 2-1) and measured for their salinity and stable isotopic O and H values. At each site, when possible, both a top (air-water interface) and bottom (water-sediment interface) sample were collected. The coordinates of each site can be found in the appendix Table 7-4.

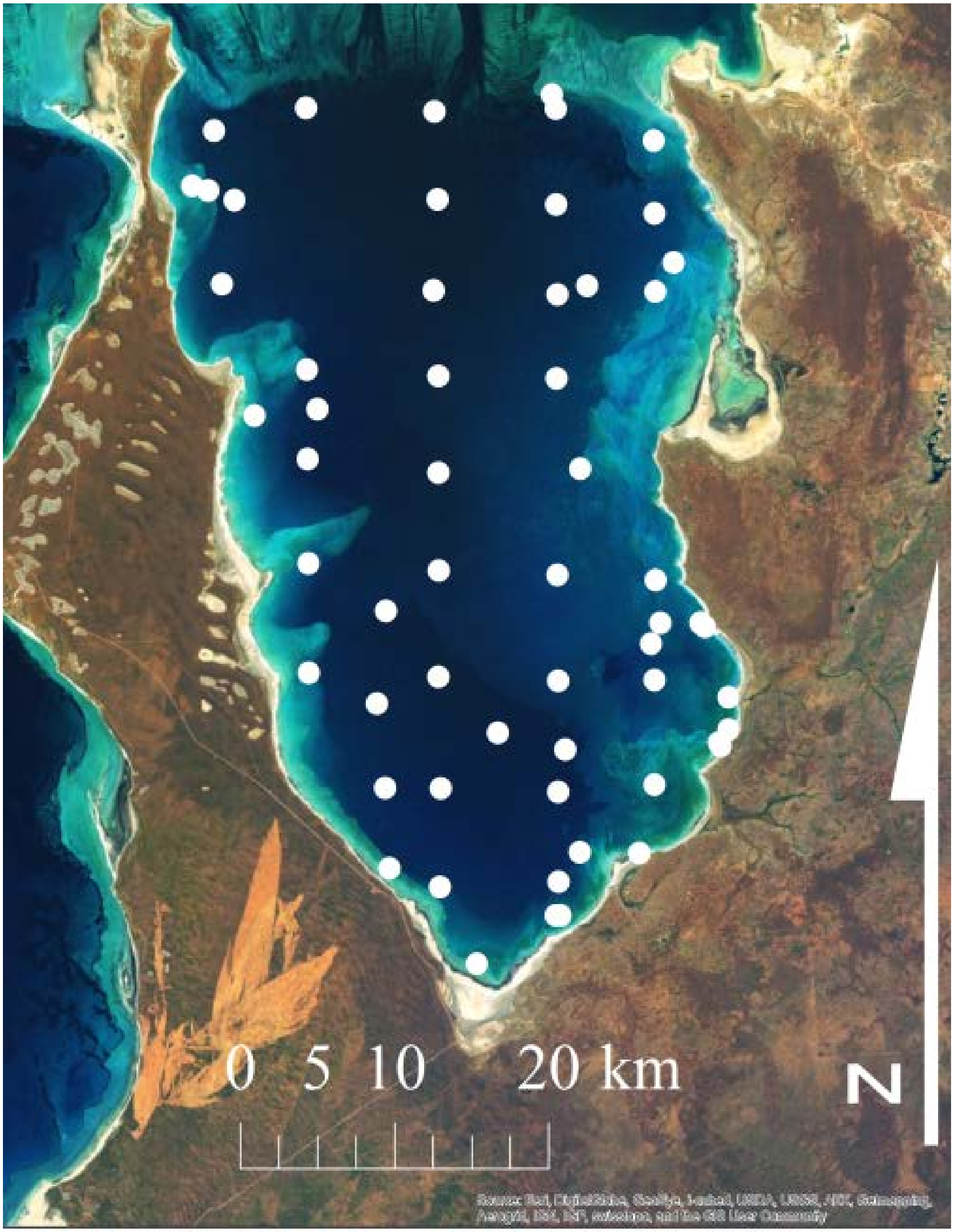

Figure 2-1 Each white circle represents a water sample collection site. Note that at site each site, when possible a top (air-water interface) and bottom (water-sediment interface) sample were collected.

2.3 ***Methods***

Salinity: In the field salinity was determined using a handheld YSI Multiparameter cable and probe meter. Salinity was recorded as conductivity, µS, and converted in to practical salinity values. Later measurements were taken at the Stable Isotope Lab (SIL) using a handheld Leica TS Refractometer. Salinity recorded on a refractive index, is directly measured as practical salinity values.

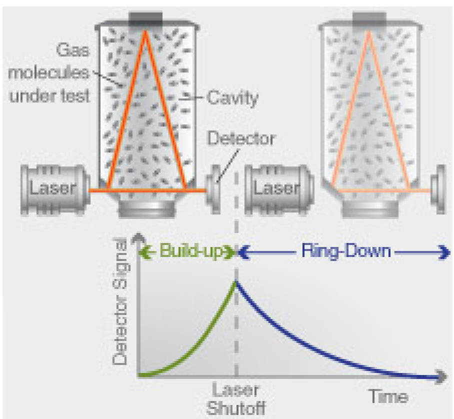

Figure 2-2. Schematic of a Picarro CRDS analyzer and graph showing which portion of the process is the "ring-down" measurement.

Stable Oxygen and Hydrogen Isotopes: The ratios (R) of $^{2}H/^{1}H$ and $^{18}O/^{16}O$ of the water samples were measured with a Picarro Cavity Ring-Down Spectrometer (CRDS). In the implementation of a CRDS analysis, a single-frequency laser diode enters a cavity that is defined by three mirrors (Figure 2-2).

Photodetectors measure light exiting the cavity and produce a signal that is directly proportional to the intensity of the light within the cavity. When the photodetector signal reaches its threshold level the continuous wave (CW) laser shuts off. The light intensity inside the cavity steadily leaks and falls to zero logarithmically. This decay, or ring-down, is measured in real-time by the photodetector. The amount of time it takes for the ring down to happen in an empty cavity, determined by the reflectivity of only the mirrors, is the baseline for light absorption. When gas molecules are present, they also absorb the laser light. This additional absorption changes the rate of the ring-down time when compared to an empty cavity. Since gas-phase molecules (e.g., CO_2, H_2O, H_2S, and NH_3) have unique infrared absorption spectrums, each molecule creates its own unique wavelength. The concentration of any molecular species can be determined by measuring the height of a specific absorption peak. Characteristic ring-down times and wavelengths are used to determine isotopic values as identical molecules with differing masses produce differing wavelengths.

For the calibration of the instrument, 2µl of four standard waters with a range of $\delta^{18}O$ and $\delta^{2}H$ values were each injected six times. The first three injections were discarded to ensure that the system has been purged of the previous sample. These standards were calibrated using Vienna Standard Mean Ocean Water scale (VSMOW), Greenland Ice Sheet Precipitation (GISP), and Standard Light Antarctic Precipitation (SLAP). The average standard deviations for all three injections used was <0.1‰ for $\delta^{18}O$ values and <0.5‰ for $\delta^{2}H$ values

2.4 ***Results***

Salinity: The average salinity of all the 2014 Hamelin Pool waters was 57.9 with a range of 40.5 to 61.6. The lower values were measured at the North end of the pool, near the Faure Sill (FS), while the highest values were found near the Southern portion of the embayment, Figure 2-3. The pool is separated in geographical portions Northern, Central, and Southern the average values are listed in Table 2-1. Data points collected at or north of latitude -26.1 are considered the Northern portion of the pool, while data point collect at or south of latitude -26.3 are considered the Southern portion of the pool. With central or mid-section being all the data points in between the two latitudes. All data are listed in the appendix table 7-5.

NORTH	Sal	$\delta^{18}O$‰	$\delta^{2}H$‰	CENTRAL	Sal	$\delta^{18}O$‰	$\delta^{2}H$‰	SOUTH	Sal	$\delta^{18}O$‰	$\delta^{2}H$‰
MEAN	56.18	3.72	21.67	**MEAN**	58.95	3.94	23.20	**MEAN**	59.81	4.12	23.59
MIN	40.50	3.16	14.32	**MIN**	53.90	3.33	20.18	**MIN**	58.60	3.61	19.22
MAX	61.00	3.73	21.72	**MAX**	61.10	4.33	24.75	**MAX**	61.60	5.27	26.73
n	45			**n**	32			**n**	39		

Table 2-1 Summary Table of salinity, $\delta^{18}O$ and $\delta^{2}H$ values split to show the Northern, Central and Southern portion of the basin.

Stable Oxygen and Hydrogen Isotopes: The mean $\delta^{18}O$ and $\delta^{2}H$ values are +3.95‰ and +22.9‰ respectfully with maxima at +5.27 and +26.73‰ and minima of +3.16 to +14.32‰. Similar to the salinity results, there is a trend in increasing values, Figure 2-4, from the north to the south (Table2-1). All data are listed in the appendix in Table 7-5.

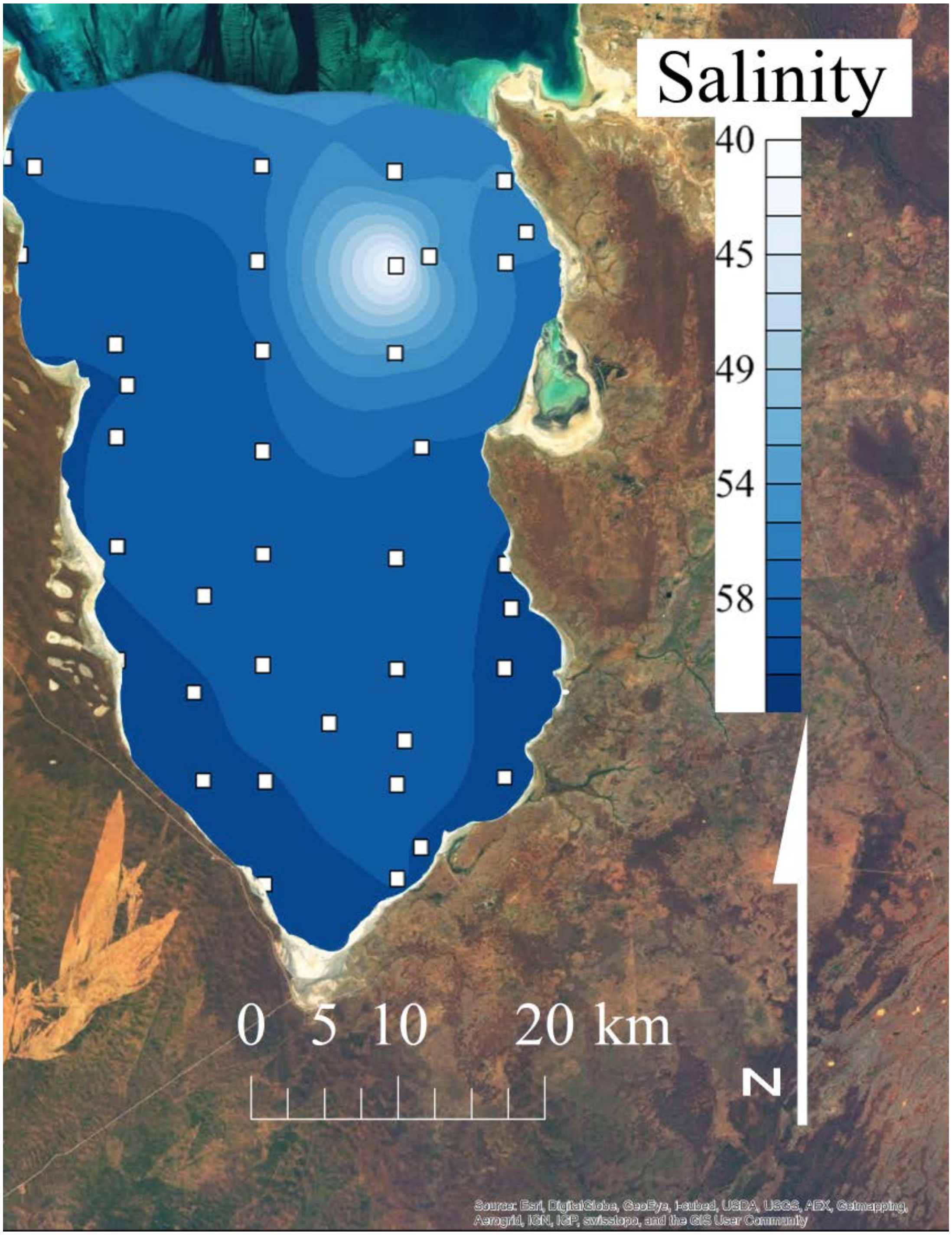

Figure 2-3 Results from the total salinities recorded from the Hamelin Pool basinal waters. There is a sharp and expected trend of increasing salinity from North to South.

Figure 2-4. Isotopic analysis, Left) hydrogen and Right) oxygen. A tending of enrichment of these values from the north to the south is observed, as expected from the salinity values.

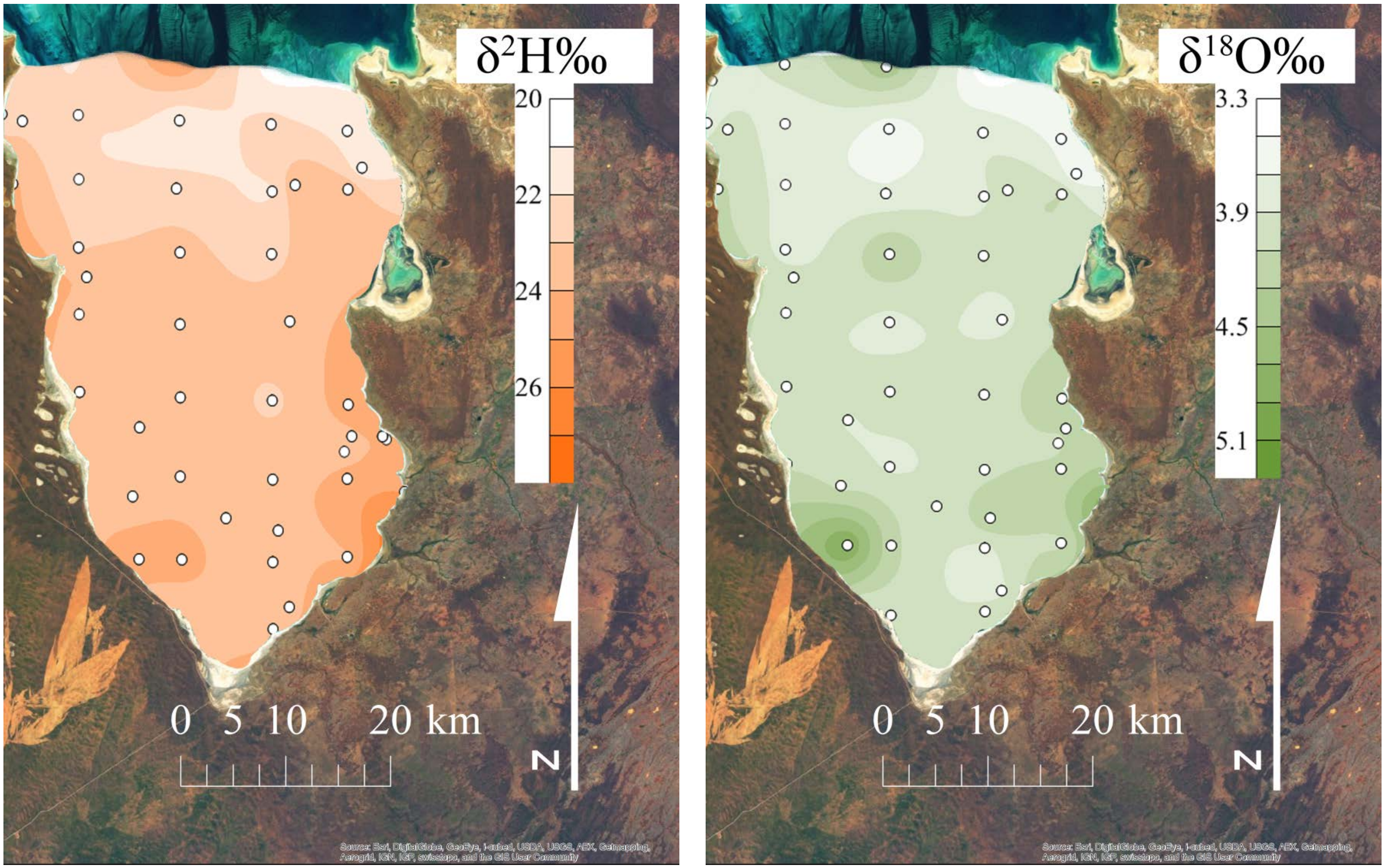

2.5 ***Discussion***

The relationships between salinity and the delta values of water (δ^2H and $\delta^{18}O$) are plotted in Figure 2-5. The $\delta^{18}O$ and δ^2H values of the water in Hamelin Pool are enriched compared to Standard Mean Ocean Water (SMOW). The values plot below The Global Meteoric Water Line (GMWL) (Figure 2-6), with a best fit line slope of 3.9 (Craig, 1961). This relationship is best explained by an evaporative basin. If Hamelin Pool was evolved from meteoric water, the best fit line would intersect the GMWL at a $\delta^{18}O$ value at about -4.0‰ and a δ^2H value at about -22.0‰ - the average rain fall values in the area (GNIP) (Gat and Gonfiantini, 1981). Instead, the line intersects at a $\delta^{18}O$ value of about -1.0‰ and a δ^2H value of about +5.0‰, a value much more similar to marine water than to rain water. The light blue dots plotted on Figure 2-6 represent rain water collected at the Hamelin Pool station. These values also plot below the GMWL, suggesting recycled marine waters are evaporating and precipitating back into the pool. The clustering together of data points in a high narrow salinity interval (~55 to 60) and a narrow range of positive delta values indicates that Hamelin Pool has few water sources.

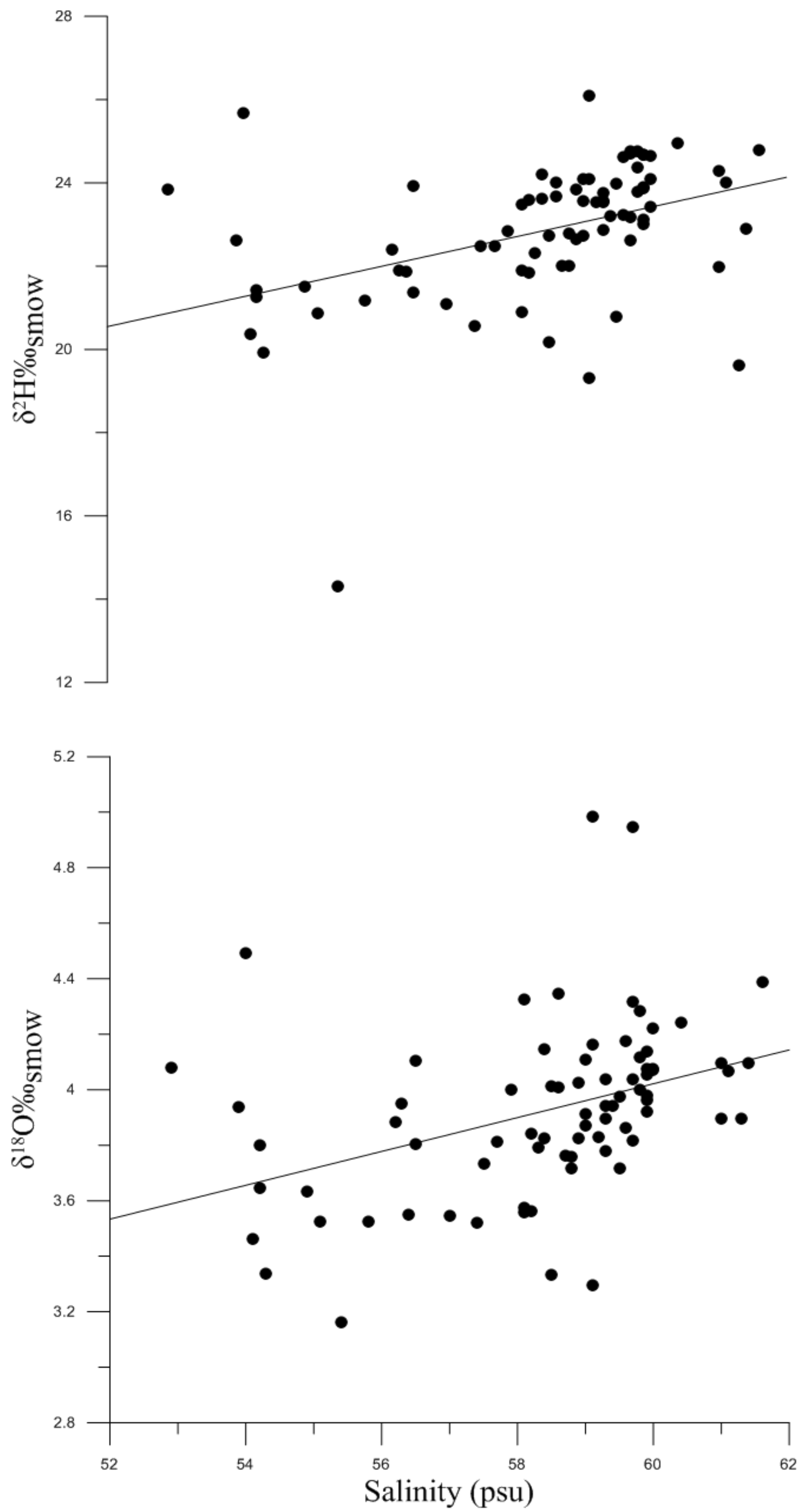

Figure 2-5. Top: salinity & δ^2H covariation. Bottom salinity & δ^{18}O covariation. The intercept with zero salinity gives the isotopic composition of the zero salinity end member.

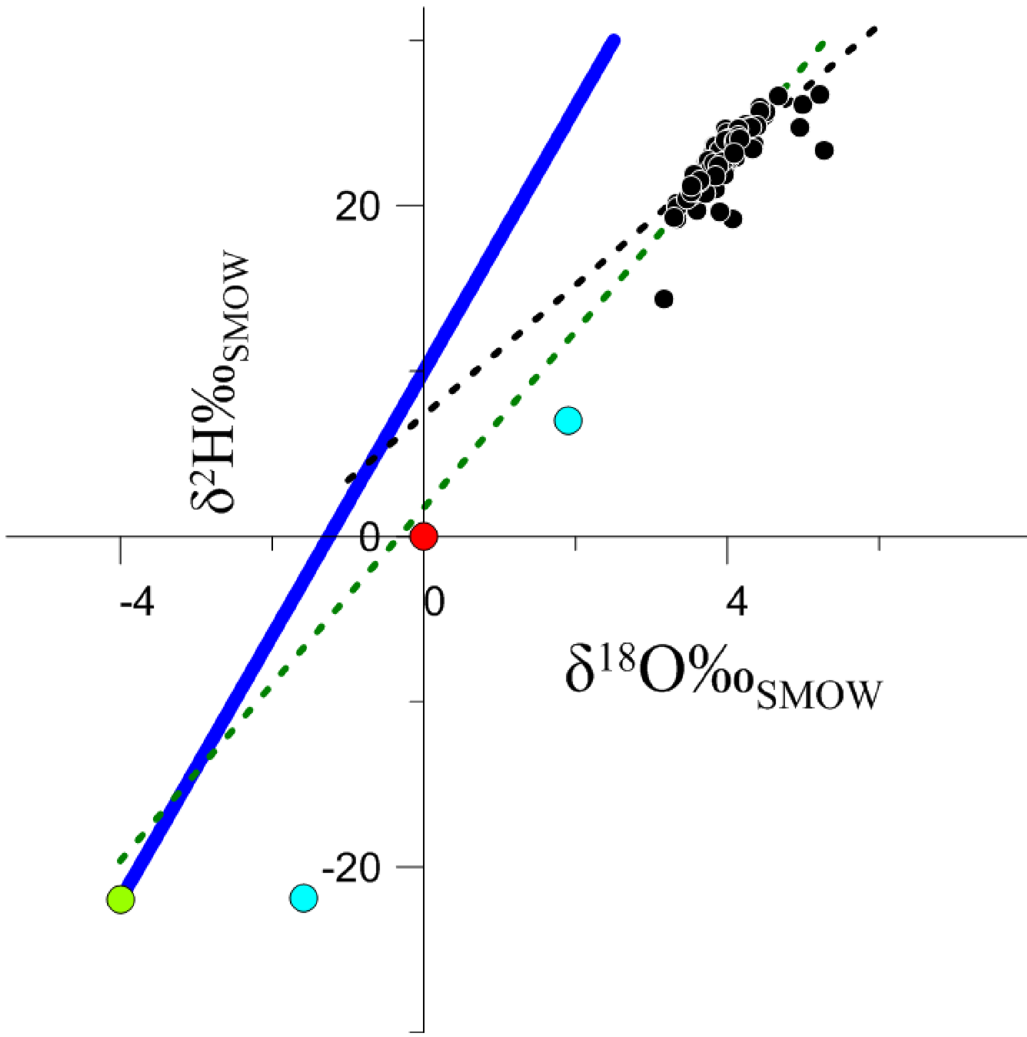

Figure 2-6. In black are the $\delta^{18}O$ & δ^2H values for the Hamelin Pool 2014 basinal water samples. In dark blue is the Global Meteoric Water Line (GMWL). Dotted in black is the best fit line for Hamelin Pool Basinal Waters. Dotted in green is a hypothetical fit based on the GMWL's estimation of Indian Ocean precipitation. The intercept with the GMWL generally indicates the isotopic composition of unevaporated freshwater water. The red solid circle is the standard for ocean water VSMOW. The light blue circles are the two meteoric water samples collected. The deviation in slope from GMWL shows an arid climate which will result in a deuterium excess.

2.6 ***Relationship Between Salinity, and the $\delta^{18}O$ and $\delta^{2}H$ Values***

Evaporation increases concentrations of the heavier isotopes of O and H, the maximum $\delta^{18}O$ and $\delta^{2}H$ values that can be attained is a function of several external factors, including the relative humidity of the atmosphere, the isotopic composition of water vapor in the atmosphere and the type and amount of salts in the evaporating solution (Gonfiantini, 1986). Salinity effects on the O and H isotopic composition arise as a result of changes in the activity coefficient of water, as an electrolyte dissolves and solvation shells form. A solvation shell describes a solvent surrounding a solute in solution, when the solvent is water a solvation shell is called a hydration shell (or sphere). The construction of hydration spheres, is dependent the activity coefficient of the electrolyte and can vary from single to multiple shells per ion. These shells change the activity coefficient of the water and have a direct impact on the delta values of the remaining evaporated waterbody as solvation shells preferentially attract the lighter fractions of water. Water activity (a_w) of a waterbody can be expressed by equation 2.9 (Gonfiantini, 1986).

$$a_w = D^*M^2 + E^*M + G \qquad \text{Eqt 2.9}$$

M, ion molarity in solution (overall salinity), can be rewritten as a fraction of initial molarity over final molarity $M_{0/}M=f$ changing equation 2.9 to equation 2.10.

$$a_w = D^*f^{-2} + E'^*F\text{-}1 + G \qquad \text{Eqt 2.10}$$

This equation relates water activity (α_w) as function of the remaining water fraction and saline molarity. 'D' diffusion coefficient, 'E' electromotive force and 'G' Gibbs free energy are constants which can be obtained by the fitting of experimental values with known water activity coefficients (Gonfiantini, 1986; Robin and Stokes, 1959). With the addition of external conditions such as humidity, temperature and calculated fractionation factors (α), evaporating waters can be modeled by the fraction of remaining water (activity of the water) to that of the amount of salinity present (ion activity). Equation 2.11 below is a condensed equation where A, and B are equal to the relationship of the above factors including water activity a_w, these equations are defined and discussed at length in Gonfiantini, 1986. With measured values of salinity, $\delta^{18}O$ and $\delta^{2}H$ a model of maximum delta values can be constructed and validated, Figure 2-7.

$$\delta = \left(\delta_0 - \frac{A}{B}\right) f^{Bz} + \frac{A}{B} \qquad \text{Eqt 2.11}$$

Isotope	α	Ɛ	δ-Ɛ	h	δ-α	δ_0	c
Hydrogen	1.067	0.067	12.5	0.765	-68.18	7.03	1
Oxygen	1.009	0.009	14.2	0.765	-10.12	1.42	1

Table 2-2 Input conditions used to calculate A, B, aW and the δ for Figure 2-7 and Figure 2-8. For a full description of these variables and how they are used to calculate the relationships between activity and delta values of O and H see Gonfiantini, 1986.

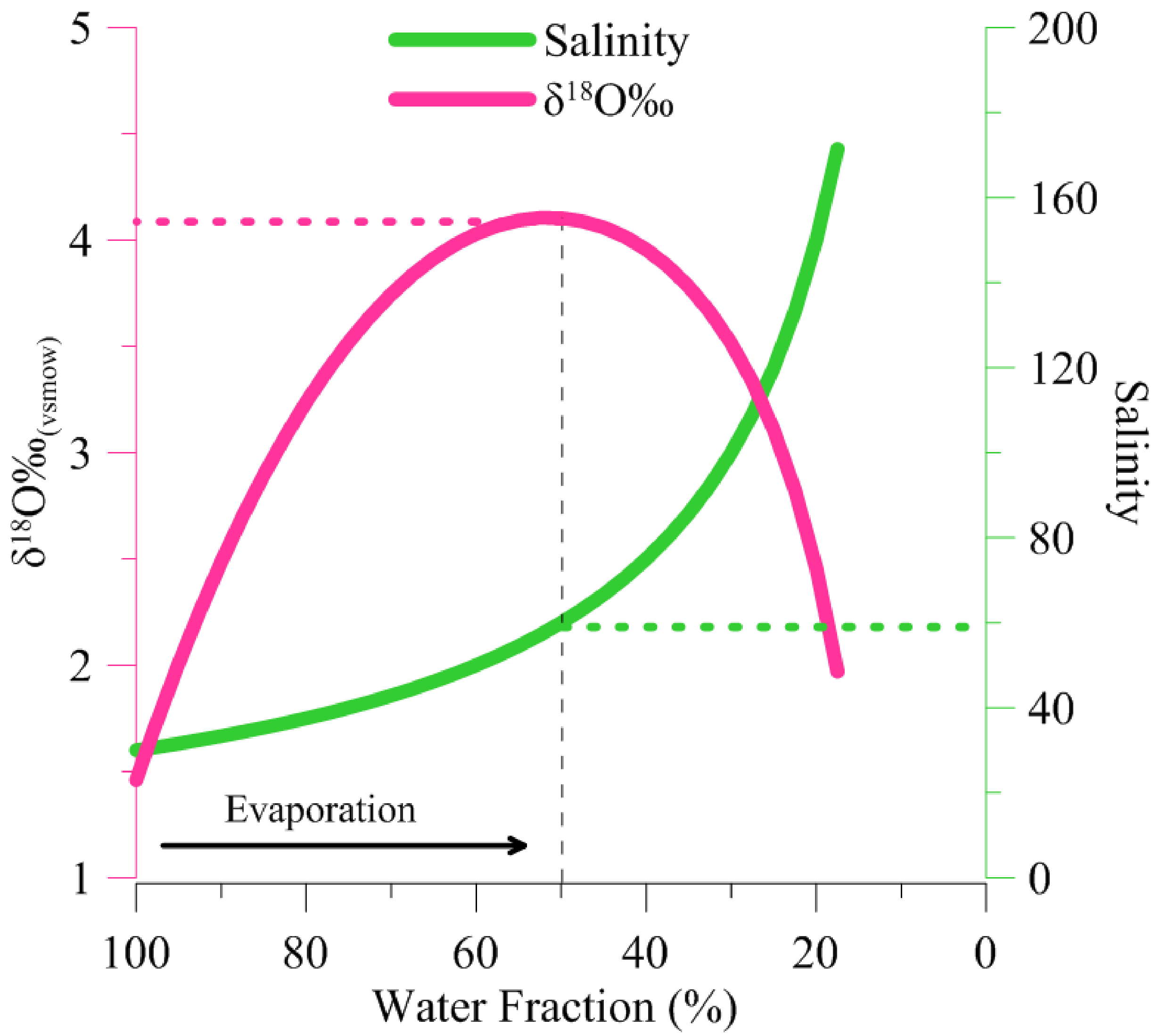

Figure 2-7. Salinity and $\delta^{18}O$ as a function of remaining sea water fraction during evaporation, highlighted are the values of salinity and $\delta^{18}O$ at 50% remaining water fraction which suggest the amount of evaporation imposed on Hamelin Pool in one years' time. These results are from the use of equation 3 where values for humidity, temperature, $\delta^{18}O$ from Hamelin Pool were input into equations from Gonfiantini, 1986.

Figure 2-7 shows modeled salinity and $\delta^{18}O$ values of Shark Bay waters (values from Price et al, 2012) evaporating under Hamelin Pool conditions. Price et al, 2012 simple math models and pan evaporation performed by the WA, BOM estimate that in one years' time up to 50% of Hamelin Pool is removed through evaporation alone. When modeling salinity in relation to the water fraction of the remaining water body, the model resembles behavior that would be expected of any evaporating sea water. Starting at ~35, as the water fraction evaporates, salinity increases (Figure 2-7 (green/right) axis). The $\delta^{18}O$ values rise during the initial stages of a evaporation, but as a consequence of a continuous decrease in water activity the solvation shells break down, causing $\delta^{18}O$ and $\delta^{2}H$ values to become more negative as lighter water fractions are released in the later stages of evaporation (Figure 2-7(pink/left) axis) (Gonfiantini, 1986). Drawn on Figure 2-7 is dotted line through the 50% water fraction remaining; the estimated amount of evaporation Hamelin Pool waters experience annually. At the 50% water fraction mark the $\delta^{18}O$ value is approximately +4.1‰ and salinity close to 60; these values agree with the measured data.

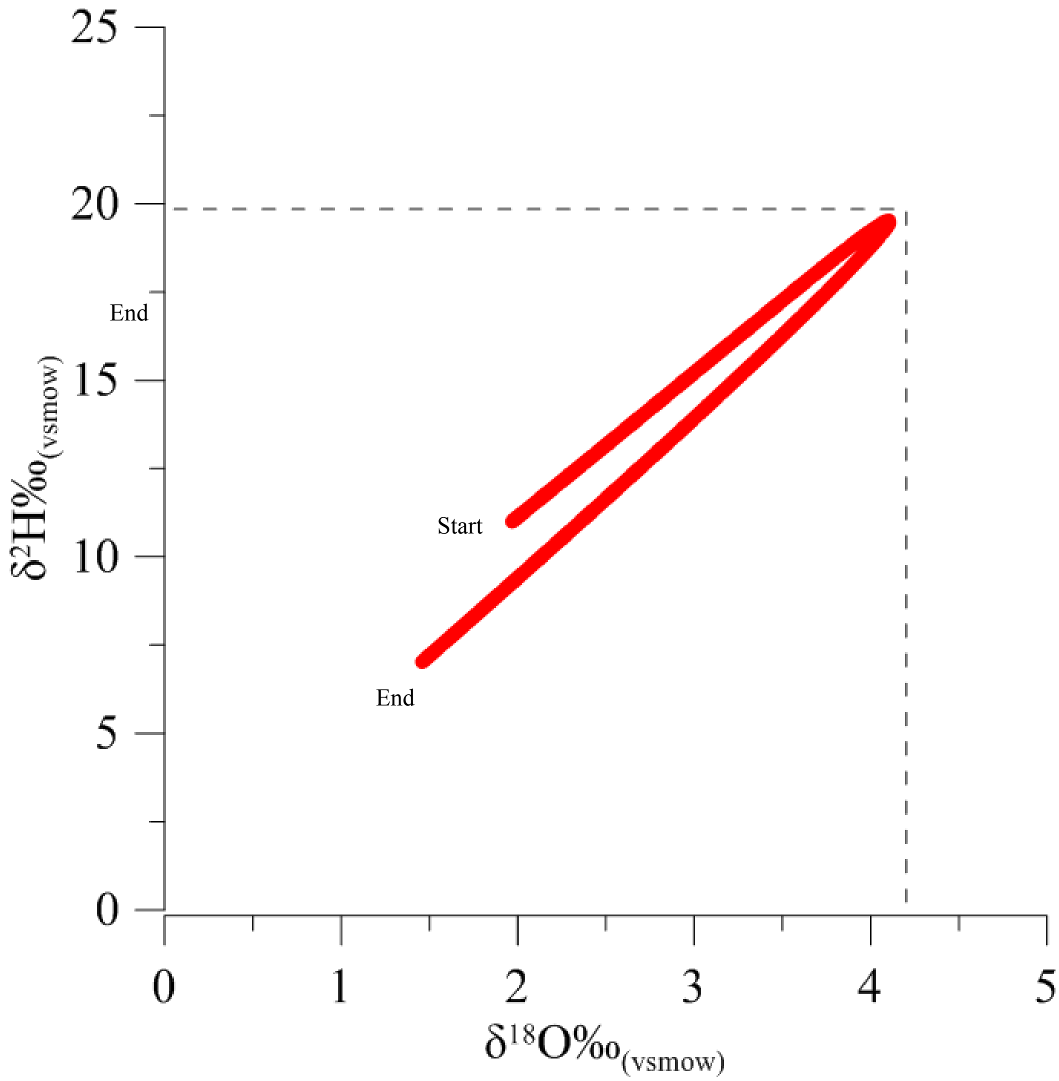

Figure 2-8 The trending of $\delta^{18}O$ and $\delta^{2}H$ during evaporation under Hamelin Pool conditions, the reversal is a result of changes in the activity of water during the final stages of evaporation. These are the results are the output from equation 3 where humidity, temperature, $\delta^{18}O$ and $\delta^{2}H$ from Hamelin Pool were entered into equations from Gonfiantini, 1986.

Furthermore, Figure 2-8 plots $\delta^{18}O$ and $\delta^{2}H$ values relative to each other during evaporation. This produces a curve that shows the possible minimum and maximum at any given stage of evaporation. The $\delta^{2}H$ modeled values are close to 20‰; the average value measured was 23‰.

In Figure 2-8, during the initial stages of evaporation both oxygen and hydrogen isotopic values begin to increase. Then during the final stage of evaporation values decrease due to hydration shell breakdown, ending with a final value that is lower than the initial value. The measured and modeled salinity and delta values agree. This suggests that modeling can accurately predict the $\delta^{18}O$ values of Hamelin Pool and can therefore by proxy estimate salinity and possible ion activity. With a valid evaporative model, steady-state modeling and evaporation modeling can be calculated over a period of time.

2.7 ***Steady-State and Flux Modeling Overview***

A mass balance model refers to a model in which the law of conservation of mass is used to define the amount of matter coming in to or leaving a physical system over a period of time. While there are tidal ranges in Hamelin Pool, caused by both astronomical and meteorological influences (Suosaari et al., 2016b), the water level over a one year period is relatively stable; water levels in July 2013 are equal to water levels in July 2014 (Suosaari et al., 2016b). With the water volume balanced, the concentrations of other matter can be measured and estimated. These types of models constrain either the composition (i.e. salinity or delta values of water) of the input/output and/or the magnitude of the fluxes imposed on the physical system. Similar models have been constructed for other closed basins such as the Black Sea (Swart, 1991a), and Florida Bay (Price et al., 2012).

Mass Balance models are also useful in determining how hypothetical fluxes will affect a physical system or in this case Hamelin Pool. This approach on a water body is more revealing with stable isotopic values than using salinity alone (Swart, 1991b). As sea water evaporates only H_2O is removed; leaving any dissolved solute behind in either the remaining solution or as precipitate. Consequently water vapor salinity is 0. Meteoric waters precipitate from water vapor in the atmosphere with little or no dissolved solutes and also have a salinity of 0. This leads to both the meteoric and evaporative fluxes having a value of 0. However, all phases of the water cycle have isotopic values, meaning that modeling with delta values accounts for meteoric and evaporative fluxes. With the data sets from Shark Bay (Price et al 2012), waters on the shores of Hamelin Pool (Baas Becking Report, 1990) and basinal waters from within Hamelin Pool (this thesis), I estimated the time needed to alter isotopic composition.

Steady-State and Flux Modeling Methodology

In a steady state condition, i.e. the water level of a basin is not changing over a period of time; the inputs must equal the outputs to achieve a steady-state balance, as defined by equation 2.12.

$$I_{(input)} = O_{(output)} \text{ or } I_{(input)} - O_{(output)} = 0 \qquad \text{Eqt 2.12}$$

The solution of zero implies that while there are both inputs and outputs into the system, the volume is unchanging; making the time period 1 year keeps volume of Hamelin Pool the fixed variable in this steady-state analysis. The inputs into Hamelin Pool (Figure 2-9) are the fluxes Q_{SB} (over flow from Shark Bay into Hamelin Pool), Q_{GW} (possible ground water infiltration) and Q_{MW} (meteoric rain fall) with the fluxes out being Q_{HP} (return from Hamelin Pool back in SB) and Q_E (evaporation). As stated, for mass balance models, the following equations must be satisfied, and at steady state.

Simple Math Model

$$I_{GW}+I_{SB} + I_{MW} = O_E + O_{HP} \qquad \text{Eqt 2.13}$$

Here the sum of fluxes from the input I_{GW}, I_{SB} and I_{MW} are equal to the sum of all output fluxes $O_{E,}$ O_{HP}. The water balance approximation expressed as flux and is equal to equations 2.14 and 2.15.

$$Q_{GW} + Q_{SB} + Q_{MW} = Q_E + Q_{HP} \qquad \text{Eqt 2.14}$$

Rearranging this becomes

$$Q_{GW} + Q_{SB} + Q_{MW} - Q_E - Q_{HP}= 0 \qquad \text{Eqt 2.15}$$

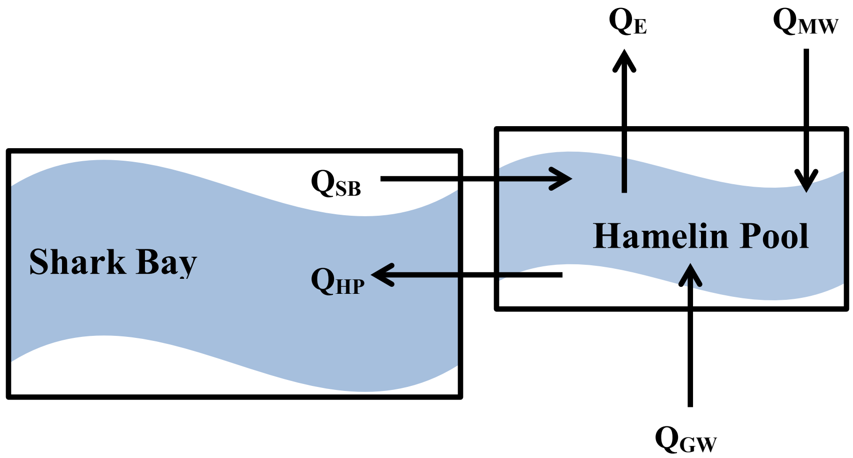

Figure 2-9 Box model of the fluxes(Q) into and out of Hamline Pool and Shark Bay.

By adding salinity (Figure 2-10) the water balance is expressed as equation 2.16, as the salinity of fresh water is essentially zero this reduces to equation 2.17.

$$S_{GW}*Q_{GW} + S_{SB}*SQ_{SB} + S_{MW}*Q_{MW} - S_E*Q_E - S_{HP}*Q_{HP} = 0 \qquad \text{Eqt 2.16}$$

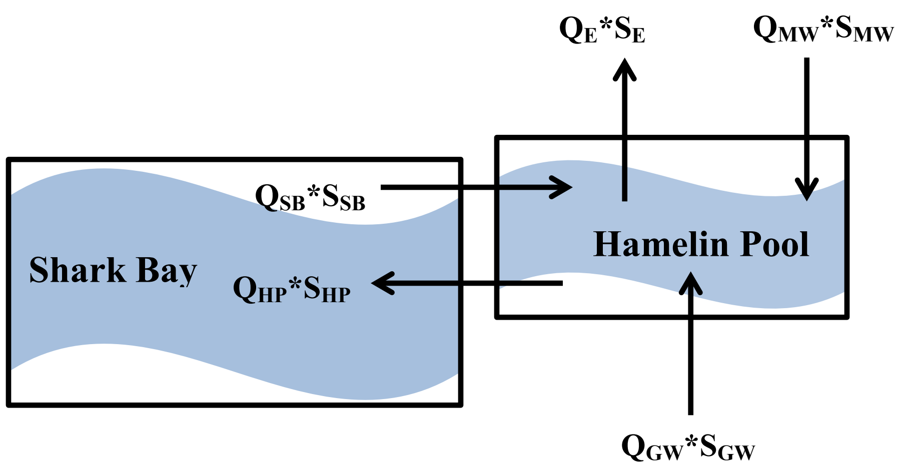

Figure 2-10 Box model of fluxes(Q) into and out of Hamelin Pool and Shark Bay with added values of salinity(S)

This reduced to,

$$S_{GW}*Q_{GW} + S_{SB}*Q_{SB} - S_{HP}*Q_{HP} = 0 \qquad \text{Eqt 2.17}$$

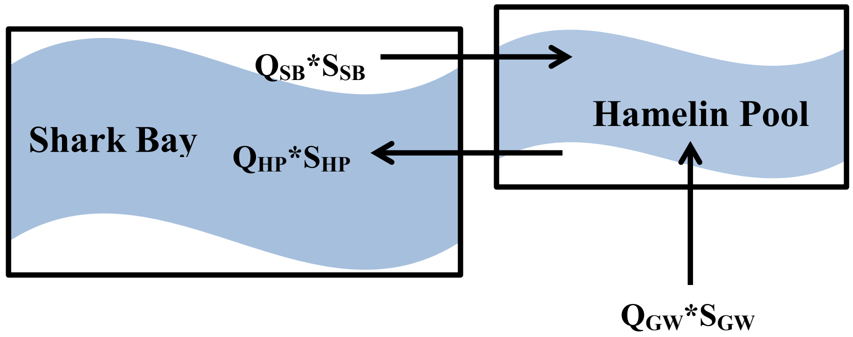

Figure 2-11 Box modeling showing the fluxes(Q) into and out of Hamelin Pool and Shark Bay with the values salinity (S) in which both evaporation and meteoric waters become zero since they have zero salinities.

The above equation is satisfied however, both evaporative and meteoric water fluxes have been eliminated (Figure 2-11).

Adding the $\delta^{18}O$ values,

$$\delta_{GW}*Q_{GW} + \delta_{SB}*SQ_{SB} + \delta_{MW}*Q_{MW} - \delta_{E}*Q_{E} - \delta_{HP}*Q_{HP} = 0 \qquad \text{Eqt 2.18}$$

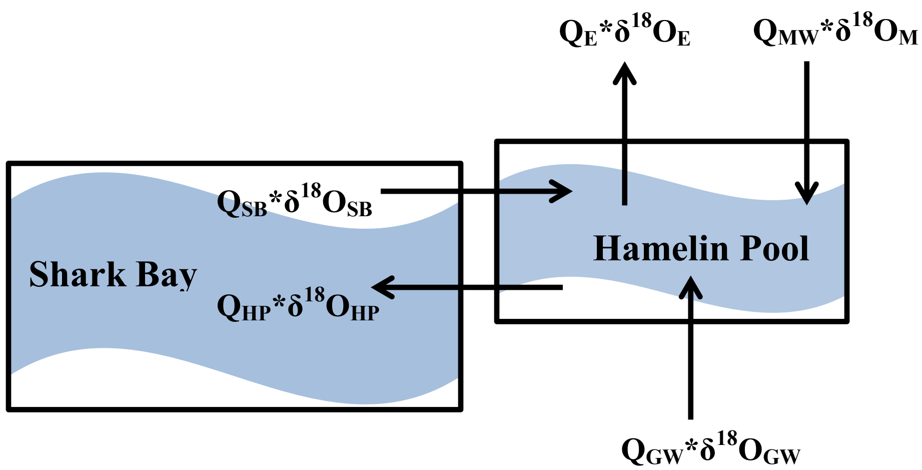

Figure 2-12 Box modeling showing the fluxes (Q) into and out of Hamelin Pool with added $\delta^{18}O$ values which cannot be reduced further.

There is no elimination of any flux using the isotopic compositions (Figure 2-12). A model with this equation can be made to constrain the isotopic composition as well as extent of the fluxes.

Steady State Evaporative Isotopic Model

$$(Vd\delta + \delta dV)/dt = Q_I\,\delta_I - Q_O\delta_O - Q_E\delta_E \text{ (Gonfiantini, 1986)} \qquad \text{Eqt 2.19}$$

In equation 2.19, V is equal to volume, Q_I refers to the amount of inflow, Q_O refers to outflow and Q_E refers to evaporation. Similarly, δ_I, δ_O, and δ_E refer to the isotopic composition of inflow, outflow and evaporation respectfully. This formula is used to calculate the isotopic composition of evaporation and therefore can be used to model the isotopic composition of a water body and solve theoretical fluxes or concentrations of delta values (Swart, 1991b; Swart, 1991c). Since the volume of the pool stays relatively constant over the course of year, all results have been calculated over a 1yr time period. In addition, all the fluxes are shown in km^3, equivalent $1*10^{12}$ liters. Using the above equations a steady state model for Hamelin Pool can be drawn as a box model shown in Figure 2-13.

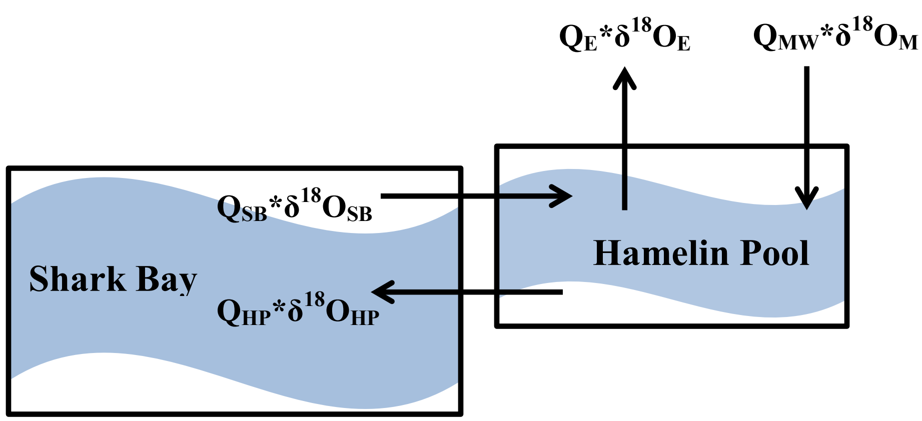

Figure 2-13 Box modeling showing the fluxes (Q) into and out of Hamelin Pool with added $\delta^{18}O$ values ground water has been removed as the flux is currently unknown.

This is a diagrammatical representation of the equations above. Groundwater influx is being currently studied in the Hamelin Pool area, groundwater will be calculated as infinitesimal or undetectable, but plausible at this point in time, once more data has been collected ground water can be entered into this model.

2.8 ***Steady-State Modeling Results***

The steady-state model suggests that it would take about 700yrs to reach an average $\delta^{18}O$ value of +3.95‰, the current measured average of Hamelin Pool. Once the water body becomes restricted and evaporation excessive (50%), the Shark Bay $\delta^{18}O$ values, which would be the initial Hamelin Pool values, have the potential to increase from +1.42 to +3.28‰ in just one year, assuming full mixing. The results also suggest that the order of magnitude by which Hamelin Pool fills with water from Shark Bay, minor sources, such as groundwater and precipitation, would be indistinguishable due to mixing. For example, Figure 2-15, at a range of 0.1 to 0.4 km^3/yr and delta value of -1.59 would have little effect on the average $\delta^{18}O$ value.

2.9***Steady State Modeling Discussion***

The model is first constructed using average inputs from measurements reported in this study (Table 2-2), but is then refined to best represent the environment as seen in Figure 2-14. The measurements collected from the Western Australia Bureau of Meteorology (WA, BOM), in blue, are slightly changed (0.15% humidity) to best mimic the natural environment.

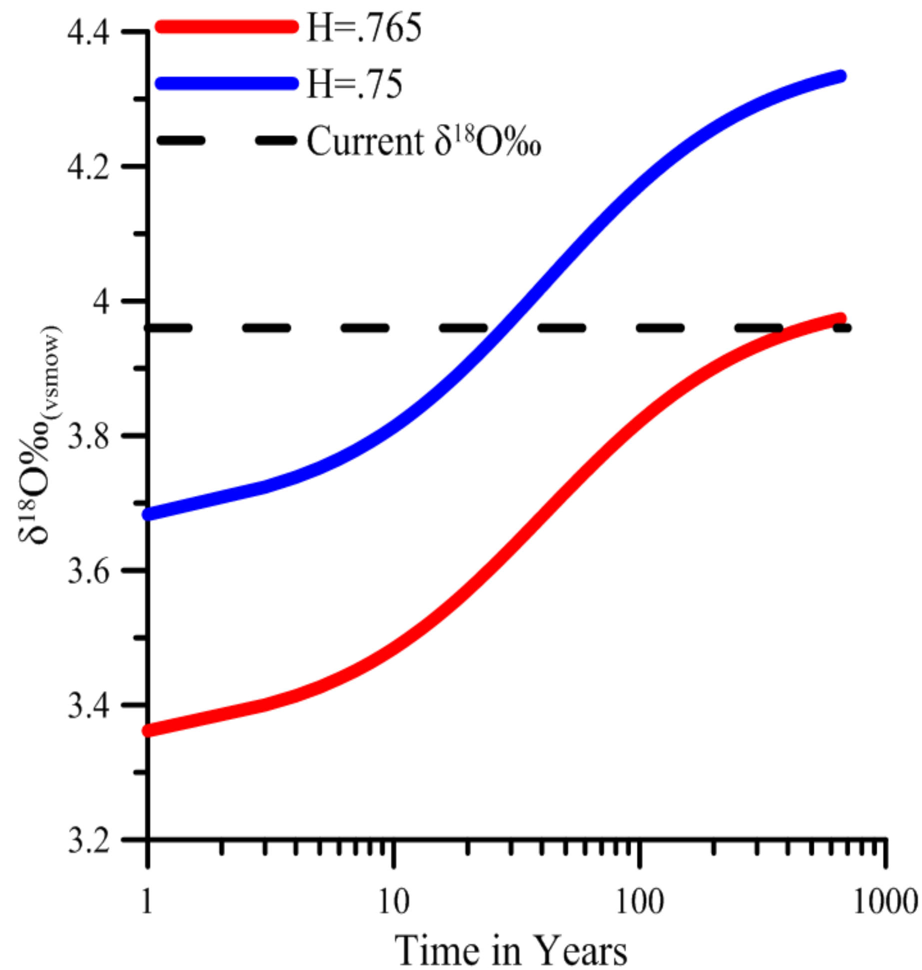

Figure 2-14 Modeled $\delta^{18}O$ values of Shark Bay waters over a 740 year period of time under Hamelin Pool environmental conditions. In blue are the modeled values using measurements from the WA, BOM. In red is a slightly modified humidity to best reflect the current state of Hamelin Pool.

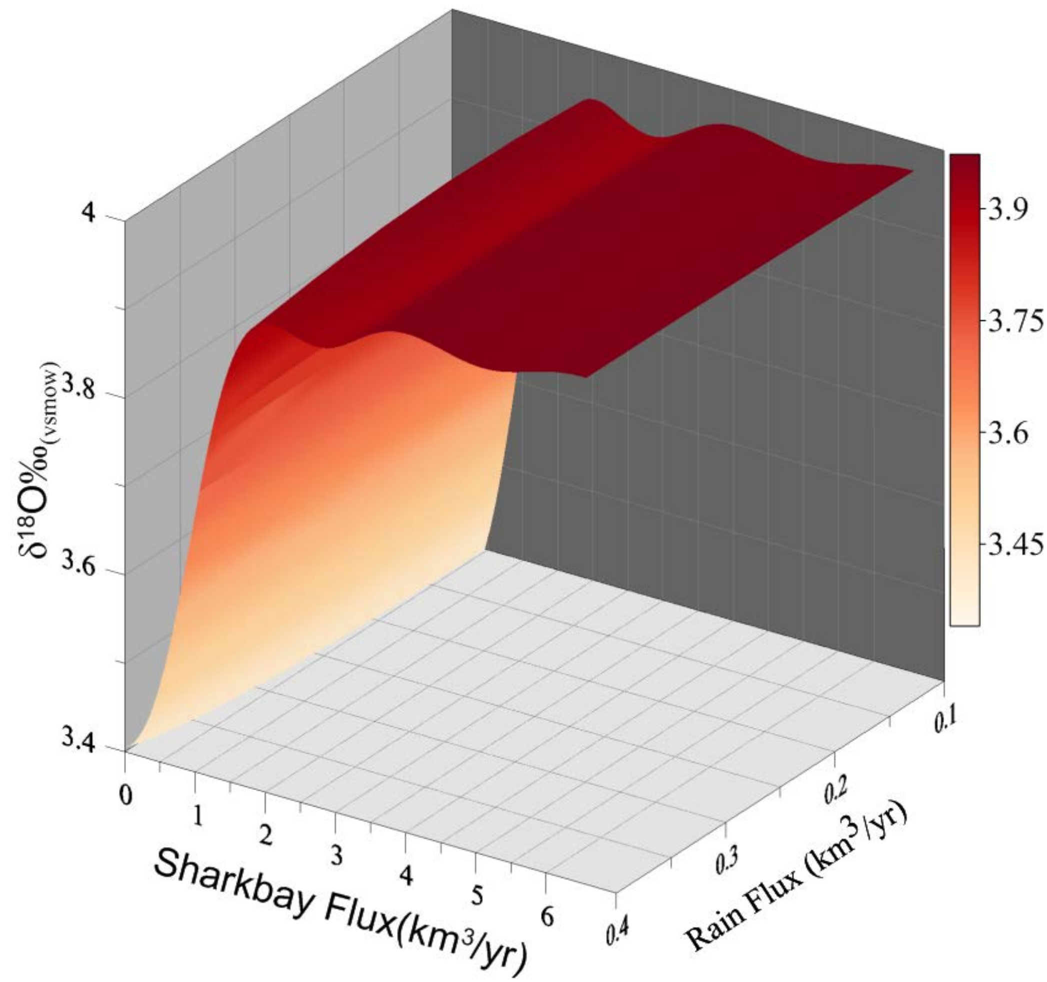

Figure 2-15. Modeled $\delta^{18}O$ values as function of changing fluxes from both Shark Bay and Meteoric Water. This figure shows how quickly the Shark Bay contribution to Hamelin Pool can mask other inputs of water into the area such as the known Meteroic Water.

Furthermore, this modeling has also given insight into the influence of Shark Bay on Hamelin Pool. When comparing the estimated flux of Shark Bay versus the measured flux of meteoric rain water (WA, BOM), Figure 2-15, it can be seen that the Shark Bay flux as the major contributor of input into Hamelin Pool has the ability to mask the rain water flux. This pattern is echoed in Figure 2-5, where the data clustering implied few sources of water recharge into Hamelin Pool. Mixing may also be making source tracking difficult to measure,

The resulting model allows for insight into the evolution of Hamelin Pool waters. The sill is known to be the major constrictor of water as well as the greatest influence on water flow into the pool. Here (Figure 2-14) I have calculated the amount of time it would take for marine waters from the greater Shark Bay area to fill the pool and reach the present measured $\delta^{18}O$ and $\delta^{2}H$ values. During the initial growth of the sill there was probably full mixing and minimal restriction, implying a low residence time of the water and therefore no elevated $\delta^{18}O$ and $\delta^{2}H$ values. In order to find the time it would take for an unaltered marine water to reach the average Hamelin Pool $\delta^{18}O$ value of +3.95‰, the simulation was run in reverse. The model suggests that it took about 740 years to reach a $\delta^{18}O$ value of 0‰. There is a sudden decrease the $\delta^{18}O$ value, at about 700 years implies that the water in Hamelin Pool may have been trapped in the pool ~700 years ago.

This model is also predictive and can be used to model $\delta^{18}O$ values from hypothetical water fluxes. The largest vulnerability to Hamelin Pool would be the inevitable invasion of seawater as a result of sea level rise (SLR). In order to best demonstrate how SLR will affect the pool chemistry, first it is important to note that while there is a global SLR there is also local SLR. Sea level rise regionally in Western Australia is estimated to be at the lower end of that predicted for the global mean of 1.8±0 .3mm to about 1.6 mm pre year (Church et al., 2004). Furthermore, the Indian Ocean, which provides water for Shark Bay and eventually Hamelin Pool has a $\delta^{18}O$ value of +0.5‰ (LeGrande and Schmidt, 2006). The resulting model, Figure 2-16, reveals a sharp decline in $\delta^{18}O$ values dropping over 70 years to +3‰, and ~320 years to +2‰. The $\delta^{18}O$ values would stabilize over a period of 3,000 years at ~1.3‰. With the known covariance of $\delta^{18}O$ values and salinity the general conductivity of the water within the pool would be expected to change as well, together with increased predation brought on by higher sea levels and normal marine salinity, Hamelin Pool's ecosystem would be subject to rapid environmental changes, which may stress stromatolitic activity.

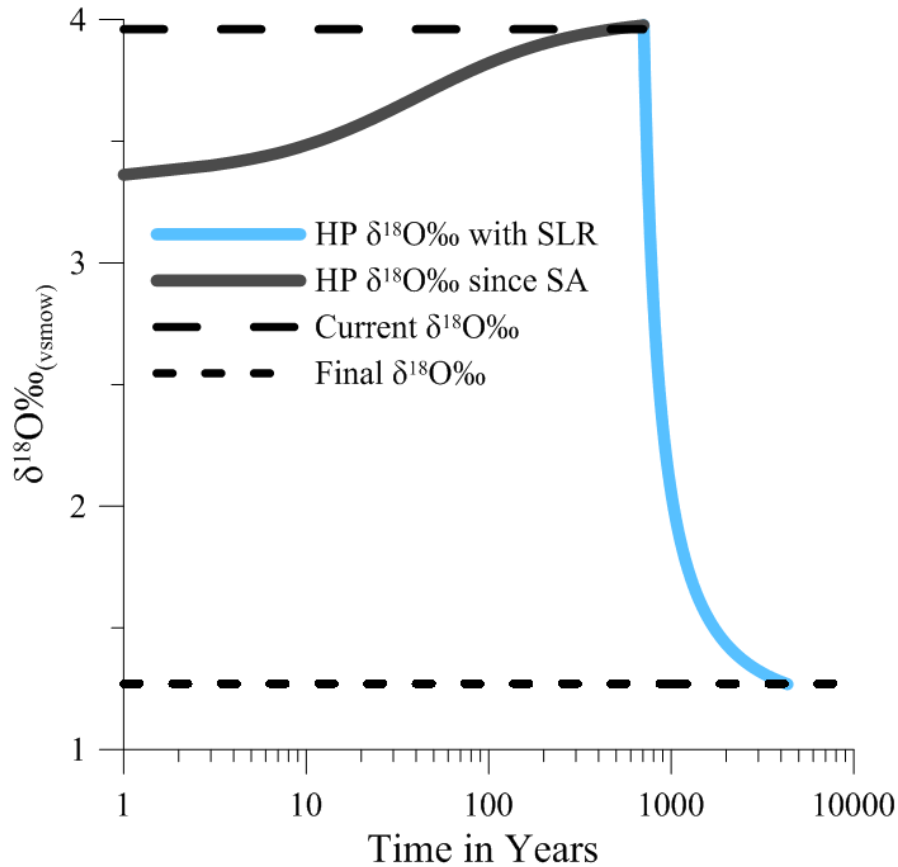

Figure 2-16 Modeled $\delta^{18}O$ values over time as function of local Shark Bay input & Indian Ocean SLR. In gray are the modeled current δ18O values. In blue is the resultant SLR which causes a drop $\delta^{18}O$ values as the sea level rises allowing more water exchange.

2.10 ***Chapter 2 Summary***

Salinity and the $\delta^{18}O$ and δ^2H values of water reveal the current state of Hamelin Pool waters and suggest not only how the water body evolved but also predict the effects of sea level rise. Salinity, $\delta^{18}O$ and δ^2H values suggest isotopically positive marine waters are the major contributor into the pool, but have only evolved to their current restricted signatures in the last 740 years. In addition, flux modeling projects that Hamelin Pool will most likely have extreme sensitivity to local sea level rise, even with continued excess evaporation and sill growth. Rapid changing conditions may lead to environmental stress on the stromatolitic activity.

Chapter 3: **Chemical Equilibrium: Major, Minor, Trace Elements and Saturation States**

3.1 ***Introduction to Water Chemistry and Carbonate Reactions in Sea Water***

Carbonates exist in nature in various polymorphs that have different element compositions. For example, aragonite an orthorhombic form of calcium carbonate, has high amounts of Sr (~7000-8000ppm), while high and low Magnesium Calcites (HMC and LMC) contain less Sr and instead incorporate Mg in varying amounts. Carbonate reactions in marine waters are driven by changes in salinity, temperatures, and biological reactions (photosynthesis and respiration). These in turn alter pH and alkalinity, driving variations in carbonate saturation. The precipitation or dissolution of any carbonate species can be traced by the concentration of trace elements as defined by distribution coefficients (D); 'D' is defined by equation 3.1 is equal to a trace element under consideration (M).

$$D = \frac{\frac{M}{Ca}\ mineral}{\frac{M}{Ca}\ seawater} \qquad \text{Eqt 3.1}$$

When carbonate reactions take place, changes in element concentration (Sr^{2+}, Ca^{2+}, and Mg^{2+}) occur in waters as a result of these varying distribution coefficients. These variations lead to changes in the element ratios relative to each other and conservative element such as Cl^- (Swart and Kramer, 1998). Furthermore, using measured chemical properties (pH, alkalinity, and available ions) saturation state (Ω) with respect to calcites (HMC and LMC) and aragonite can also be measured. The saturation state of a mineral in water predicts how likely that mineral is to precipitate. In this chapter I will discuss the expected changes in the elemental ratios during carbonate reactions and what these reactions suggest about the behavior the basinal waters.

3.2 ***Objectives***

The water samples collected from Hamelin Pool (Chapter 2) have also been analyzed for their concentrations of Ca, Sr, Mg and Na with the objective to use the dissolved metal data to predict carbonate saturation (Ω) and likelihood of precipitation. This is accomplished by comparing reactive elements ratios to each other (Sr^{2+}, Ca^{2+}, Mg^{2+}) as well comparing those reactive elements to the non-reactive element Cl^-.

3.3 ***Methods***

Alkalinity and pH: Water samples were measured in the Stable Isotope Lab (SIL, RSMAS) for initial pH and alkalinity by titration with pH probe using a Gran titration. Precision was determined with an internal 2.0 mM sodium bicarbonate ($NaHCO_3^-$) standard run along with samples and reported as one standard deviation from the mean. Precision for the internal standard was ± 0.30 (1σ) for pH and ± 0.16 (1σ) for alkalinity. For comparison, reference material for oceanic CO_2 measurements (Scripps UCSD, batch 139) with a known alkalinity of 2.25mM, was measured to be 2.46mM ± 0.19(1σ).

Chloride: The Cl^- ion concentration measurements were calculated using the ICP-OES data for Na^+ as proxy. The Na^+ concentration was multiplied by a factor of 1/0.86 (IAPSO Sea Water) to account for the natural covariance of Na to Cl ions in sea water.

<u>Trace Metals:</u> Trace metal abundances were measured using a Varian Inductively Coupled Plasma Optical Emission Spectroscopy (ICP-OES). This type of emission spectroscopy uses an inductively coupled plasma torch to excite atoms and ions that emit electromagnetic radiation at wavelengths characteristic of a particular element.

Each sample is delivered to an analytical nebulizer by peristaltic pump where is it changed into a mist and introduced to the plasma flame. The intensity of the emission is indicative of the concentration of the elements within the sample. The machine was calibrated using a range four IAPSO Sea Water Standards diluted in 1:100 in nitric acid. Ratios of 0.06:100, 1:100, 1.3:100 and 2:100 and normalized with a natural South Florida water. Precision was measured with an internal standard made with IAPSO standard seawater at a dilution of 1:100. The Sr/Ca, Mg/Cl, Mg/Ca and Ca/Cl ratios we measured to a precision of 0.074, 1.94, 0.05, 0.36 respectively.

<u>Saturation State:</u> Saturation state (Ω) of seawater with respect to carbonates can be defined as the product of the activities of dissolved calcium and carbonate ions in seawater divided by their product at equilibrium.

$$\Omega = \frac{[Ca^{2+}] \bullet [CO_3^{2-}]}{[CaCO^3]} \qquad \text{Eqt 3.2}$$

When Ω is equal to 1 then the seawater being measured would be in equilibrium or saturation with the carbonate, meaning that no dissolution or precipitation is taking place. $\Omega > 1$ and $\Omega < 1$ correspond to supersaturated and undersaturated. The carbonate (i.e. Calcite/Aragonite) saturation state (Ω) is dependent on carbonate (CO_3^{2-}) available, the concentration of Ca^{2+}, pressure, temperature and salinity. Surface waters are generally supersaturated with respect to $CaCO_3$; however it is rare for $CaCO_3$ to precipitate inorganically due to complex ion-ion interactions, which inhibit the precipitation. Cold and fresh water promote lower $CaCO_3$ saturation states (Chierici and Fransson, 2009). The saturation state of the basinal pool waters was calculated using geochemical modeling software *The Geochemist Workbench*®. The software calculates the saturation state using a Debye-Hueckel equation (see Larson et al, 1942) modified for high ionic strength.

3.4 ***Results***

Alkalinity and pH: Table 3-3 shows a summary of results; the average, minima and maxima of the pH, alkalinity concentrations. The average pH measured was 7.82 well within the normal range for marine waters (~8). The pH ranged between 8.36 and 6.81(Figure 3-1). The average alkalinity measured was 3.06 mM with the highest values being 4.09mM and the lowest values being 0.73mM. The distribution of these values shows no strong spatial relationship around the pool area (Figure 3-1).

Trace metals: The average concentrations of Sr, Ca, Mg and Cl are listed in Table 3-1. The average ratios are found in Table 3-2 Sr/Ca and Ca/Cl values tended to be higher than Standard Sea Water SSW (Figure 3-5). While Mg/Cl and Mg/Ca values were lower (Figure 3-6, Figure 3-7).

Saturation state: The values are all greater than 0, which is typical in marine waters. The Ω for aragonite had an average value of 2.27 (0.16 to 6.97). The Ω for calcite had an average value of 3.31 (0.23 to 10.19). The two maps in Figure 3-2 appear to have matching distributions, where aragonite saturation is high so is calcite saturation. All data for this chapter can be found in the appendix in Tables 7-6 through 7-10.

	pH	Alk	Sr_{umol}	Ca_{mmol}	Mg_{mmol}	Cl_{mol}
North $_{Avg}$	7.80	2.93	136.23	16.49	79.02	866.93
Mid $_{Avg}$	7.85	3.11	139.39	16.76	81.38	884.13
South $_{Avg}$	7.80	3.11	158.61	18.62	89.50	987.65
Mean	7.82	3.05	145.73	17.39	83.72	918.50
Max	8.36	4.09	251.08	31.06	11.42	1547.86
Min	6.81	0.73	89.99	10.74	59.13	561.37
n	117	119	117	117	117	116

Table 3-3 Summary Table of the results from the pH, Alk and trace metal results, highlighting the average geographical units of North, Mid and South. The full list of all results can be found in Tables 7-6, 7-7, and 7-8 of the appendix.

Figure 3-1. Left) Alkalinity results and Right) pH results contoured over Hamelin Pool. There are no spatial relationships for these

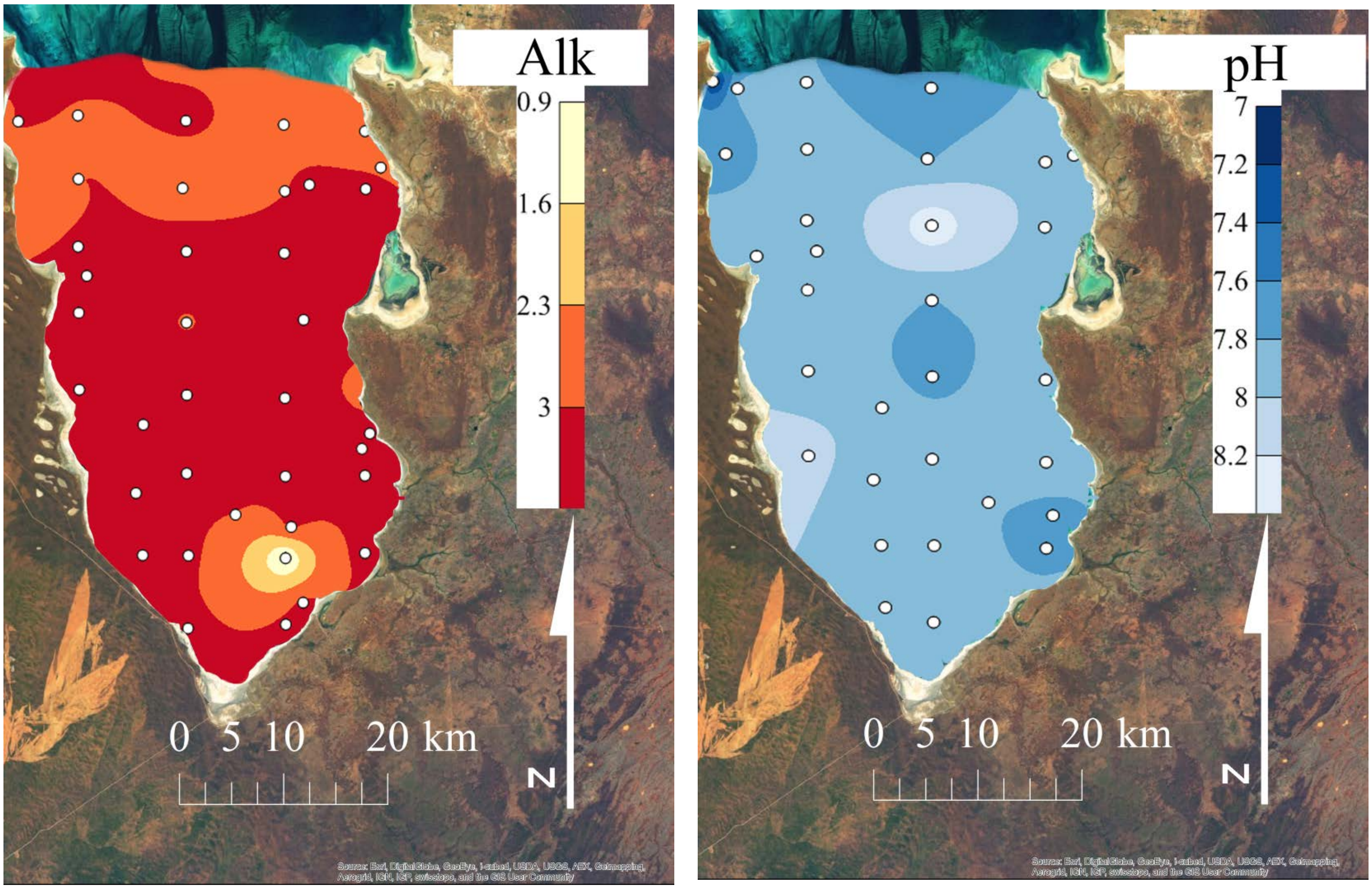

Figure 3-2. Saturation state values for aragonite (Left) and calcite (Right) for the pool waters collected in Hamelin Pool. There is no strong spatial relationship.

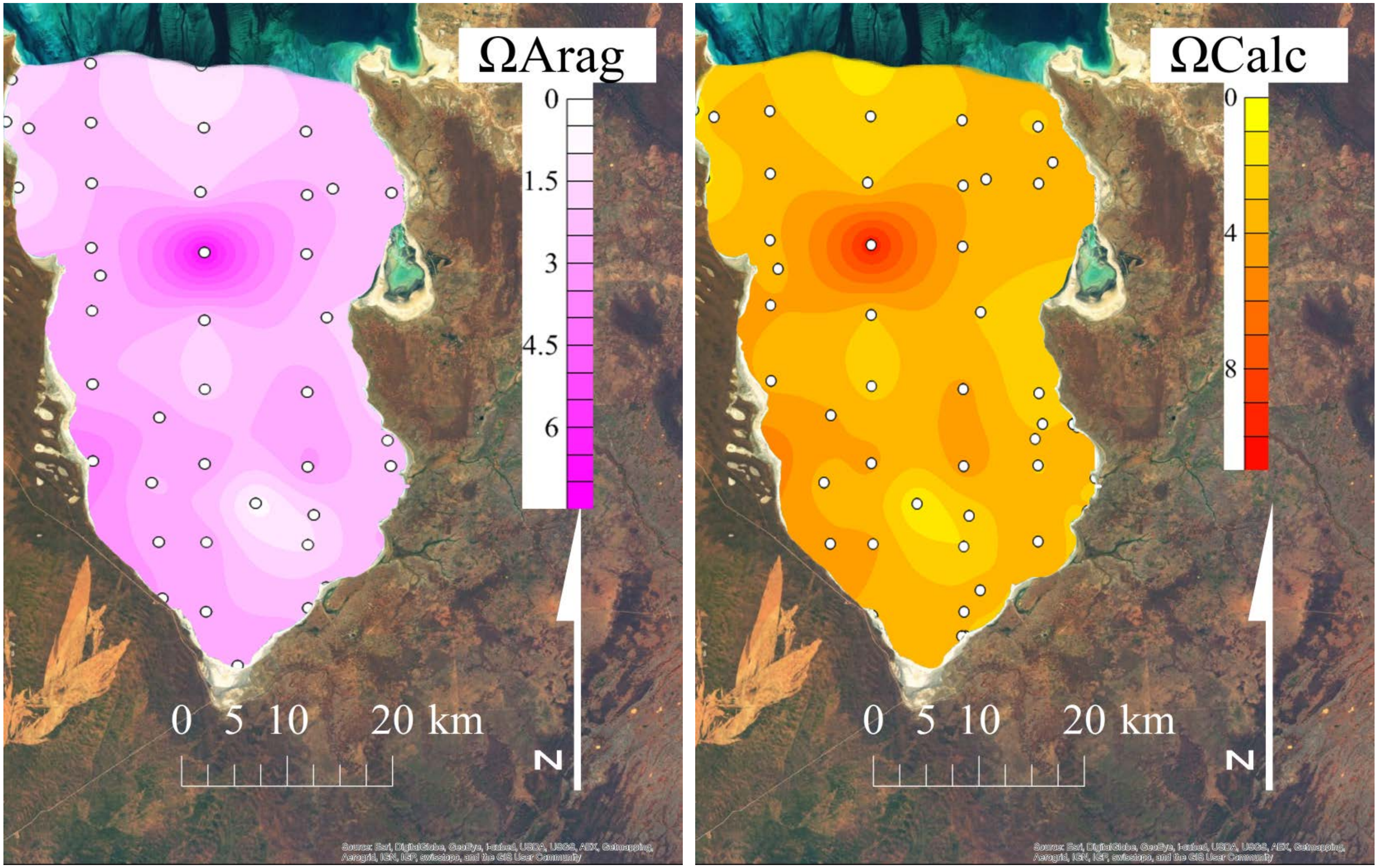

3.5 ***Discussion***

Precipitation and Dissolution

Dissolution and precipitation of calcite (HMC or LMC), aragonite and dolomite have pronounced influences on Sr/Ca, Ca/Cl, Ca/Mg, and Mg/Cl ratios in solution. Assuming Cl^- ions are conservative, i.e. not reactive, increases and decreases in the Ca/Cl ratio arise from dissolution (increases in solution) and precipitation (decreases in solution) reactions. Changes in Sr^{2+}, Ca^{2+} and Mg^{2+} concentrations relative to Cl^- are indicative of which carbonate minerals are involved in dissolution or precipitation. Ratio differences are a result of the differing distribution coefficients of these elements (Equation 3.1) (Swart and Kramer, 1998).

Strontium/Calcium and Calcium/Chloride

Aragonite: The precipitation (and dissolution) of aragonite, while changing the Ca/Cl ratio of the precipitating fluid, will not change the Sr/Ca ratio of seawater as the distribution coefficient for Sr into aragonite is close to unity. In other words aragonite is removing and precipitating Sr and Ca at the same ratio as that contained in seawater. Hence these reactions plot as a horizontal line on Figure 3-3.

Low-Mg Calcite: The precipitation of LMC on the same diagram, Figure 3-3 will produce waters which plot diagonally, as calcite preferentially excludes Sr during precipitation leading to elevated Sr concentration (higher Sr/Ca and lower Ca/Cl ratios). During dissolution the reverse is true.

<u>High-Mg Calcite:</u> As the distribution coefficient for Sr into HMC is intermediate between that of aragonite and LMC, precipitation and dissolution of HMC will fall on a line with an intermediate slope between aragonite and LMC. The Sr/Ca values increase with calcium utilization while the Ca/Cl is dropping, Figure 3-3.

<u>Dolomite:</u> Precipitation or dissolution of dolomite will affect the values in a similar manner to HMC and LMC.

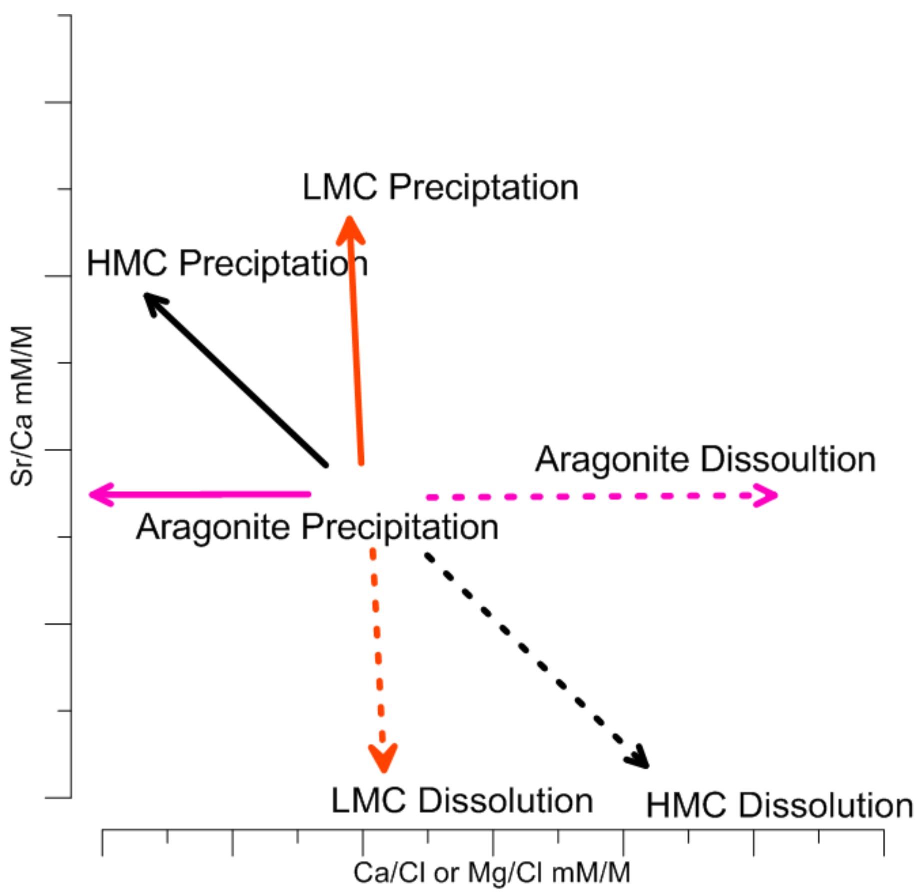

Figure 3-3 The expected relationships of Sr/Ca ratios compared with Ca/Cl and Mg/Cl. In pink Aragonite trends along a horizontal line as the Sr/Ca ratio is similar to seawater, with only Ca/Cl and Mg/Cl concentration varying during dissolution or precipitation. LMC (orange) HMC (black) trend horizontally as while Ca/Cl and Mg/Cl ratios rise during precipitation, Sr/Ca ratios drop the opposite is true for dissolution as Ca/Cl and Mg/Cl ratios drop Sr/Ca ratios rise.

Strontium/Calcium and Magnesium/Chloride

Aragonite: Aragonite contains very little Mg and therefore although dissolution and precipitation will change the absolute concentration of Mg in the fluid, these changes are likely to be within analytical error. As mentioned previously dissolution and precipitation will not change Sr/Ca ratio.

Low-Mg Calcite: Low-Mg calcite contains small amounts of Mg and therefore precipitation and dissolution of LMC would shift have a minor effect Mg/Cl value of the fluid.

High-Mg Calcite: In contrast to LMC precipitation and dissolution, precipitation and/or dissolution of HMC (or dolomite) would greatly influence the Mg/Cl ratio of the fluid Figure 3-3.

Dolomite: Precipitation or dissolution of dolomite will behave in a similar manner to HMC, but with greater changes in the Mg/Cl ratios to the Sr/Ca ratios of the fluid.

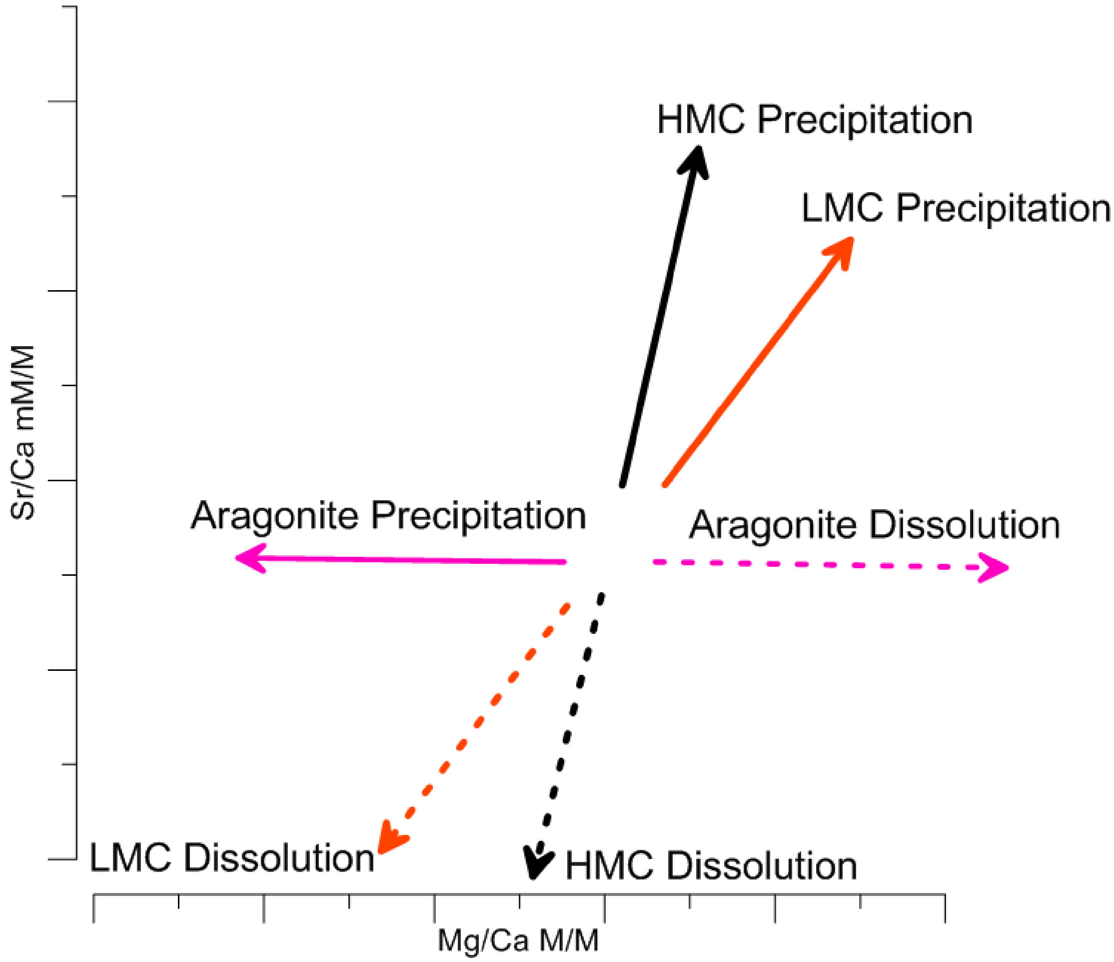

Figure 3-4 The expected relationships of Sr/Ca ratios compared with Ca/Mg. In pink Aragonite trends along a horizontal line as the Sr/Ca ratio is similar to sea water, with only Ca/Mg concentration varying during dissolution or precipitation. LMC (orange) HMC (black) trend horizontally as while Mg/Ca ratios rise during precipitation so does Sr/Ca ratios the opposite is true for dissolution as Mg/Ca ratios drop the Sr/Ca ratio also drops.

Strontium/Calcium and Magnesium/Calcium

Aragonite: Precipitation of Aragonite does not alter the Sr/Ca ratio of the fluid, but increases the Mg/Ca ratio during dissolution and decreases it during precipitation (Figure 3-4).

Low-Mg Calcite: Precipitation of LMC increases Mg/Ca and Sr/Ca ratios, while dissolution decreases Sr/Ca and Mg/Ca ratios of the fluid (Figure 3-4).

High-Mg Calcite: The Sr/Ca and Mg/Ca ratios increase during precipitation and both decreases during dissolution, but at a higher rate, Figure 3-4.

Dolomite: Precipitation or dissolution of 1:1 Mg/Ca ratio leaves the Mg/Ca ratios unchanging. Sr/Ca ratios however, will increase during the precipitation of dolomite and decreases during dissolution.

Hamelin Pool Water Trace Metal Chemistry

In order to correctly predict the nature of the minerals being precipitated or dissolved, it is necessary to define the initial composition of the water body. Standard Sea Water (SSW) as defined by Ocean Drilling Program (ODP) Technical Note 15(1991) has on average Ca^{2+}, Mg^{2+}, Sr^{2+}, and Cl^{-} concentrations of 10.55 mM, 54mM, 87µM, and 560 mM respectively. This gives seawater a Sr/Ca ratio of 8.2 mM/M, a Mg/Cl ratio of 96.6mM/M, a Mg/Ca ratio of 5.1 M/M and a Ca/Cl ratio of 18.8 mM/M. These ratios are shown in Figures 3-5, 3-6 and 3-7 below as a red circle. The initial values for seawater entering Hamelin Pool would be the water closes tot the Faure Sill, the average for the waters collected in the northern part of the pool, the Faure Sill Water (FSW), is shown in Figures 3-5, 3-6 and 3-7 as a yellow triangle. The values of the individual elements measured can be found in Tables 7-7 and 7-8 of the Appendix. In order to evaluate mixing in Hamelin Pool, water samples were collected at both the air-surface interface (blue circles in Figures 3-5, 3-6, 3-7) as well as the water sediment interface (black circles in Figures 3-5, 3-6, 3-7). When comparing SSW and FSW, data suggest that the water entering the pool from Shark Bay has already been chemically altered. The extensive seagrass beds, which are home to an abundance of calcifying organisms and water restriction in Shark Bay, change the water chemistry before reaching Hamelin Pool.

Ratio Distributions

The data from Hamelin Pool are shown below in Figures 3-5, 3-6 and 3-7 have analytical error plotted on one sample value to represent the overall error for all data points. In order to describe the variation within Hamelin Pool the basin has been separated into three regions (north, mid and south). The northern portion of the pool are all data points on and north of latitude 26.1˚S, the southern portion of the pool are all data points, on and south of latitude 26.3˚S with central or mid-section are being all the data points in between.

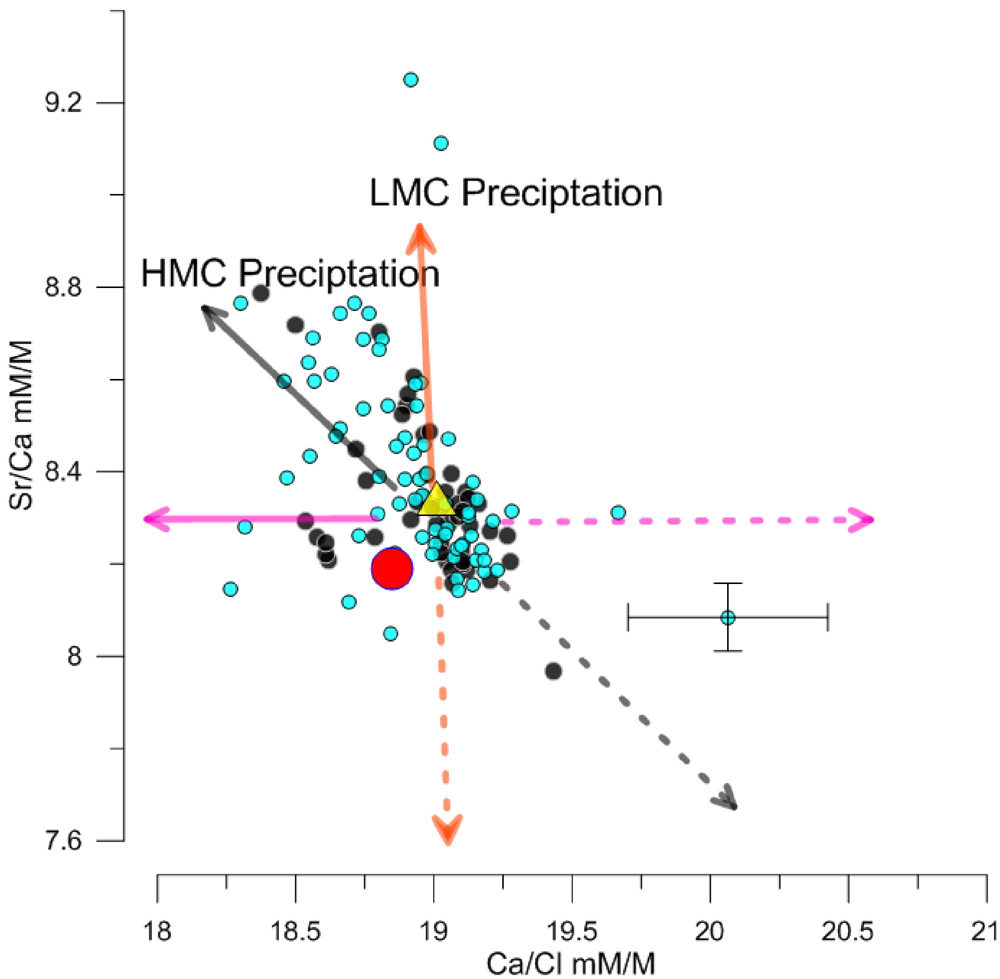

Figure 3-5 The Sr/Ca ratios compared with Ca/Cl ratios for Hamelin Pool waters, blue dots are surface samples, black dots are bottom samples. The solid red circle is indicative of sea water standard and the yellow triangle is Sill Water. Dotted lines show trend directions for dissolution while solid lines show trends for precipitation (Swart and Kramer, 1998) Sr/Ca error = 0.074 Ca/Cl error = 0.36.

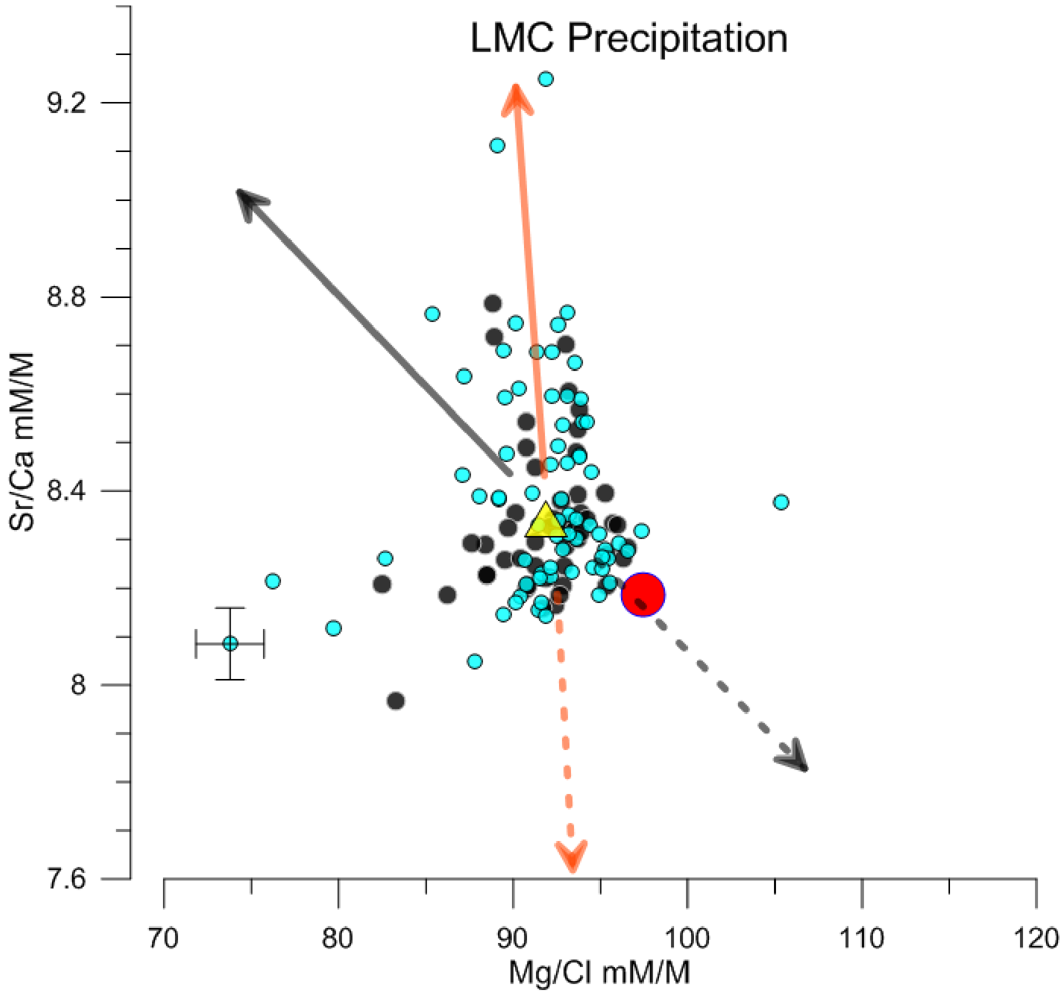

Figure 3-6 The Sr/Ca ratios compared with Mg/Cl ratios of Hamelin Pool waters, blue dots are surface samples, black dots are bottom samples. The solid red circle is indicative of sea water standard and the yellow triangle is Sill water. Dotted lines show trend directions for dissolution while solid lines show trends for precipitation (Swart and Kramer, 1998) Sr/Ca error = 0.074 Mg/Cl error = 1.94.

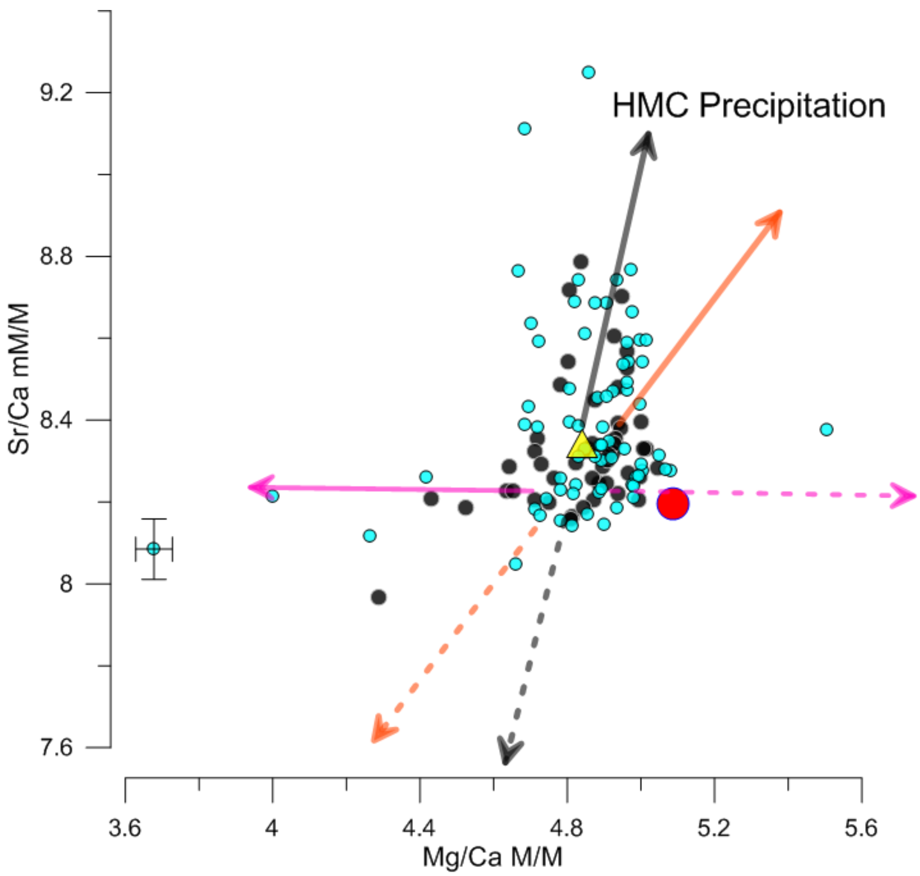

Figure 3-7 The Sr/Ca ratios compared with Mg/Ca ratios for Hamelin Pool waters, blue dots are surface samples, black dots are bottom samples. The solid red circle is indicative of sea water standard and the yellow triangle is Sill water. Dotted lines show trend directions for dissolution while solid lines show trends for precipitation (Swart and Kramer, 1998) Sr/Ca error = 0.074 Mg/Ca error = 0.05.

The differences between the geographical regions have been compared using a two-tailed t-test (Table 3-2) and graphically (Figures 3-8, 3-9, 3-10). The two-tailed t-test p-values show no significant difference, in any of the ratios measured, when comparing the north and central regions (yellow triangle and gray square Figures 3-8, 3-9, 3-10). However, there are significant differences in the south (black upside down triangle) compared to the north as well as the south compared to the central (mid) regions. The Sr/Ca ratios and the in the southern region are significantly higher than in both the mid and northern regions. The Ca/Cl ratios are significantly lower in the southern region when compared to mid and northern regions with the Sr/Ca values being much more significant than the Ca/Cl. The Mg/Cl ratios only showed a significant difference with the southern compared to the central regions with the central region being higher. Graphically, in the north and central the average results (yellow triangle and gray square) in suggest that the water in the northern and central parts of the pool are chemically similar Figures 3-8, 3-9, 3-10. These differences are due to mixing of Shark Bay Waters with Hamelin Pool waters through the channels within the sill. The water that flows through the channels would mix in the northern portions of the pool past the sill and continue to mix as they approach the south.

	North (mean)	Mid (mean)	South (mean)	Standard deviation	North/Mid (p-value)	South/Mid (p-value)	North/South (p-value)
Sr/Ca	8.27	8.31	8.51	0.07	0.09	<<0.01	<<0.01
Mg/Ca	4.84	4.86	4.82	0.05	0.63	0.25	0.71
Ca/Cl	19.01	19	18.86	0.36	0.88	<0.01	0.02
Mg/Cl	91.99	92.44	90.92	1.94	0.64	0.05	0.26
n	45	32	39				
Ω Calc	2.99	3.67	3.34	1.15	0.29	0.02	0.00
Ω Arag	2.04	2.51	2.29	0.78	0.29	0.02	0.11
n	39	32	42				

Table 3-4 Elemental ratios and saturation states (Ω) separated geographically, mean values for the northern, southern and central (mid), standard deviations of from the mean. On left colored are P-values for the comparison of the geographical locations to one another. T-Test parameters: Null Hypothesis: there is no difference, 2 tail no directional assumptions, $p>0.05$ = Red no significance, $p<0.05$=Green significant difference.

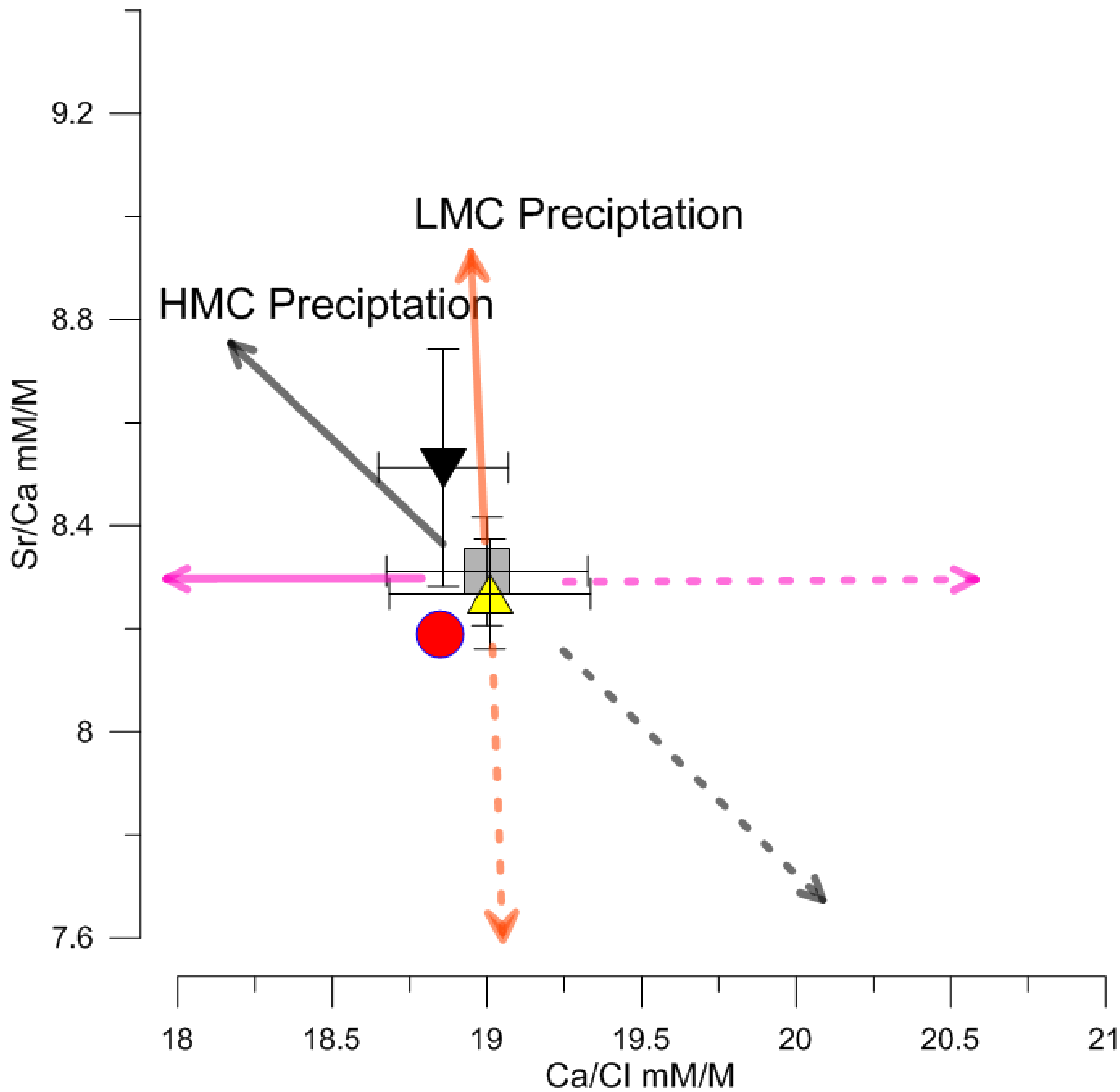

Figure 3-8 Geographical averages of Sr/Ca and Ca/Cl ratios of northern (yellow triangle) central (gray square) and southern (upside down black triangle) Hamelin Pool basinal waters compared with Stand Sea Water (red circle) and Hamelin pool Sill water (yellow circle). Water in the northern portion differs from the central and southern waters, indicating mixing in the northern portion of the pool past the sill.

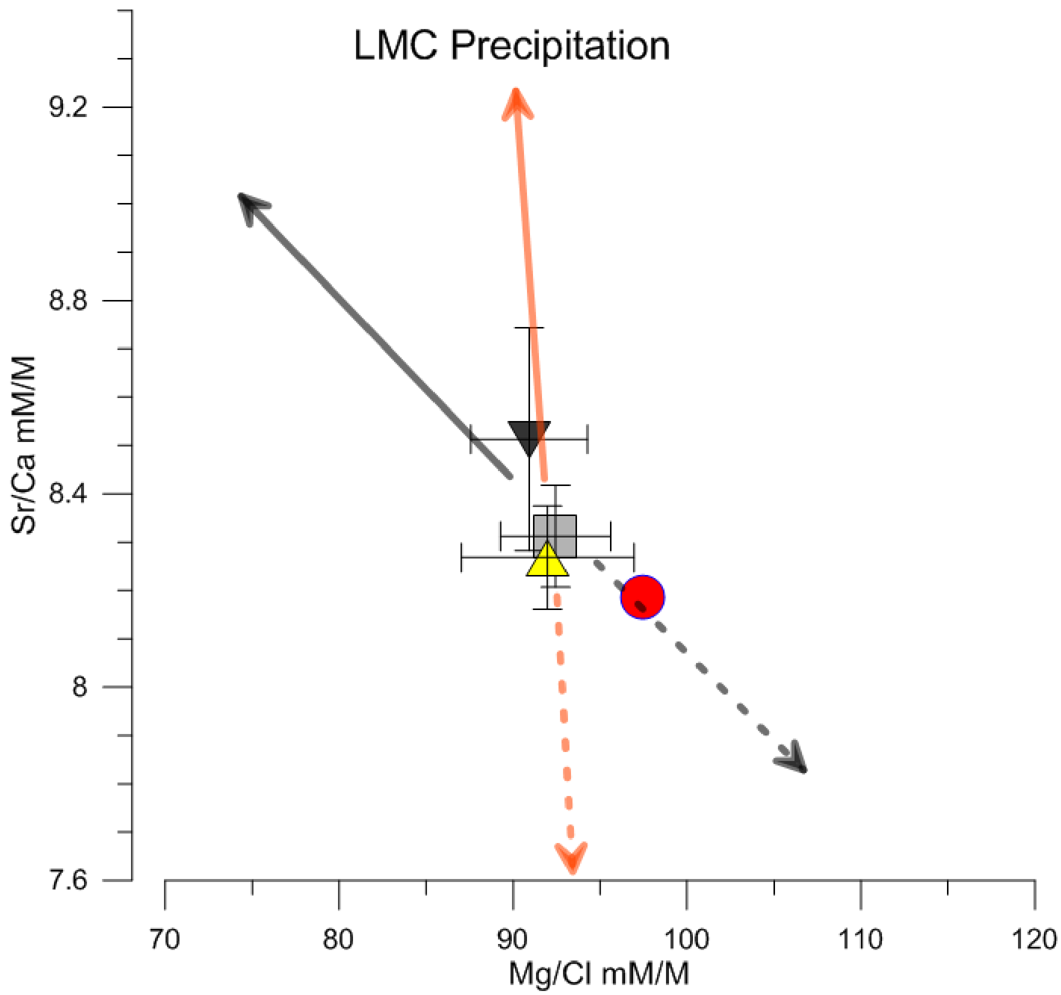

Figure 3-9 Geographical averages of Sr/Ca and Mg/Cl ratios of northern (yellow triangle) central (gray square) and southern (upside down black triangle) Hamelin Pool basinal waters compared with Stand Sea Water (red circle) and Hamelin pool Sill water (yellow circle). Water in the northern portion differs from the central and southern waters, indicating mixing in the northern portion of the pool past the sill.

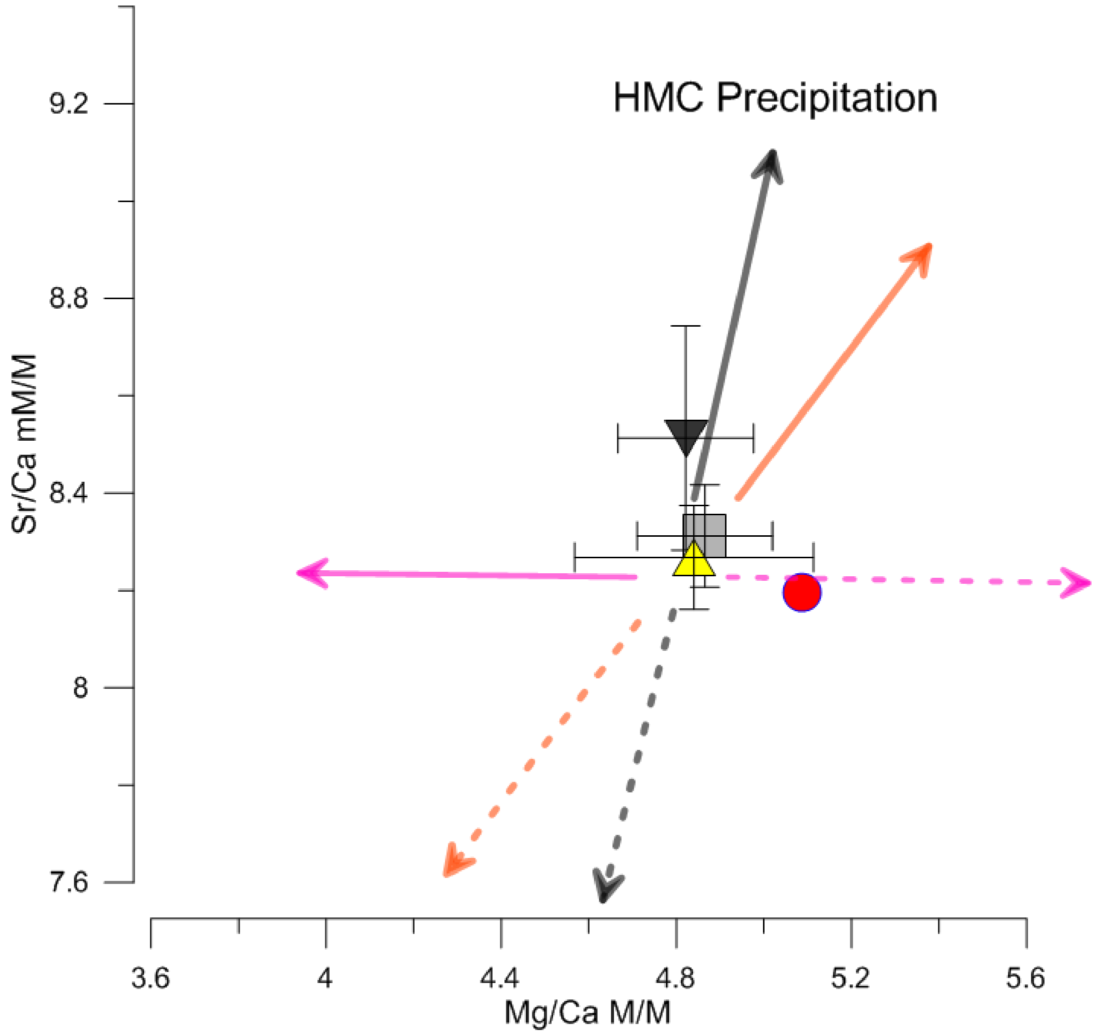

Figure 3-10 Geographical averages of Mg/Ca and Ca/Cl ratios of northern (yellow triangle) central (gray square) and southern (upside down black triangle) Hamelin Pool basinal waters compared with Stand Sea Water (red circle) and Hamelin pool Sill water (yellow circle). Water in the northern portion differs from the central and southern waters, indicating mixing in the northern portion of the pool past the sill.

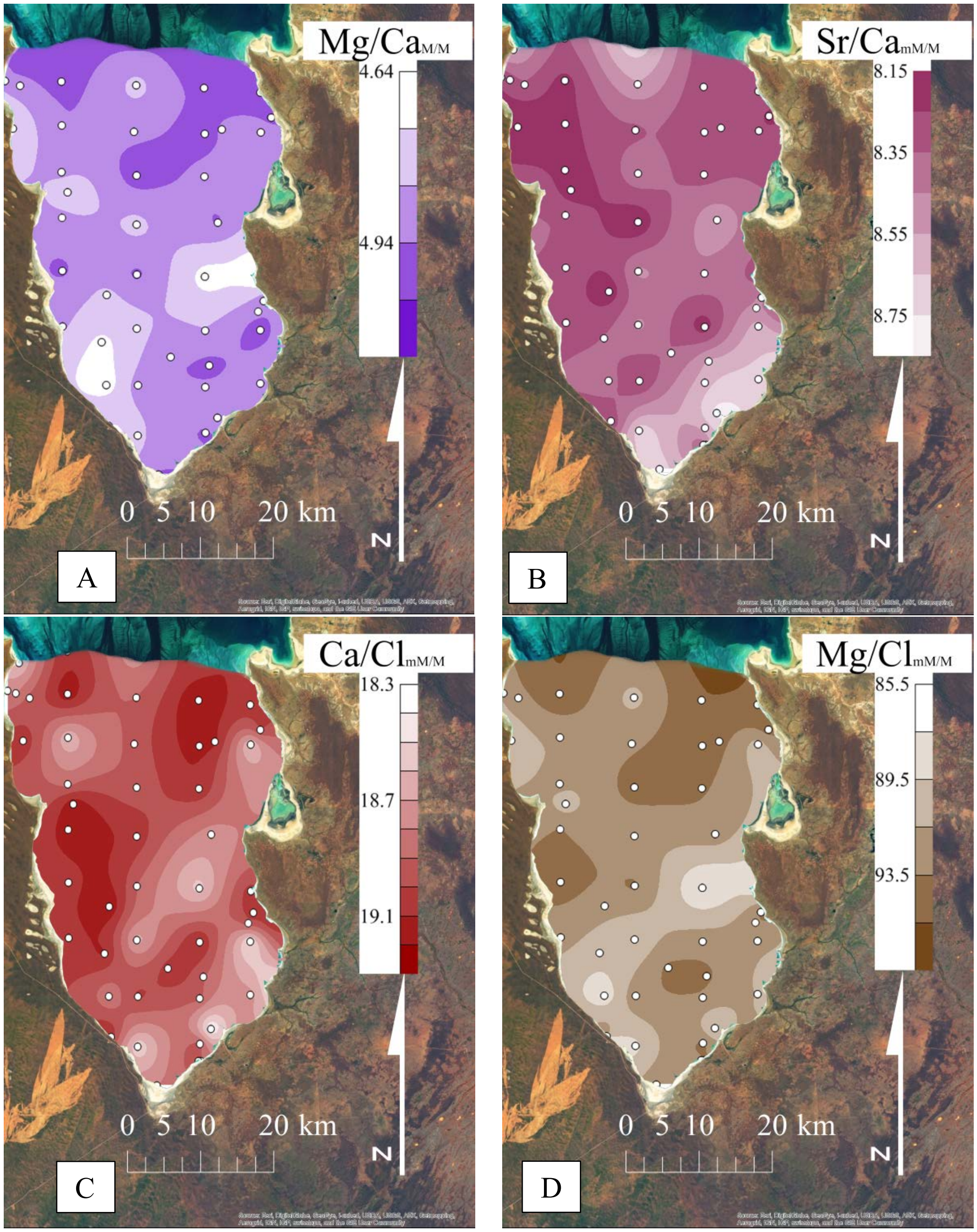

Figure 3-11 A) Mg/Ca ratios B) Sr/Ca ratios C) Ca/Cl ratios D) Mg/Cl ratios of the Hamelin Pool water samples. While there are no strong spatial relationships in these figures, they do suggest that the metal ratios can be broken down into smaller sections for a better understanding of their distributions.

Saturation Index

There is no significant difference in the aragonite and/or calcite saturation in the northern compared to the central regions. The southern region is both significantly more saturated in calcite and aragonite than the central regions and the South compared to the North is significantly more saturated in calcite. This is likely linked to high saturation and hyper salinity of pool waters coupled with higher residence time of water in the southern region of the basin.

Hamelin Pool Compared to Great Bahama Bank

The elemental ratio data from this thesis has been compared with waters from Great Bahama Bank (GBB) collected and analyzed at RSMAS. Since cyanobacterial and microbial mats are found in both of these areas this comparison may hold a critical key to understanding microbial environments. The absolute ratios and ranges of GBB and Hamelin Pool vary significantly. While Hamelin Pool values differ from Standard Sea Water (SSW) by almost double with average concentrations of Sr, Ca, Mg and Cl of 145.73 ± 21.98, 17.39 ± 2.51, 83.72 ± 8.57, 918.50 ± 132.84 (Table 3-1), Great Bahama Bank is close to SSW with average amounts of Sr, Ca, Mg and Cl of 84.79 ± 1.75, 10.87 ± 0.19, 58.96 ± 1.04, 545.04 ± 12.10. However, when examining the metal ratios, the inverse is true. Hamelin Pool waters have ratios much closer to SSW, Figures 3-12, 3-13, 3-14, whereas GBB is significantly different. This is likely due to Hamelin Pool water being directly altered from restricted seawater, whereas GBB is an open marine environment with several other hydrological processes affecting the sea water chemistry.

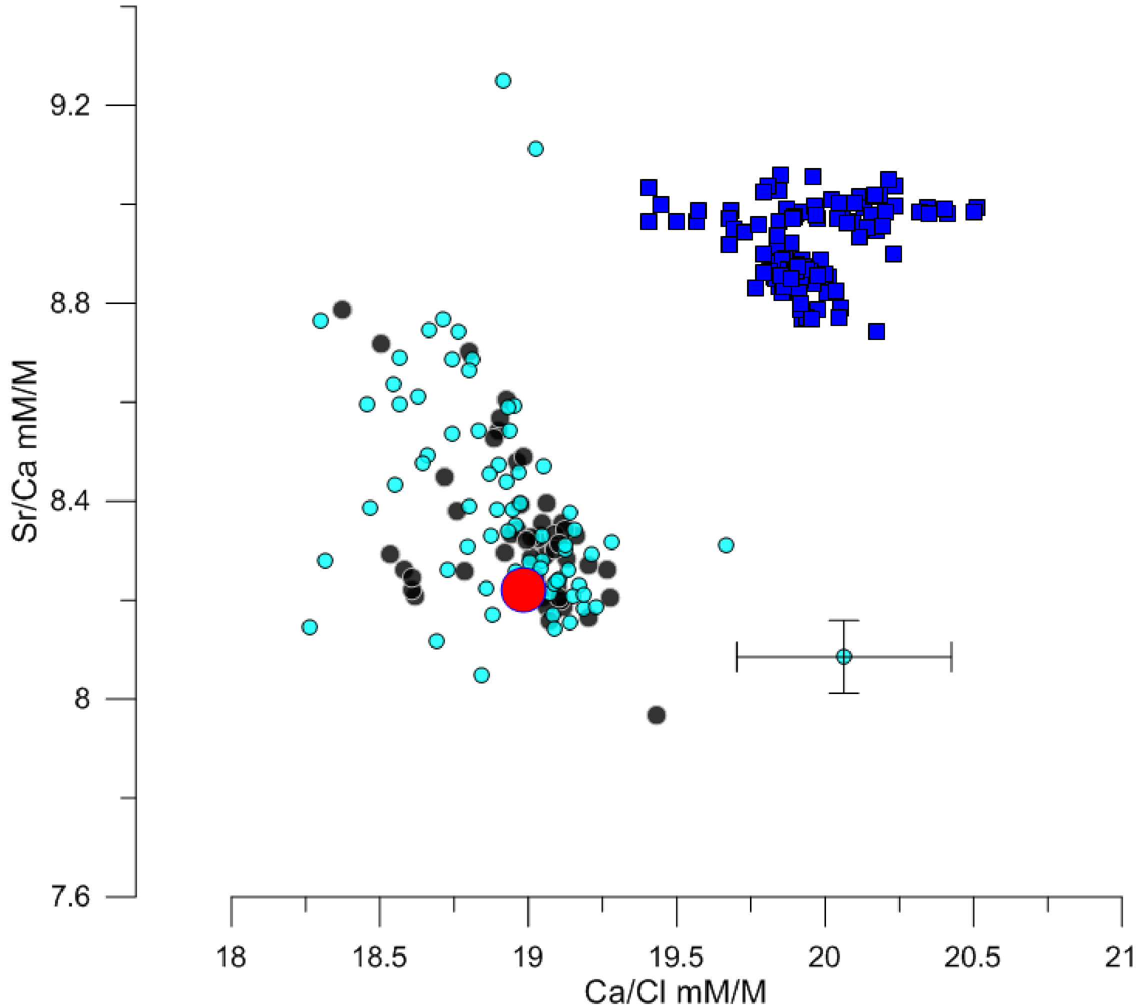

Figure 3-12 Hamelin Pool (black and blue dots) and Great Bahama Bank (blue squares) Ca/Cl ratios compared with Sr/Ca ratios. The error shown is the analytical error of the ICP-OES and can apply to all data points. Great Bahama Bank waters appear to be a more evolved water from that of standard sea water (red circle), however given the error the waters do not appear to be preferring the precipitation or dissolution of any specific carbonate mineral.

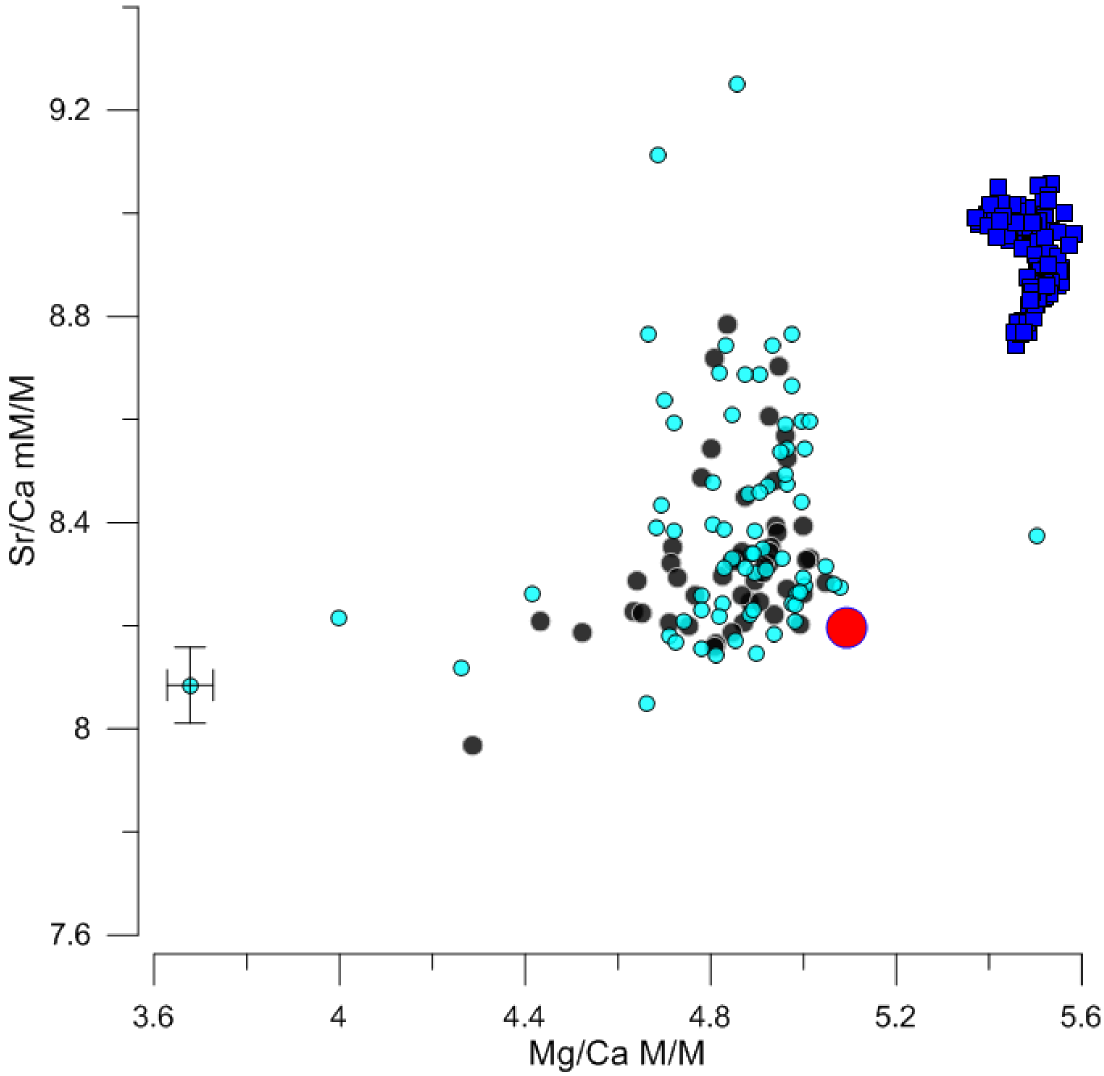

Figure 3-13 Hamelin Pool (black and blue dots) and Great Bahama Bank (blue squares) Mg/Ca ratios compared with Sr/Ca ratios. The error shown is the analytical error of the ICP-OES and can apply to all data points. Great Bahama Bank waters appear to be a more evolved water from that of standard sea water (red circle), however given the error the waters do not appear to be preferring the precipitation or dissolution of any specific carbonate mineral.

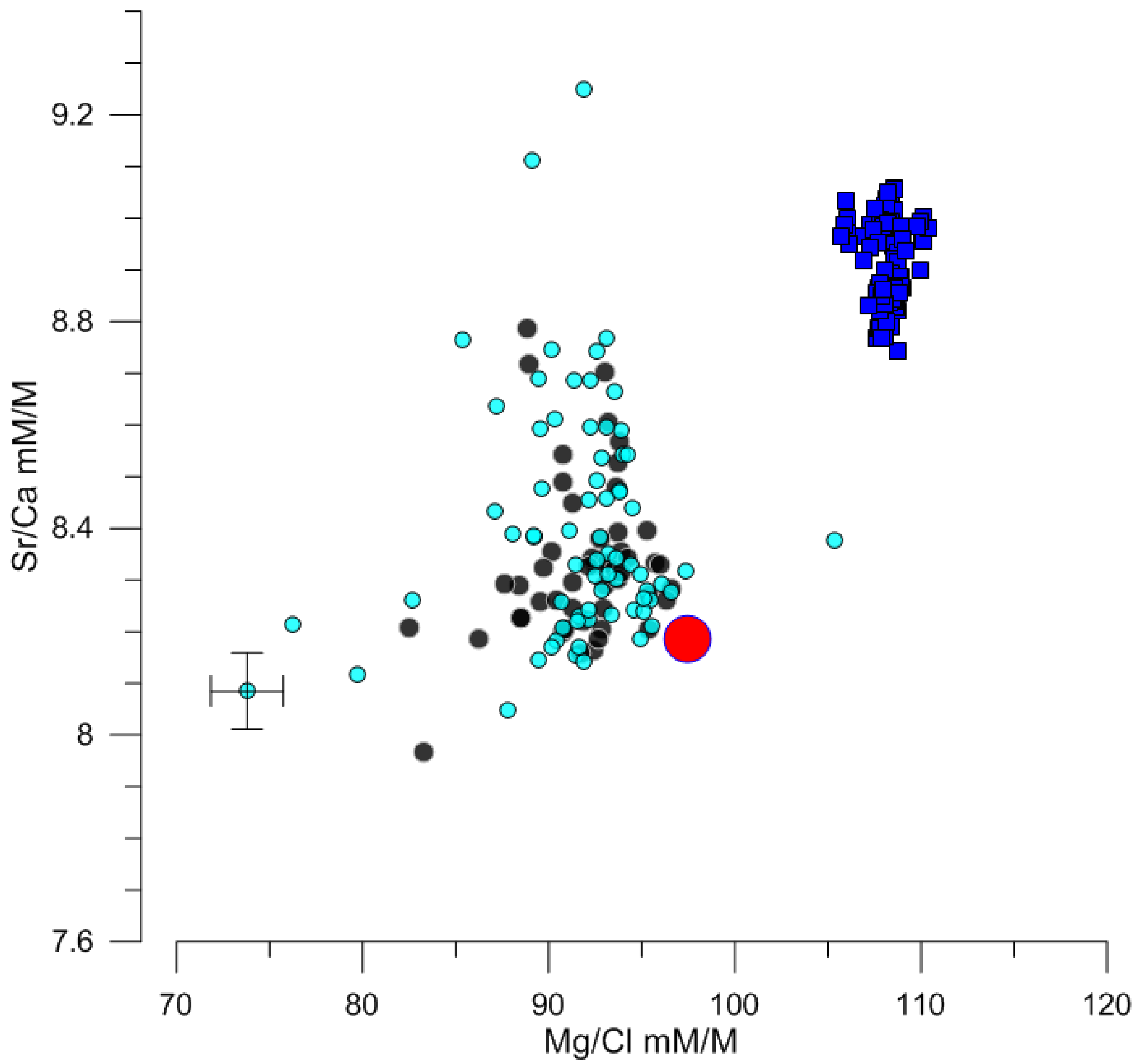

Figure 3-14 Hamelin Pool (black and blue dots) and Great Bahama Bank (blue squares) Mg/Cl ratios compared with Sr/Ca ratios. The error shown is the analytical error of the ICP-OES and can apply to all data points. Great Bahama Bank waters appear to be a more evolved water from that of standard sea water (red circle), however given the error the waters do not appear to be preferring the precipitation or dissolution of any specific carbonate mineral.

Strontium and Calcium

Based on the geographical division of Sr, Ca, Mg, Cl ratios, the southern portion of the pool has a higher Sr/Ca ratio when compared to the Northern and Central units (Table 3-1). This is likely due to the precipitation of LMC rather than HMC considering that there are no differences in the Mg/Ca ratios, but a significant increase in the Sr/Ca ratios of the waters (Figure 3-8, 3-9 and 3-10). This would suggest that water in the southern portion of the pool becomes trapped and experiences a longer residence time. This scenario is also supported in the salinity and stable isotopic value results which suggest that the residence time of water in the southern portion of the pool is higher. If the southern portion of the pool had another major source of input, such as water ground water recharge, the input is not recognized in the minor element concentrations.

Dolomite

When investigating Sr^{2+} and Mg^{2+} compared to Ca^{2+} there is no evidence for dolomitization as the concentrations of Mg^{2+} show no major shifts from the initial waters. Increases in the Ca^{2+}/Cl^{-} ratio of fluids can arise from the dissolution of HMC, aragonite or dolomitization. If there was dissolution or precipitation of dolomite the Mg^{2+} ratios would be dramatically shifted from the initial waters as dolomite incorporates Ca^{2+} to Mg^{2+} at nearly and one to one ratio.

3.6 ***Chapter Summary Water Chemistry, Major, Minor, Trace Elements and Saturation States Summary***

The trace metal analysis of Hamelin Pool waters shows that basinal pool waters are modified seawaters, specifically as it pertains to carbonate reactions, with nearly double the amounts of Sr, Ca, Mg and Cl in solution. Although the waters of Hamelin Pool are over saturated with respect to aragonite and HMC (and LMC), the values are not dissimilar from modern seawater. The Sr/Ca ratios suggest that the waters in the southern portion of Hamelin Pool have been modified further after entering the pool during the precipitation calcite. The longer residence time of the water in the southern portion of HP leads to an increase in the Sr/Ca ratios reflecting the precipitation of LMC. These results fit well with data from the stable isotopes of water and salinity trends found in Chapter 2 and suggest there is no major input of water directly into the southern portion of Hamelin Pool.

Chapter 4: **Sediment Description, Distribution and Geochemical Signatures**

4.1 *Introduction to Sediment Geochemistry*

The sedimentary environment of Hamelin Pool has been described by Logan and Cebulski 1970. The Pool is dominated by carbonate sediments produced by marine organisms presently found in the pool with the distribution being controlled by the environment and energy regime. In this chapter I will focused on basinal sediments and their chemical properties as they relate to water chemistry.

4.2 *Methods*

Sediment Collection: Between 2012 and 2014, nearly 400 sediment samples were collected around the margin and basin of Hamelin Pool. These samples are considered to be "grab" samples as they were collected by machine (Ponar) or by hand at the water sediment boundary. The samples were then split, one half rinsed with fresh water, the other half bleached to remove organics, then left to dry for several hours before being packaged.

Size Fractions: The sediment size fractions were determined by standard laboratory sieving methods using standard sieves, sizes phi (ϕ) $x>4$ to $x<-1$ in whole number intervals. A sediment fraction was weighed, and then poured through the series of sieves in decreasing aperture. The sieves were then thoroughly shaken (30 minutes) in an automated agitator. Each subsequent size fraction was then weighed, and a percent size fraction calculated. The data measured from sieving was entered into *GRADISTAT v 8,* a grain size analysis tool for classifying sedimentary environments, developed by Blott and Pye (Blott and Pye, 2001).

<u>Mineralogy:</u> Bulk and individual components of selected sediment samples were homogenized and prepared for X-Ray powder Diffraction (XRD) Analysis. Using a Panalytical Xpert Pro the mineralogical composition of carbonate end-members was verified prior to analysis with a set of 5 standards which vary from 0 to 60% respectively (Swart et al., 2003). Each mixture was homogenized in a ball mill for a period of 10min. If it is assumed that the sediment is composed of only carbonate minerals (end members): dolomite (D), LMC, HMC and aragonite(A), then Equation 1 is valid and can be used to quantify mineralogical composition and concentration (Swart et al., 2003).

$$D+A+LMC+HMC=1 \qquad \text{Eqt 4.1}$$

The peak areas for each relevant mineral were determined by scanning a smear mount of the sample between 24° and 32°2ϴ (CuKα radiation). The ratio of the peak areas for the appropriate peaks for aragonite, HMC, and dolomite were determined relative to LMC + HMC and correlated to the same ratio in the weighed components of each standard.

Inorganics: The $\delta^{13}C$ and $\delta^{18}O$ values of the carbonates were analyzed by dissolution in phosphoric acid using the common acid bath method. The CO_2 produced by the reaction of phosphoric acid and carbonate matter were then analyzed on a Finnigan MAT 251 (Thermo Fisher Scientific, Bermen, Germany) (Swart et al., 1991). In each run of 30, there were 24 unknown samples, as well as six standards four of which are measured at the start and two at the end. Data were then corrected for any fractionation in the reference gas during the run and for the usual isobaric interfaces modified for a triple collector mass spectrometer. Data are reported relative to the Vienna Pee Dee Belemnite (VPDB) scale, defined for carbonates by $\delta^{13}C$ values of NBS-19‰ versus Pee Dee Belemnite (PDB). The error for these analyses is <0.01‰ as indicated by replicate analyses of internal standards.

Organics: Sedimentary organic matter co-occuring with grains was analyzed following Oehlert and Swart 2014. Organic matter was separated via dissolution in 10% HCl acid overnight, followed by vacuum filtration onto glass microfiber filters (Whatman GF/C). The insoluble residue (IR) on the filter was allowed to dry for at least 48 h, or until a constant dry weight was achieved. The weights of the insoluble material were quantified by subtracting the weight of the empty filter from the weight of the dried insoluble material and filter after filtration. Samples of the insoluble material were scraped off of the filters, weighed and packed into tin capsules and loaded into a Costech ECS 4010 (Costech Analytical Technologies Inc., Valencia, CA, USA), where they were combusted. The resulting CO_2 gas was then delivered to a to a continuous flow isotope-ratio mass spectrometer (Delta V Advantage, Thermo Fisher Scientific). For every run of

36 samples, 12 internal standards were analyzed to calibrate the machine and to assess the precision of the measurements. An analytic blank as well as 6 internal standards preceded the first sample analysis, and two standards were run for every 10 samples analyzed. The reproducibility of δ^{13}C values is ±0.1‰ as indicated by the s.d. of replicate analyzes of internal standards of glycine (n=54, δ^{13}C value=−31.8‰ VPDB).
All δ^{13}Corg data are reported relative to the VPDB scale, defined for organic carbon as the δ^{13}C value of graphite (USGS24) =−16.05‰ versus VPDB. To calculate weight percent carbon in the IR, a calibration line was established that related the peak area measured by the Delta V Advantage (Thermo Fisher Scientific) to the known weight of carbon in the internal standard, glycine. The weights of the standards were chosen to bracket the expected range of organic carbon in the samples. The s.d. of these analyses is 0.4% based upon repeated analyses of glycine (n=54). Delta V Advantage peak area measurements for each sample was transformed to mg of organic carbon in the insoluble residue using the equation of the calibration line. Organic carbon concentration in the insoluble residue in mg was converted to TOC by the following equation:TOC=((Org C in IR (mg) × total IR weight (mg))/initial weight of the sediment (mg)) × 100 (Oehlert and Swart, 2014).

4.3 ***Hamelin Pool Sediments Results***

Sediment Sizes

Below (Figure 4-1) shows a generalization of Hamelin Pool sediment size fractions, The sieving results have been averaged in order to measure the frequency of the size fractions around the pool area. The results from the individual samples can be found in appendix (Tables 7-11, 7-12, 7-13, 7-14 and 7-15).

Hamelin Pool basinal sediments, in general, fell between 63µm to 2mm (4 to -1 phi or coarse silt to granule sized). There was little mud collected by the grab samples; also most of the sediments that measured to be less than -1 phi or greater 2mm were the made of the bivalve *Fragum Erugatum*. The Folk and Ward mean results describes the pool as being predominantly very coarse sand (53%), followed by very fine gravel (20%), coarse sand (14%), medium sand (10%) and finally with fine sand & fine gravel (both at 1%). Nearly all analyzed samples were found to be poorly sorted (85%) with very few moderately sorted samples (19%) and very rare well-sorted samples (2%). Samples showed various skewedness values as well as variable clustering among the mean (kurtosis).

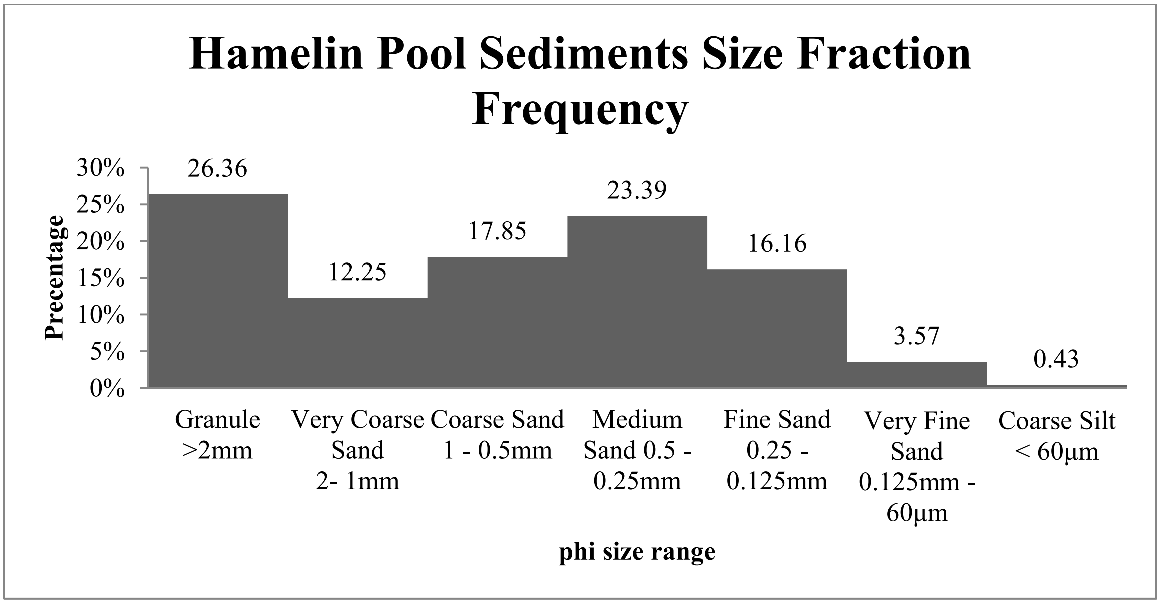

Figure 4-1. Frequency chart of sediment sizes found through Hamelin Pool. This chart is a generalization of the entire pool, done by averaging the sieved results.

Mineralogy

The carbonate mineralogy of the sediments samples consisted of aragonite and HMC with the HMC reaching as high as 58% in some areas, Tables 7-16, 7-17, 7-18 and 7-19 (Appendix). The highest percentage of aragonite was found along the coast notably on the southeast portion, with intermediate ranges in the basin, and the lowest amount of aragonite and therefore the highest amount of HMC was found in the north near the sill (Figure 4-2).

Inorganic $\delta^{13}C$ & $\delta^{18}O$ values

The $\delta^{13}C$ and $\delta^{18}O$ values measured on the inorganic components of the sediments averaged from +4.68‰ and +3.19‰ and varied from +6.18 to +2.83‰ and +4.07 to +2.17‰ respectively, with a trend for values to increase from north toward the south (Figure 4-3).

Insoluble Residue values

The insoluble residue collected from Hamelin Pool sediments, Figure 4-4, consisted of both organic insoluble residue as well as silicate eolian debris which erode from the western Peron Peninsula. The insoluble fraction ranged from ~1% to upwards of 50% with the larger fractions having more siliciclastic debris and being the most dominant on the western side of the pool.

Carbon and Nitrogen weight values (C:N ratios)

Organic carbon matter ranged from <0.01 to 3.54%wt with an average of 0.33%, and organic nitrogen matter ranging from 0.04 to 0.42%wt with an average value of 0.04%. The C:N ratios from the Hamelin Pool organic sediments ranged from a 0.00 to 24.67 with an average of 9.72 (Figure 4-6). Higher values are found sporadically around the margin of both the lower eastern and western sides of Hamelin Pool.

Organic $\delta^{13}C$ & $\delta^{15}N$ values

The $\delta^{15}N$ values of organic matter ranged from -4.28 to +9.06‰ (Figure 4-7) with an average value of 0.77‰. The $\delta^{13}C$ values of the organic matter ranged from -21.88 to -8.59‰ (Figure 4-7) with an average value of -15.38‰. Neither contour map shows any reasonable trending, but rather patchy distributions of heightened areas.

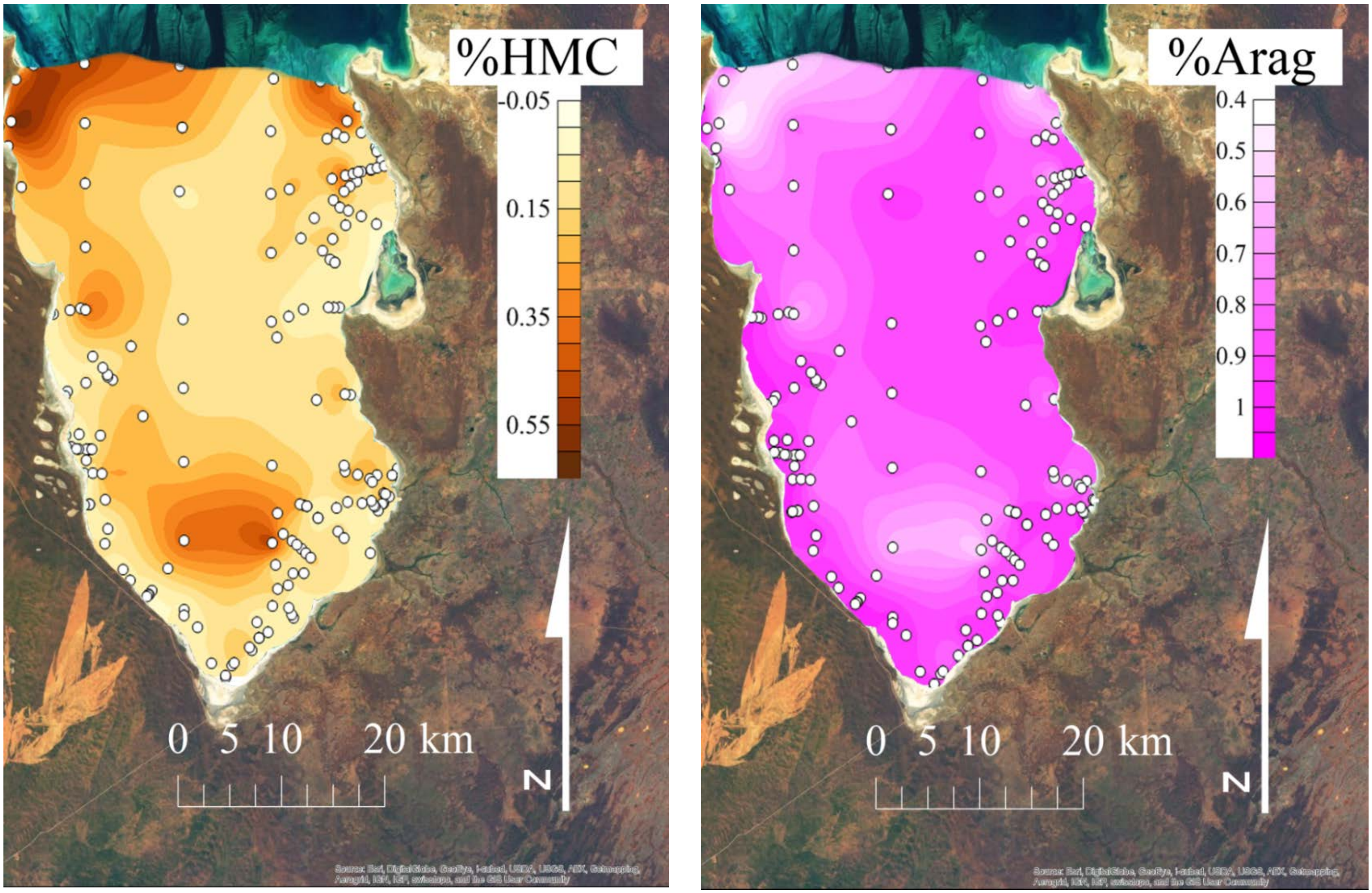

Figure 4-2. Mineralogy of bulk sediments collected from Hamelin Pool. Left in brown shows the varying amount of High Mg Calcite (HMC). Right in pink shows the percent aragonite measured. The basinal sediments were predominantly aragonite. There is no strong spatial relationship in the distribution of HMC to Aragonite.

Figure 4-3. Inorganic sediment $\delta^{13}C$ and $\delta^{18}O$ values, Left shows the $\delta^{13}C$ values Right shows $\delta^{18}O$ values. Both figures show a strong spatial relationship of increasing values from north to south, which is consistent with higher residence time in the southern area of Hamelin Pool.

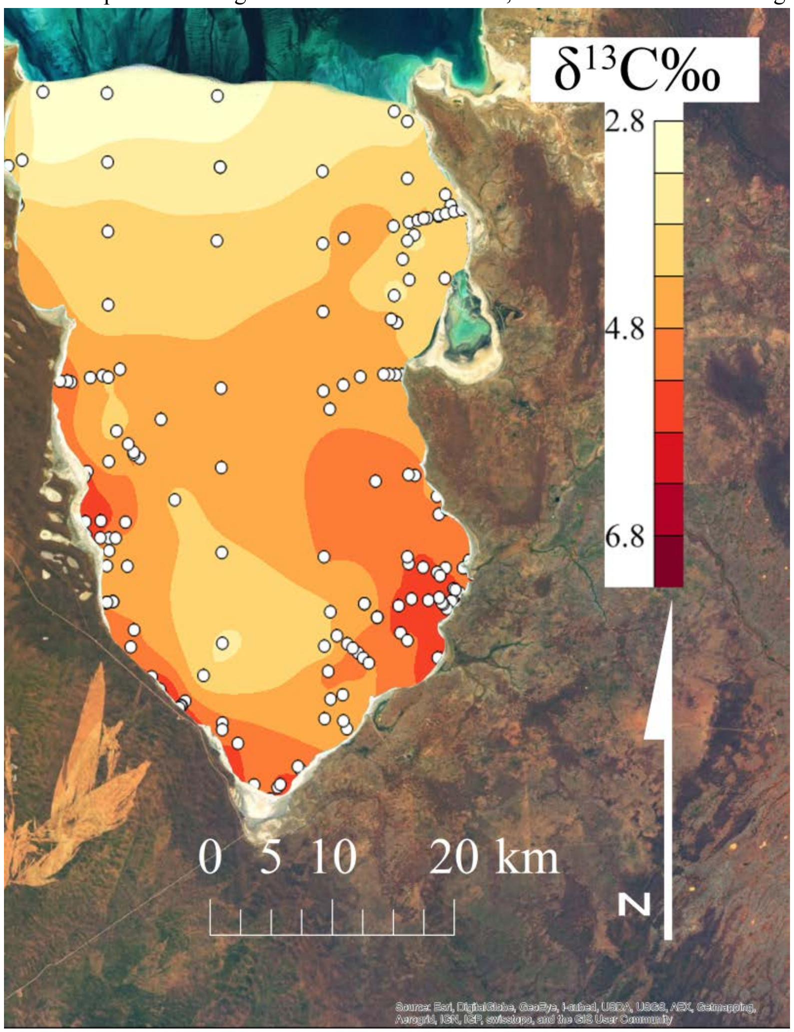

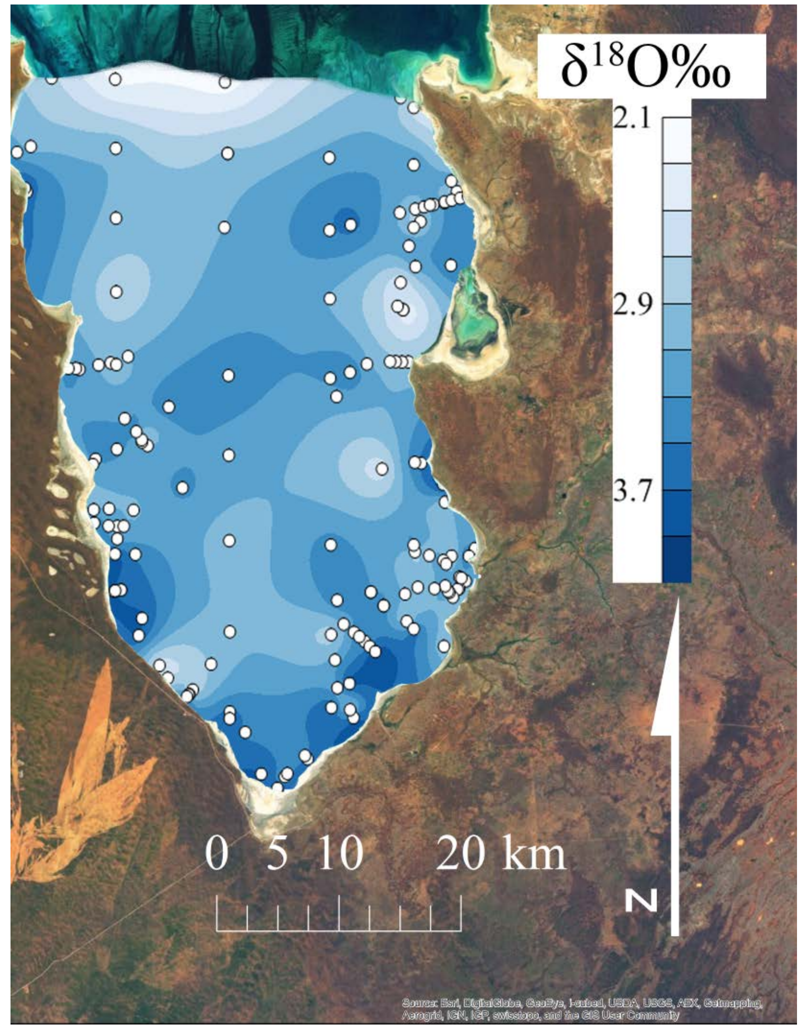

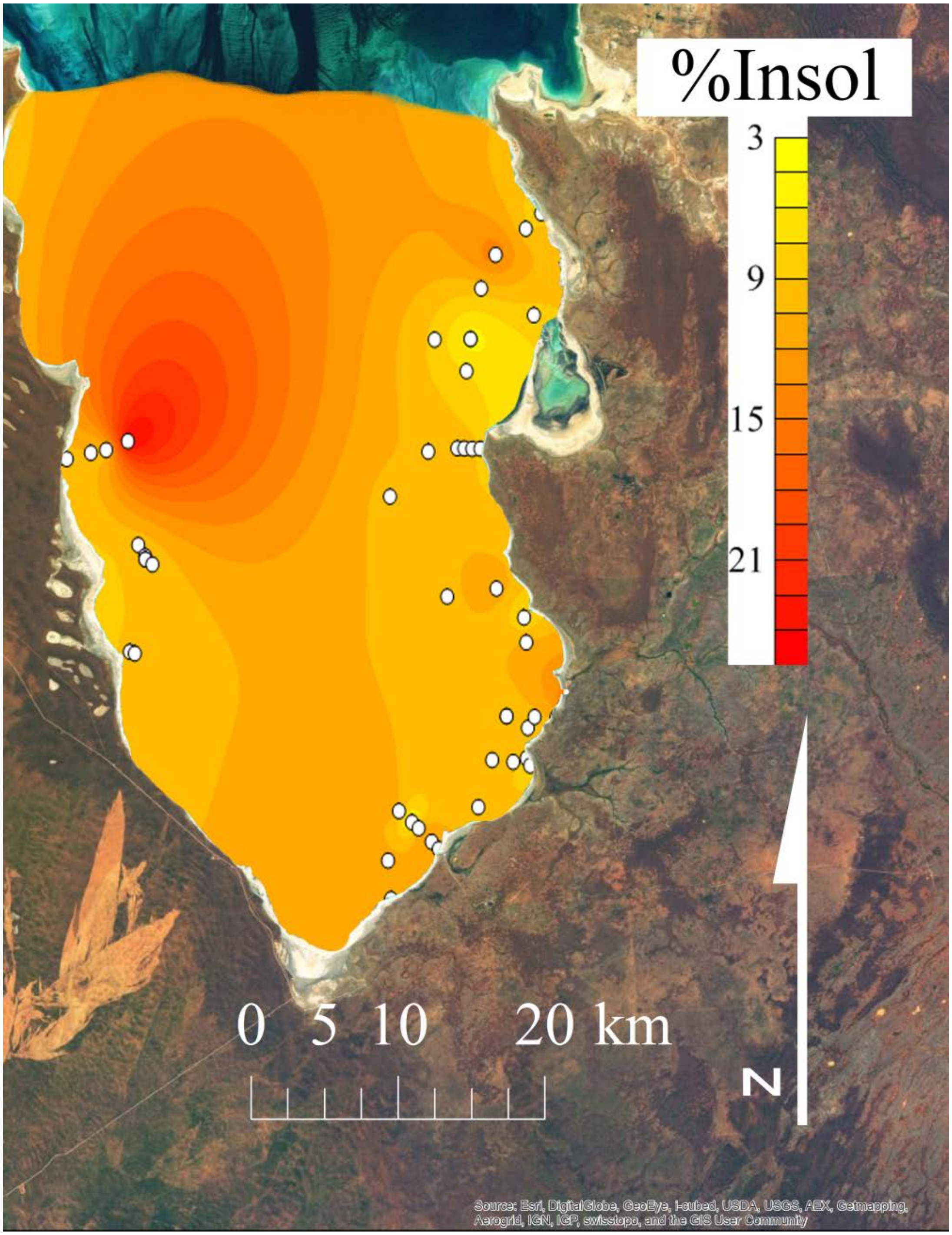

Figure 4-4 Shows the distribution of insoluble fraction from the sediments collected during the 2014 field season at Hamelin Pool, WA. These results are a combination of both insoluble silicate debris eroding of the *Peron Peninsula* as well as the insoluble organic carbon and nitrogen residue. This figure show fewer data points as only unbleached samples are appropriate for organic content analysis, many sample collected in the field were bleached prior to this analysis and were therefore not included.

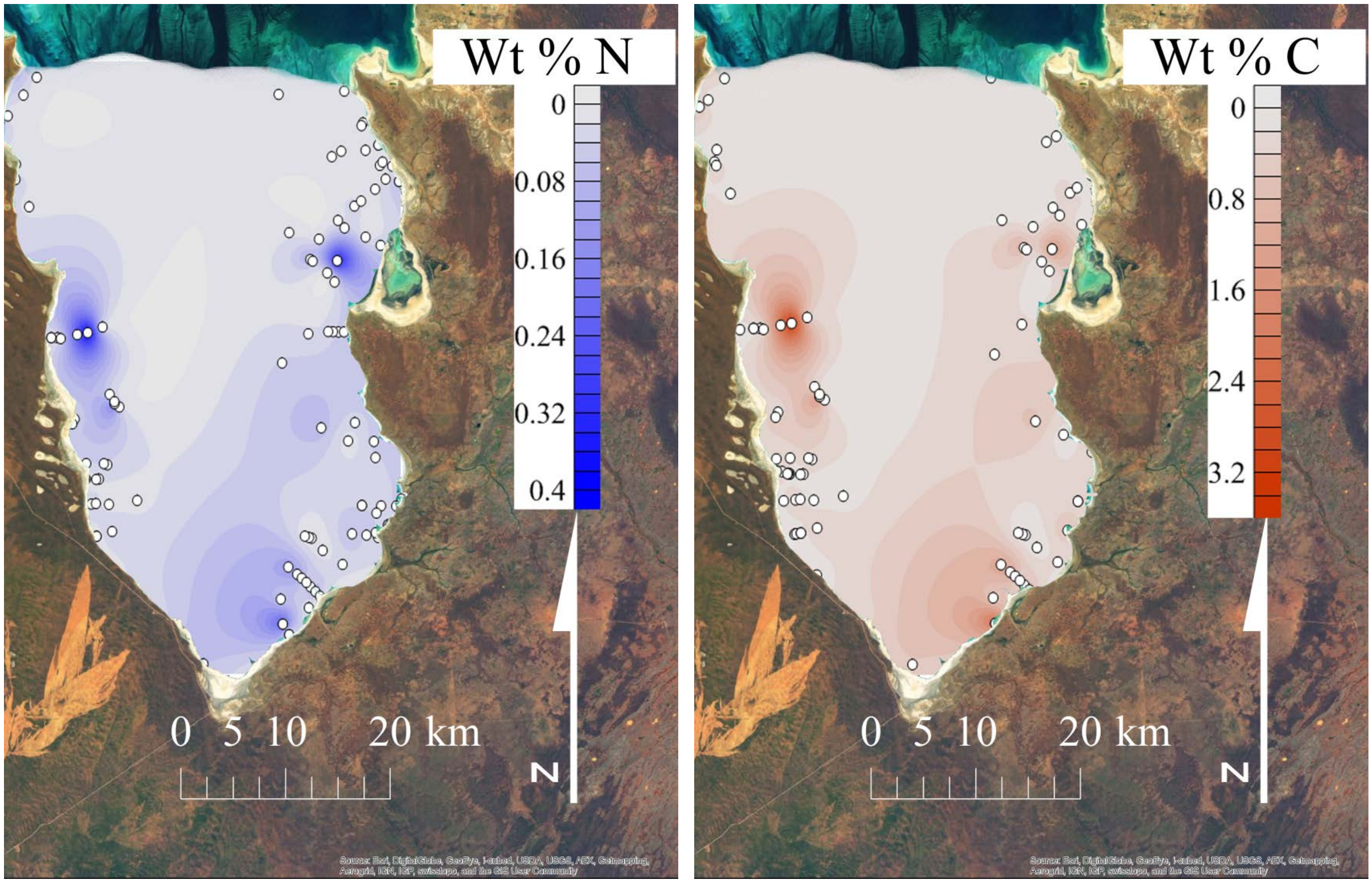

Figure 4-5 Shows the percent nitrogen (Left) and carbon (Right) from the sediments collected during the 2014 field season at Hamelin Pool, WA. The percent weights of carbon and nitrogen are co-occurring, hence both figures appearing nearly identical. There are no strong spatial relationships, but some 'hot spots' of elevated points.

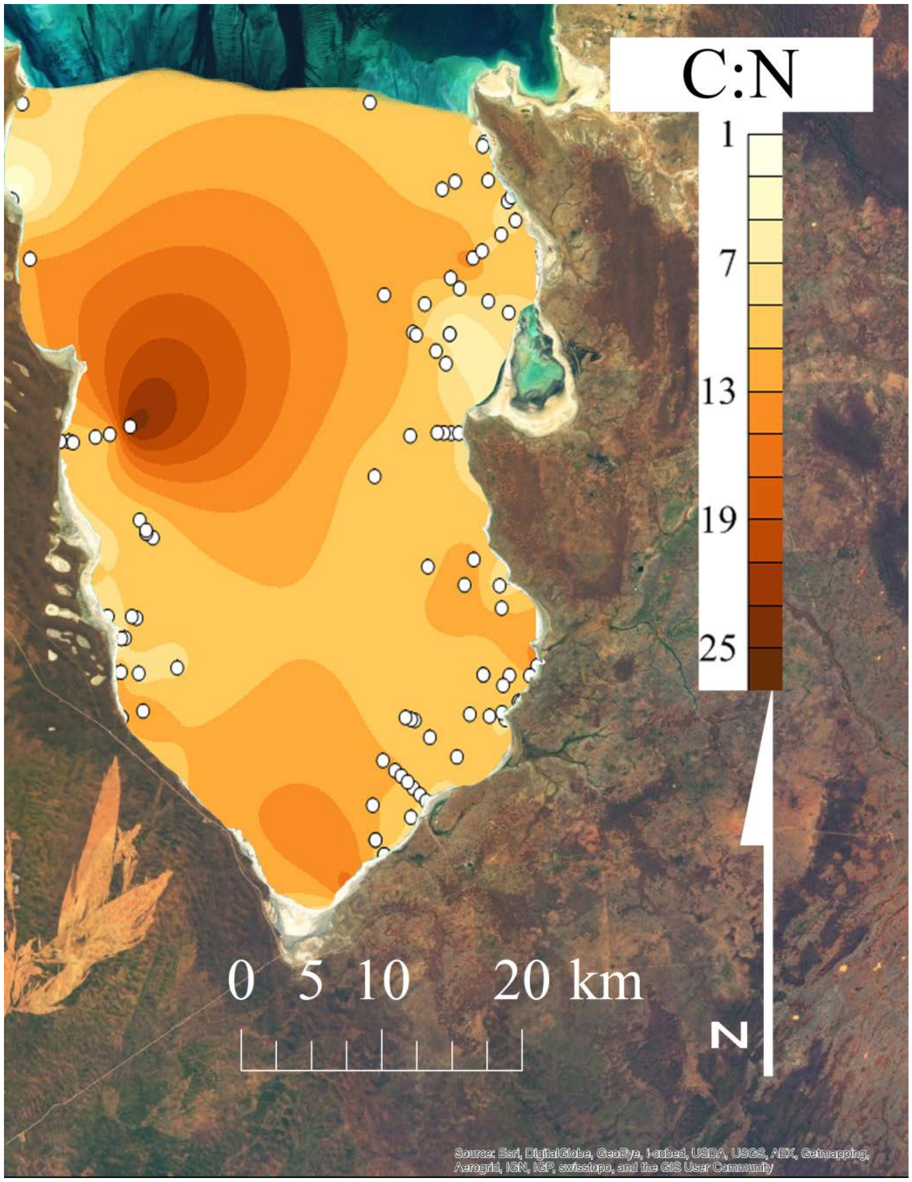

Figure 4-6 Shows the distribution atomic C:N ratios of the sediments collected during the 2014 Hamelin Pool field season. The C:N ratios are consistent with the weight percent and show no strong spatial relationship within the basin.

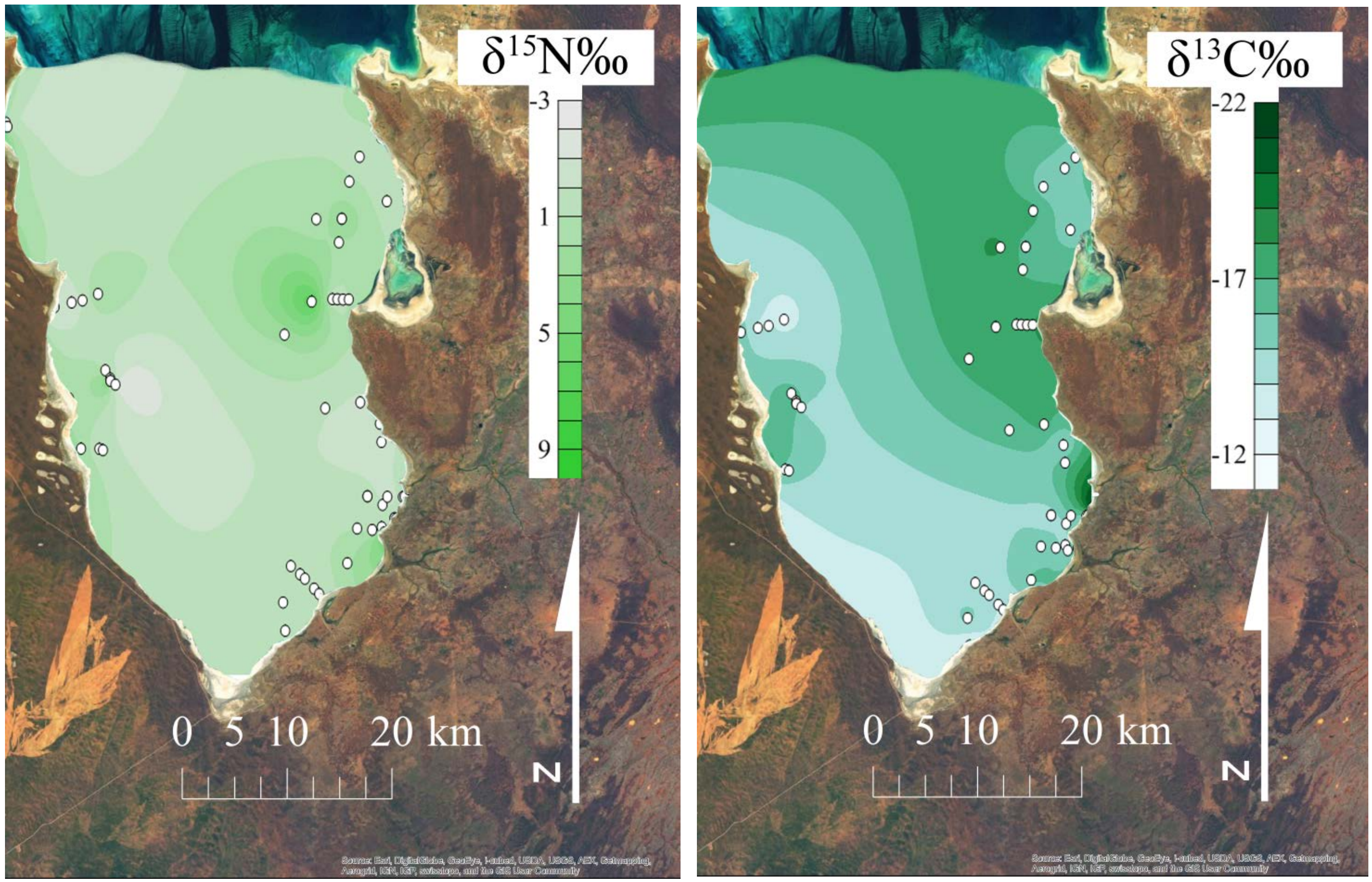

Figure 4-7 Left) The distribution of the organic $\delta^{15}N$ values Right) The $\delta^{13}C$ values from the sediments collected during the 2014 field season at Hamelin Pool, WA. The $\delta^{13}C$ values show a trending of more positive values approaching the south, this enrichment is consistent with higher residence time of water. The nitrogen values show no spatial relationship within the basin.

4.4 ***Discussion***

Sediment Size Fractions

Hamelin Pool is a carbonate dominated sedimentary environment with a salinity gradient controlling the distribution of facies, with the most dramatic imposition being the restrictive nature of the Faure Sill (Logan and Cebulski, 1970). The sediments in the majority of the pool are skeletal and micritic grains that are less then 2mm (-1 phi), with little mud. They are classified as grainstones, in Dunham classification (Dunham, 1962). There are however, some areas that are dominated by the bivalve *Fragum eragatum* and are better classified, as rudstones patches, as illustrated in Suosaari (2015).

Present in the greater then 2mm (phi<-1 interval, Table 7-1) is *Fragum eragatum*, a small bivalve is which dominates the sublittoral platform of Hamelin Pool and is the most typical grain type found, both articulated and inarticulate. *Fragum eragatum* is not only abundant in Hamelin Pool, but also within the greater Shark Bay region and is the species that comprises the majority of the sediment on Shell Beach (Figure 1-1); Fragum shells may also have encrusted serpulids tubes on their surfaces. In addition, present in this size class, are clumps of precipitate/micrite, which appear through the size fractions in various dimensions. Last, the benthic foraminifera *Marginopora vertebralis* occurs, in both isolated flat looking discs with thin centers, as well as twinning plates.

In the next interval 2 to 1 mm(-1> phi >0, Table 7-1) *Marginopora vertebralis* are present albiet in a smaller life stage. Broken tube worms encrustations are also present although this occurance may be due to abrasion caused by sieving. Newly found are gastropods, as well the stalks of *Acetabularia peniculus* and *A. calyculus* which tend to grow in shallow waters and attach themselves to shells and rock debris (Logan et al., 1970). Both species are present in the pool but the caylax, cup or bulbous top portions, are readily disintegrated leaving only their stalks which are difficult to distinguish.

Table 7-2 (Appendix), displays the sediment composition for size fractions 1mm to 0.5mm (0>phi>1) and 0.5mm to 0.25mm (1>phi>2). Here the players change as the variety of foraminifera appear, *Marginopora vertebralis*, as well as *Penerpolis planatus* and *Spirolina sp.,*these are most likely the most mature speicmens as they have not been found in any larger size fraction, and juveniles can be seen in the small mixed fractions.

Table 7-3(Appendix), shows the remaining fractions 0.25mm to 0.125mm (2>phi>3) and 0.125 to 60µm (3>phi>4), <60µm (4< phi) has been ommited since the photos have poor resolution and for some samples this size fraction had an insignificant (less than 1%) contribution to the bulk. These fractions are made up of mostly debris from the larger fractions as well as juvenile stages of formainifera, bivalves and gastropods.

Analysis by Province

Hamelin Pool has been separated into 7 major provinces based on the distinct geographical characteristic of stromatolite morphologies and associated lithofacies (Suosaari et al., 2016a)(Figure 4-8). As such, the sediments collected were divided into their respective provinces. Figures 4-9, 4-10, 4-11 and 4-12 show the frequency charts of Folk and Ward Descriptions ($\bar{x}$), Sorting (σ), Skewness (Sk_1), and Kurtosis (K_G); Hamelin Pool basinal sediments were grouped into their stromatolitic provinces. The Southern tip of Hamelin Pool, the Nilemah province grain size is coarse to fine sand, the provinces north of Nilemah; Booldah, Flagpole, Spaven & Carbla grain sizes group together as coarse sand and finally the most Northern provinces, Nanga and Hutchinson range from being very coarse sand to fine sand. This variation in grain size may be attributed to the position of Faure Sill, which feeds well-sorted sediment into the more northern providences; this can be seen in the sorting.

Sorting of carbonate sediments is an indication of the size of the organisms living in the environment as well as calcified hardparts, with some indication of energy, rate and duration of depositional environmental conditions (Tucker, 2003). Sorting in carbonate sediments can be affected by the reworking of material after deposition as in bioturbation, and activity of other organisms (Tucker, 2003). Carbonate sediment sorting is also correlated with porosity; poorly sorted sediments tend to be less porous then well-sorted sediments (Tucker, 2003). Hamelin Pool sediments are for the most part cohesive and not well sorted.

Figure 4-8. Morphological stromatolitic distribution provinces, each province has a characteristic morphological feature. The variance in size, shape and width is likely driven by the physical and chemical environment along the margin of the coastline.

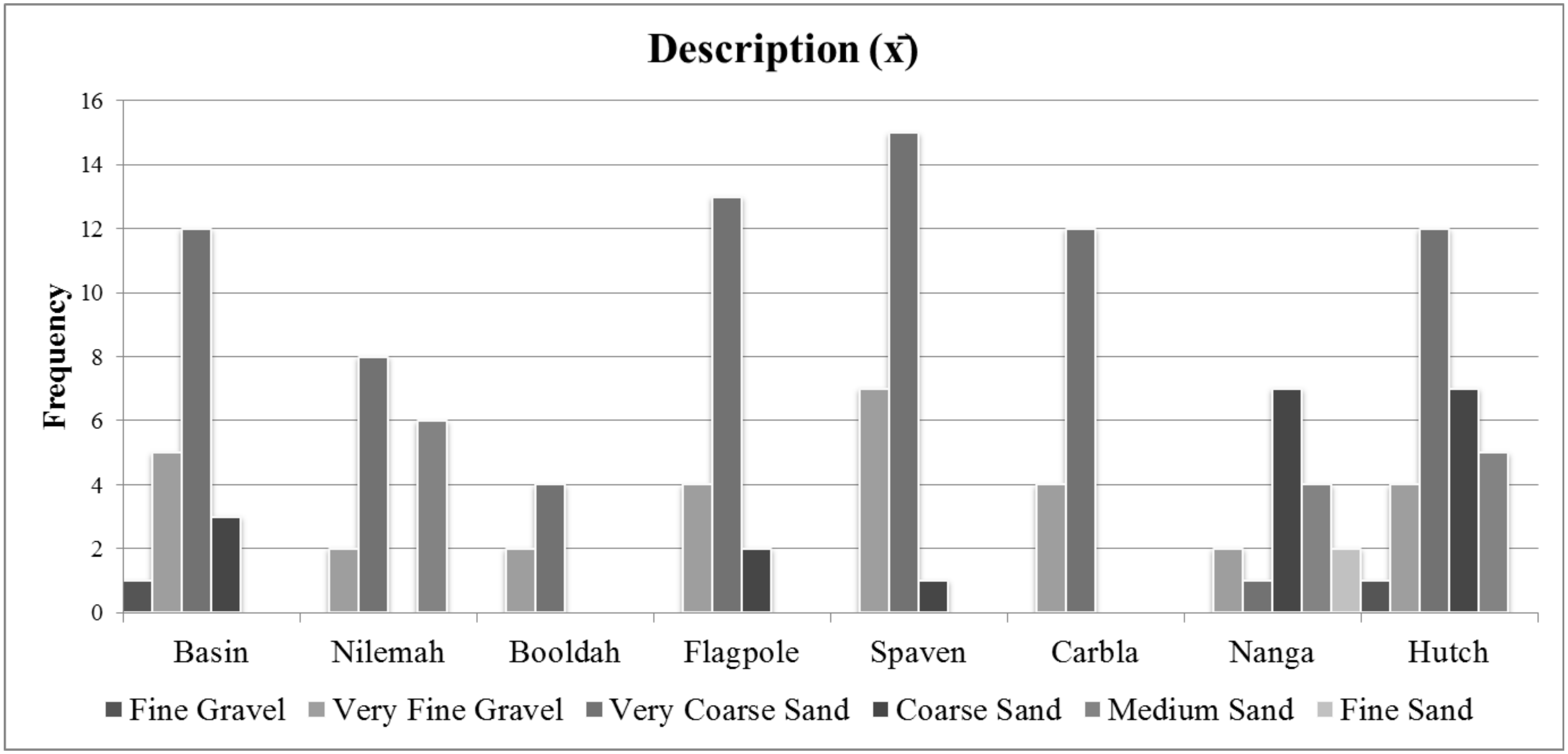

Figure 4-9 Frequency charts showing the Folk and Ward Description ($\bar{x}$) for Hamelin Pool sediments by stromatolitic provinces.

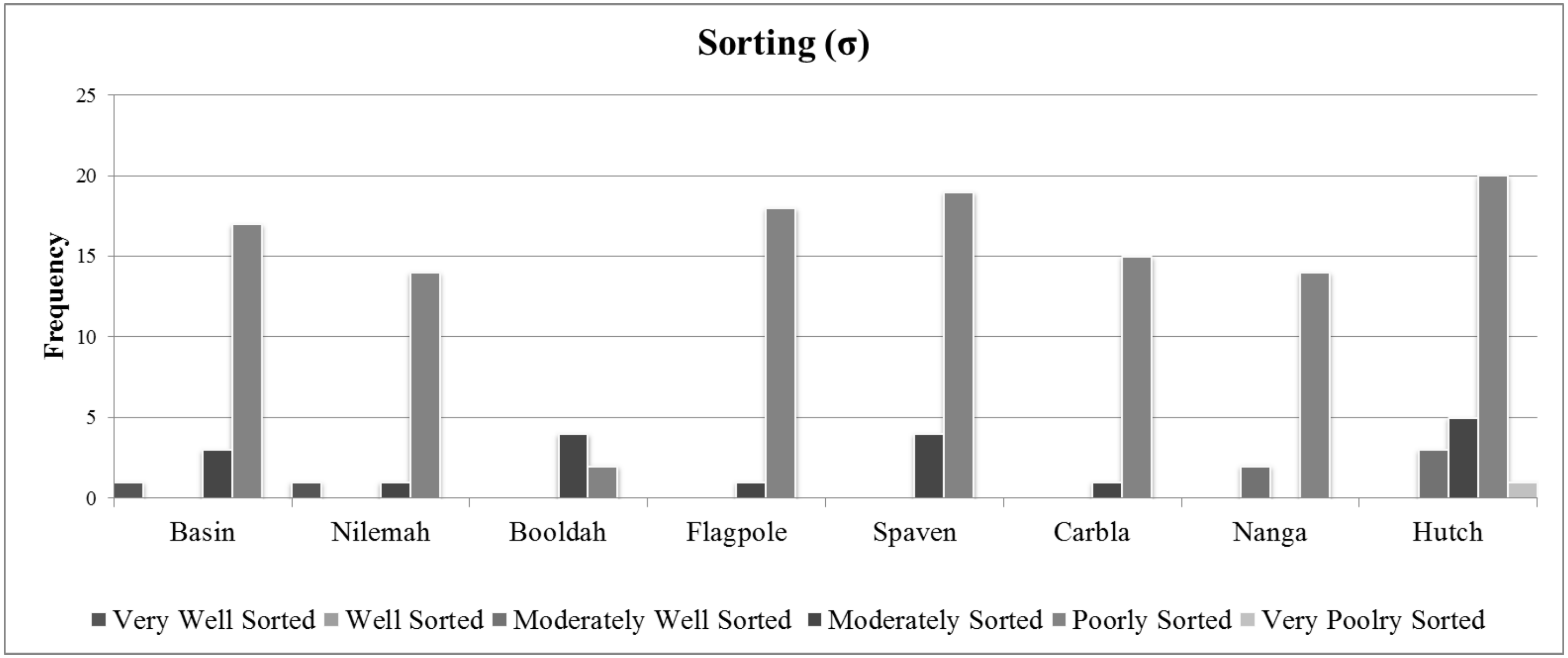

Figure 4-10 Frequency charts showing the Folk and Ward Sorting (σ) for Hamelin Pool sediments by stromatolitic provinces.

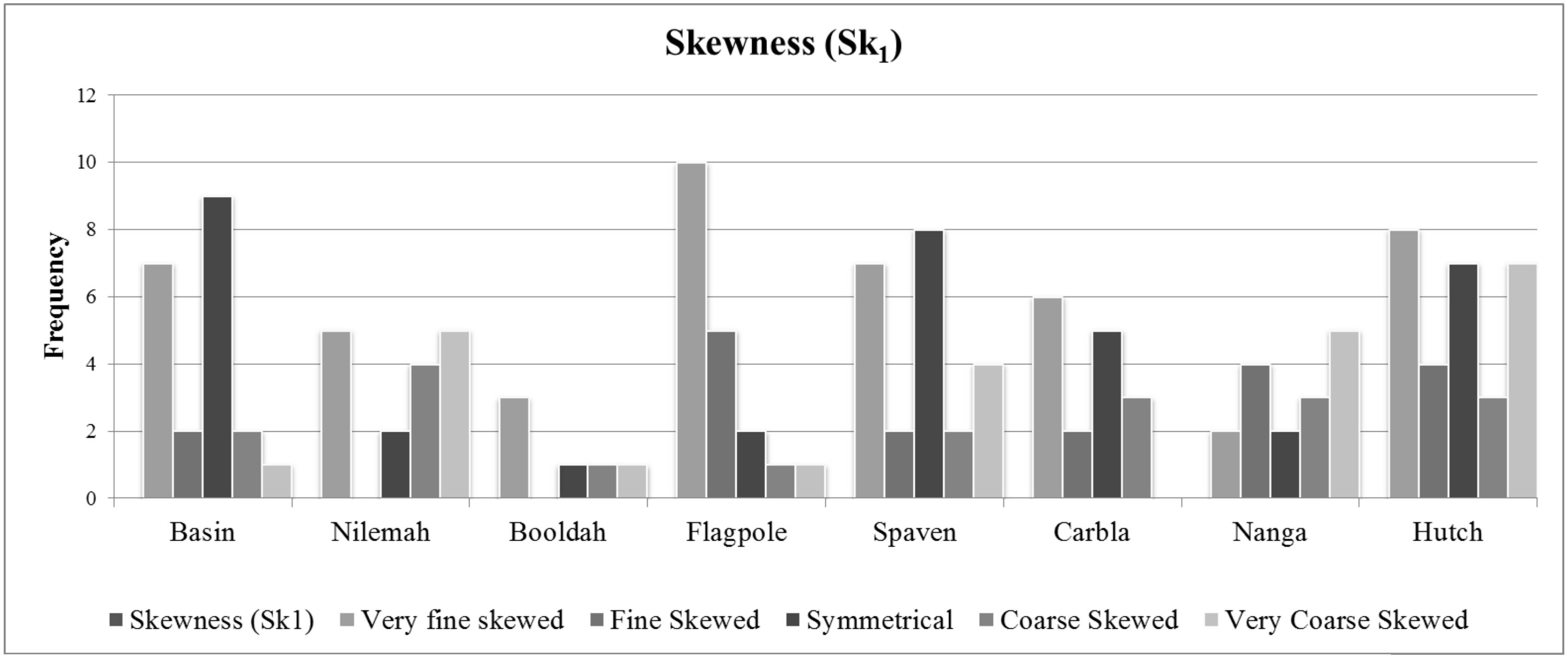

Figure 4-11 Frequency charts showing the Folk and Ward Skewness(Sk_1) for the Hamelin Pool by stromatolitic provinces.

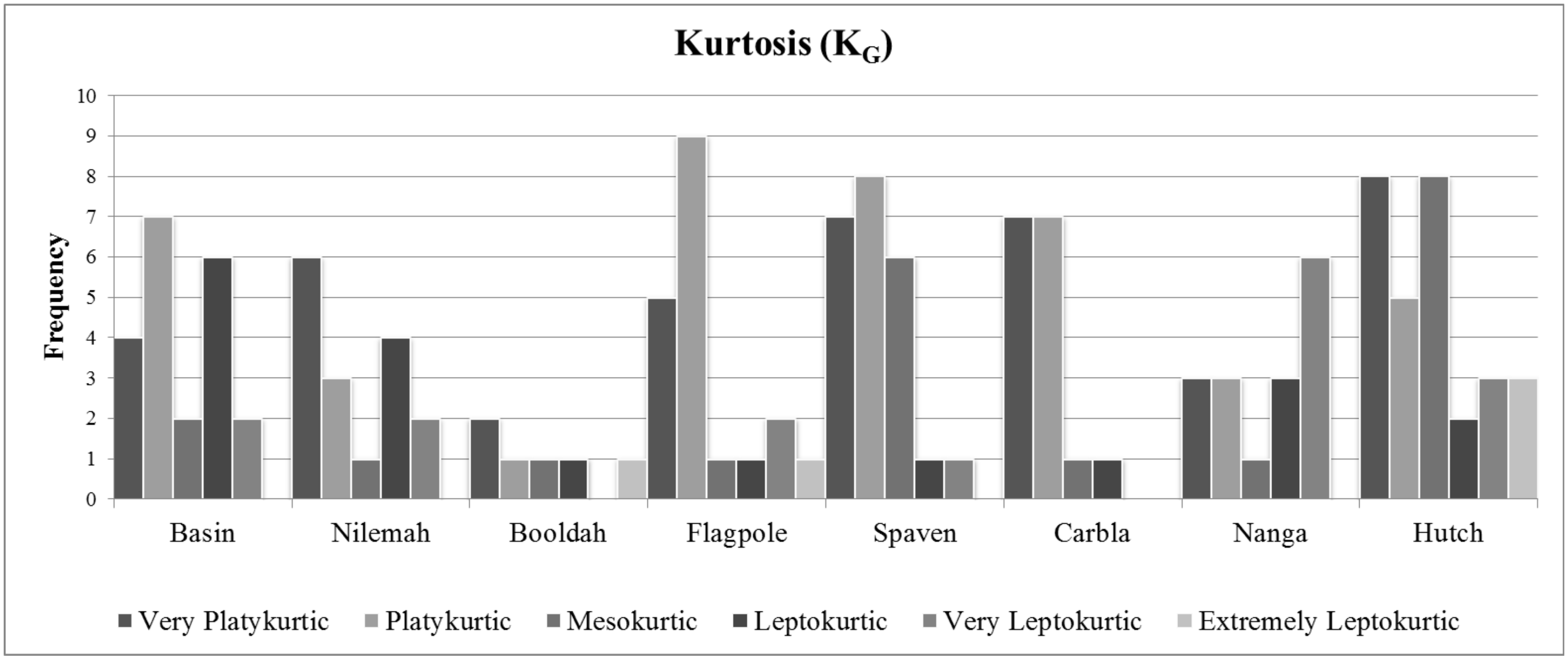

Figure 4-12 Frequency charts showing the Folk and Ward Kurtosis (K_G) for the Hamelin Pool by stromatolitic provinces.

Inorganic $\delta^{13}C$ and $\delta^{18}O$ values

Positive $\delta^{13}C$ values of the inorganic components in the sediments reflect a change in the $\delta^{13}C$ value of the DIC in water, which is caused by utilization $^{12}CO_2$ by photosynthetic bacteria, algae, macro algae etc. living in a water body. This process is particularly evident where residence times are high. The contour map of the $\delta^{13}C$ values (Figure 4-3) in Hamelin Pool show increased values in the mid and southern regions, a pattern similar to the water isotopic values, supporting the previous conclusion (Chapter 3) of longer residence times in the southern portion of the basin. The average $\delta^{13}C$ values of unaltered marine carbonates is close to 0‰ (VPDB) and typically range from -2‰ to +2‰ (Sharp, 2007). The $\delta^{13}C$ values of carbonates in equilibrium with surface waters are about +2 to +4‰. The lowest value seen within the southern portion of the basin is +4‰ and the highest overall just under +6‰. Whilst marine carbonates typically have low $\delta^{13}C$ values close to 0‰, lacustrine carbonates tend to have lower even lower values (-5‰ or less) as they incorporate CO_2 derived from the decay of plant material in soil. Lower values are also associated with vital effects and diagenesis (Sharp, 2007). Therefore, while Hamelin carbonates are forming in a restricted system, they have a marine signature. There is an overall pattern of increasing $\delta^{13}C$ values from north to south supporting the idea that the Faure Sill is a major driver of geochemical signals in the sediments as well as the waters as discussed in Chapter 2. This pattern is also prominent when looking at the $\delta^{18}O$ values of the inorganic fraction of the sediment data contoured, Figure 4-3. The $\delta^{18}O$ values range from 2.17‰ to 4.07‰. Both photosynthesis and evaporation fractionate the dissolved inorganic oxygen in a solution and driving up the $\delta^{18}O$ values of the precipitated carbonates.

<u>Organic Carbon and Nitrogen delta values and C:N ratios</u>

The C:N ratio is a commonly used as tool to understand the origin of organic matter. Marine organic matter, derived from phytoplankton & zooplankton have a C:N ratios ranging close to 16:1 (Redfield Ratio; Rumolo et al., 2011), whereas terrestrial vascular plants have C:N ratios that range >20 (Rumolo et al., 2011). This distinction arises from the absence of cellulose in algae and it abundance in vascular plants (grasses, shrubs, trees, land-rooted plants) (Meyers, 1994). The C:N ratios and $\delta^{13}C$ values of total organic matter retain source signatures which, despite some possible early digenetic modifications, remains intact extended periods of time (Meyers, 1994). Organic matter in a water body can vary from being predominantly algal to being land dominated or in some cases a mixture of both (Meyers and Ishiwatari, 1993).

Biogeochemical processes that effect the DIC and NO_3^- in solution ultimately effect the particulate organic matter(POM) and consequently the organic $\delta^{13}C$ and $\delta^{15}N$ values (Finlay and Kendall, 2007). In Figure 4-13 the $\delta^{15}N$ values show a consist scatter close to zero, these values are diagnostic of nitrogen fixation which tend to cause minimal if any fractionation of ^{15}N to ^{14}N (Swart et al., 2014). Cyanobacteria as well other biological communities fix nitrogen showing that the organic matter is highly affected by microbial communities inside of Hamelin Pool. Excessive amount of evaporation known to correlate with higher amounts of DOM (Cawley et al., 2012), are also known to drive DIC values to be more positive. This effect can only be augmented with higher residence times of restricted water.

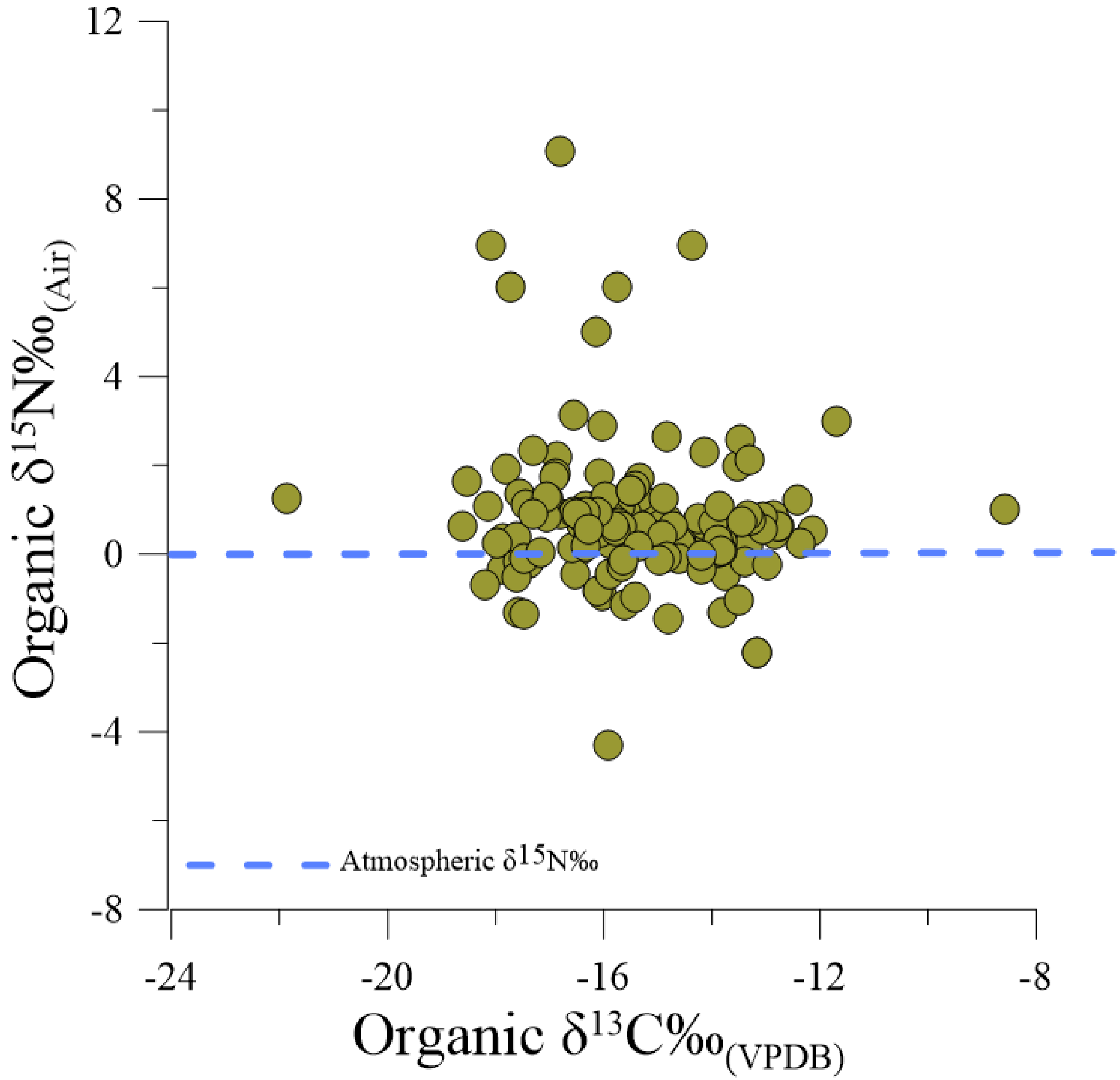

Figure 4-13 Shows the relationship between the organic $\delta^{13}C$ and $\delta^{15}N$ values of sediments collected from the 2014 Hamelin Pool field season.

It is to be expected that the Shark Bay POM contributes to Hamelin Pool POM in some part, as water in Hamelin Pool originates from Shark Bay. The thriving seagrass communities of Shark Bay have a significant contribution to the DOM in Shark Bay (Cawley et al., 2012). Globally seagrasses tend to have $\delta^{13}C$ values ranging from -19.6‰ to -4.8‰ with an average of -10.3‰ (Kennedy et al., 2010). C:N ratios of seagrasses can vary from as low as 7 and as high as 37 (Fourqurean et al., 1992). Shark Bay was found to have an average $\delta^{13}C$ value of -19.3‰ (Cawley et al., 2012) which is on the lower end of $\delta^{13}C$ values found in Hamelin Pool. C:N ratios in Western Australia, which are slightly higher than the C:N ratios found in Hamelin, can vary from 24 to 37 (Fourqurean et al., 1992).

Hamelin Pool sediment organic matter C:N ratios to $\delta^{13}C$ values cluster just above expected typical marine algae (Figure 4-14). The C:N ratios from the Hamelin Pool organic sediments ranged from a 4.99 to 24.67 with an average of 9.72; in some cases sediment has a 0 ratio or no organic matter present (Figure 4-14). The organic matter from the Hamelin Pool stromatolites heads measured between -16.76 to -13.32‰ with an average of -14.68‰ .The C:N ratios varied from 8.27 to 10.69 with an average of 9.25; Figure 4-14 (Giusfredi, 2014).

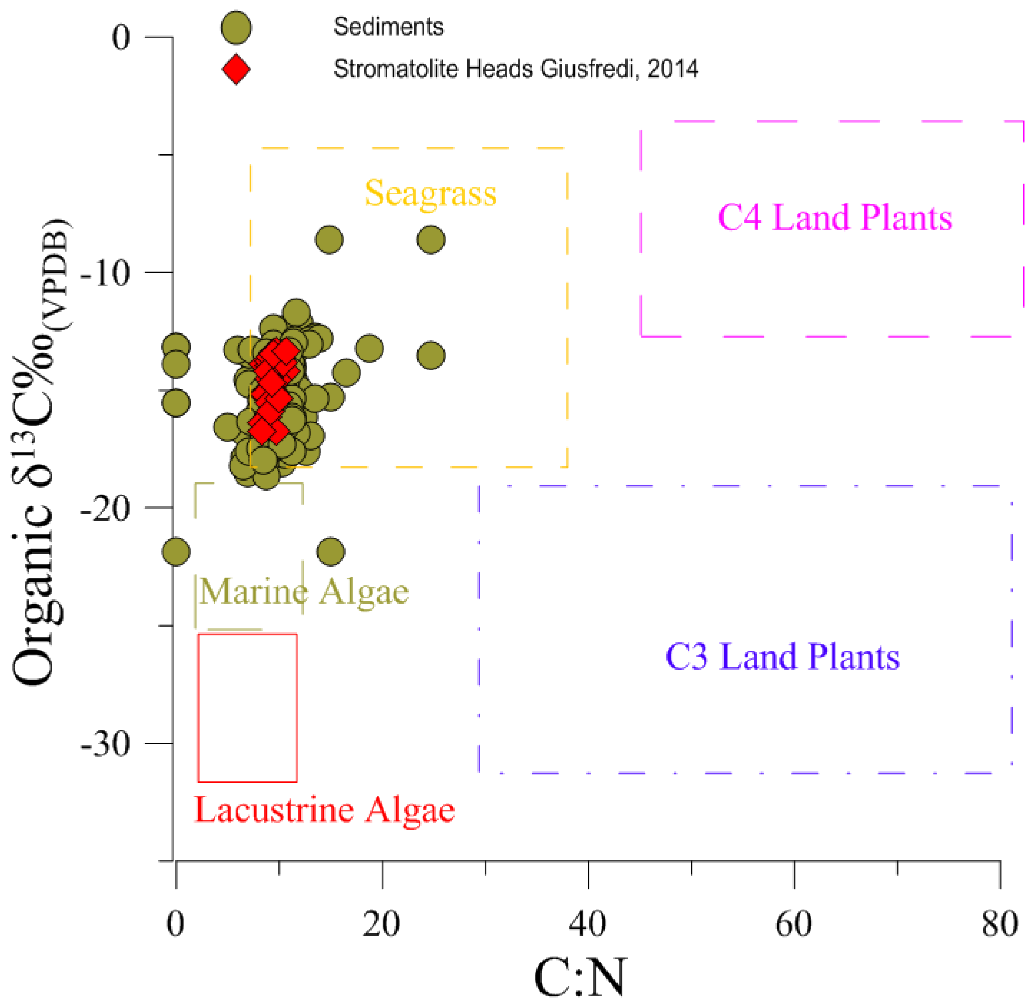

Figure 4-14 Shows the relationship between organic $\delta^{13}C$ and the atomic C:N ratios highlighting ranges of expected sources of organic matter from Fourqurean et al, 1992, Kennedy et al., 2010 and Meyers, 1994. The values from Hamelin Pool group within seagrass organic matter sources skewing towards marine algae. The values of the sediments are consistent with values found form the Hamelin Pool stromatolite heads.

The stromatolite organic matter results cluster within the organic sediment matter results (Figure 4-14). All points plotting at a typical C:N value for marine algae but at an elevated $\delta^{13}C$, which may be the result of a higher residence time of host waters. The organic matter in Hamelin Pool sediments therefore are derived, in part, from local microbialite activity and debris.

The organic matter in Hamelin Pool, like the sediments, is autochthonous. Local microbialite activity, debris, seagrass detritus (from northern Hamelin Pool and spill over from Shark Bay), macro and micro algae growing in Hamelin Pool are all sources of organic matter. All of these sources are subjected to high residence time in an essentially closed system; the microbialite values fall within sediment values because they are related by the water body in which they reside and with which they exchange ions.

4.5 *Chapter 4 Summary*

Hamelin Pool sediments were found to be on average skeletal and micritic grains that are less then 2mm (-1 phi), with little mud. Most sediments are classified as grainstone with some patches that are dominated by *Fragum eragatum,* classified as rudstones (Suosaari, 2015). The Nilemah province grain size is coarse to fine sand. Booldah, Flagpole, Spaven & Carbla grain sizes group together as coarse sand and the northern provinces, Nanga and Hutchinson range from being very coarse sand to fine sand. The inorganic fractions of the sediment have enriched marine $\delta^{13}C$ and $\delta^{18}O$ values (greater than 0‰), which increase from the north to the south, in agreement with the water isotopic values. The organic fraction of the sediments had $\delta^{15}N$ values that scattered close to zero, diagnostic of nitrogen fixation, suggesting that the organic matter is highly affected by microbial communities inside of Hamelin Pool. Furthermore, $\delta^{13}C$ values when compared to C:N ratios appear to be sourced primarily from organic mat activity and decay, but are likely also partially sourced from sea grass matter from Shark Bay.

Chapter 5: **Geochemical Conclusions**

The presence of the actively growing stromatolites is exceedingly rare in the modern, making Hamelin Pool a valuable site to study their microbialite growth. In an effort to better understand this environment, in this thesis, I have examined the geochemical setting of Hamelin Pool. The goal of the study was to measure geochemical parameters that can then be used to make a baseline for future interpretations and studies, of seasonal and/or annual variations and predictions of water evolution.

5.1 ***Empirical Proofs***

As hypothesized, the main source of water contributing to Hamelin Pool is derived from the greater Shark Bay. Using the salinity (Figure 2-3), $\delta^{18}O$ and $\delta^{2}H$ values (Figure 2-4) I have shown empirically that Hamelin Pool is a partially mixed waterbody with isohalines of increasing value southward, also implying that the highest residence time of the pool waters is in the southern embayment.

By modeling the salinity $\delta^{18}O$ and $\delta^{2}H$ values using the environmental conditions prevalent in Hamelin Pool (relative humidity, temperature, $\delta^{18}O$, $\delta^{2}H$) it is possible to confirm that at least 50% of the water body is lost by evaporation per year and that there has been an increase over time of both salinity and isotopic values (Figure 2-6). This model also revealed that the magnitude of the influence Shark Bay waters is have on Hamelin Pool waters can mask the input of smaller water input fluxes (Figure 2-15). Utilization of the dissolved fraction before entering Hamelin Pool is evident in the minor and trace metal results show a skewedness compared to standard sea water(SSW) (Figure 3-5, Figure 3-6, Figure 3-7). Excessive amounts of water evaporation results in

Hamelin Pool being an ion saturated water body, with tendency to precipitate aragonite and HMC. The increased Sr/Ca ratio and Ca/Cl ratios in the southern portion of the pool support no other major input of water directly into the southern portion of the pool.

Comparing the δ^{13} C and δ^{18}O values of the inorganic sediment and the water δ^{18}O and δ^{2}H values confirms that the southern portion of the pool has the highest residence time. This residence time exerts a geochemical imprint upon the sediments.

5.2 ***Water Restriction Role on Diversity***

The basinal sediment distribution is a testament to the role of heightened salinity, as a function of water restriction, resulting in a discrete assemblage of halotolerant biota. The majority of sediments collected (~74%) measured at or less then 2mm and showed a wide spread distribution of the halotolerant cockle, *Fragum eragatum*, along with macro algae fragments, micrite, and gastropod shells.

5.3 ***Geochemical Predictions***

The modeling of salinity and the stable O and H isotopic composition of water have also allowed for future water chemistry predictions of Hamelin Pool (Figure 2-16). While it may have taken nearly 700yrs to transform Hamelin Pool into saline water body it is today, the δ^{18}O values and also δ^{2}H values, and salinity (total dissolved metal fraction) predictions suggest that in as little as 70 years the Sea Level Rise impacts will begin to show its effects on Hamelin Pool. While hyper salinity is not essential for the growth of stromatolites, there is a high chance that lowering salinity could increase grazing, leading to the decline of stromatolites. This is not to say that other factors may not compensate for SLR, for example if extreme weather causes even higher levels of evaporation, or the sill growth rate suddenly increases, but if conditions stay the same or close to it, human intervention may need to be taken in order to preserve the stromatolites.

5.4 ***Sources of Organic Matter in Hamelin Pool***

The results from the insoluble fraction of Hamelin Pool sediments strongly suggest microbial mat production and decay as the main sources of organic matter (Figure 4-15). The stable isotopic signatures showed independent "hot spots" of enriched values and may prove to be the best tool for tracking changes in the environment. The $\delta^{15}N$ values, of the organic matter (Figure 4-14), also emphasizes the importance of nitrogen fixation. Since there is minimal fractionation during fixation of nitrogen, $\delta^{15}N$ values are close to atmospheric i.e. 0‰. In interpreting and predicting basinal evolution the organic matter C:N ratios and delta values may be the strongest points of evidence to investigate an area thought to have been a stromatolitic reef complex.

5.5 ***Future Work***

In order to best evaluate and certify the chemical results and predictions suggested in this thesis, a multi-isotopic and geochemical investigation should be conducted on continuous bases. Furthermore, sampling from around the margin amongst the stromatolites will allow for better resolution of the coastal chemistry and how it compares to the basin. Although this thesis is a good snap shot of the Hamelin Pool waters in 2014 this study by no means characterizes Hamelin Pool over the course of a year; water level and salinities are different during different time of the year (Suosaari et al., 2016b). Studies also predict ground may be entering the pool between May and September along the margins (Suosaari et al., 2016b). This type of study can help identify ground water flux and elemental contributions to the pool. For the present data set the dissolved element fractions and mass-balance models can be broken into subsections, in doing this a mass balance prediction can be refined as well the precision of the expected precipitations within specific areas of Hamelin Pool. Further investigations in to the organic matter may also prove to be a good indicator of the response to stresses that may be placed on the pool. If coring in the area was possible a study of pore water inclusion as well as diagenetic effects on such hypersaline precipitated carbonates may also help in understanding how prehistoric stromatolitic reef complexes are recorded in the geologic record and evolve.

References

Awramik, S., Margulis, L., Barghoorn, E., 1976. .4 Evolutionary Processes in the Formation of Stromatolites, Developments in Sedimentology. Elsevier, pp. 149-162.

Awramik, S.M., 1992. The history and significance of stromatolites, Early Organic Evolution. Springer, pp. 435-449.

Blott, S.J., Pye, K., 2001. GRADISTAT: a grain size distribution and statistics package for the analysis of unconsolidated sediments. Earth surface processes and Landforms, 26(11): 1237-1248.

Burne, R.V., Bauld, J., Hunt, G., 1990. The geobiology of Hamelin Pool: Research reports of the Baas Becking Geobiological Laboratory's Shark Bay Project. Bureau of Mineral Resources, Geology and Geophysics.

Cawley, K.M., Ding, Y., Fourqurean, J., Jaffé, R., 2012. Characterising the sources and fate of dissolved organic matter in Shark Bay, Australia: a preliminary study using optical properties and stable carbon isotopes. Marine and Freshwater Research, 63(11): 1098-1107.

Chierici, M., Fransson, A., 2009. Calcium carbonate saturation in the surface water of the Arctic Ocean: undersaturation in freshwater influenced shelves. Biogeosciences, 6(11): 2421-2431.

Church, J.A., White, N.J., Coleman, R., Lambeck, K., Mitrovica, J.X., 2004. Estimates of the regional distribution of sea level rise over the 1950–2000 period. Journal of Climate, 17(13): 2609-2625.

Clary, R., Wandersee, J., 2013. Stromatolites. Science Teacher, 80(2): 60.

Cockbain, A., 1976. Chapter 8.2 Modern Algal Stromatolites at Hamelin Pool, A Hypersaline Barred Basin in Shark Bay, Western Australia. Developments in Sedimentology, 20: 389-411.

Craig, H., 1961. Isotopic Variations in Meteoric Waters. Science, 133(3465): 1702-1703.

Dill, R.F., Shinn, E.A., Jones, A.T., Kelly, K., Steinen, R.P., 1986. Giant subtidal stromatolites forming in normal salinity waters. Nature, 324(6092): 55-58.

Dravis, J.J., 1983. Hardened subtidal stromatolites, Bahamas. Science, 219: 385-386.

Dunham, R.J., 1962. Classification of carbonate rocks according to depositional texture. Memoirs American Association of Petroleum Geologists, 1: 108-121.

Finlay, J.C., Kendall, C., 2007. Stable isotope tracing of temporal and spatial variability in organic matter sources to freshwater ecosystems. Stable Isotopes in Ecology and Environmental Science, 2: 283-333.

Fourqurean, J.W., Zieman, J.C., Powell, G.V.N., 1992. Phosphorus limitation of primary production in Florida Bay - Evidence from C-N-P ratios of the dominant seagrass *Thalassiatestudinum*. Limnology and Oceanography, 37(1): 162-171.

Gat, J.R., Gonfiantini, R., 1981. Stable isotope hydrology. Deuterium and oxygen-18 in the water cycle.Internatoinal Atomic Energy Agency (IAEA):IAEA

Giusfredi, P.E., "Hamelin Pool Stromatolites: Ages and Interactions with the Depositional Environment"(2014). Open Access Thesis. 501. https://scholarlyrepository.miami.edu/oa_theses/501

Gonfiantini, R., 1986. Environmental Isotopes in Lake Studies. In: Fritz, P., Fontes, J. (Eds.), Handbook of Environmental Isotope Geochemistry. Elsevier, Amsterdam, pp. 113-168.

Jahnert, R.J., Collins, L.B., 2012. Characteristics, distribution and morphogenesis of subtidal microbial systems in Shark Bay, Australia. Marine Geology, 303: 115-136.

Kennedy, H. et al., 2010. Seagrass sediments as a global carbon sink: isotopic constraints. Global Biogeochemical Cycles, 24(4).

LeGrande, A.N., Schmidt, G.A., 2006. Global gridded data set of the oxygen isotopic composition in seawater. Geophysical Research Letters, 33: L12604.

Logan, B.W., Cebulski, D.E., 1970. Sedimentary environments of Shark Bay, Western Australia.Carbonate Sedimentation and Enviornments, Shark Bay, Western Australia. American Association of Petroleum Geologist, 1-37

Logan, B.W., Read, J.F., Davies, G.R., 1970. History of carbonate sedimentation, Quaternary Epoch, Shark Bay, Western Australia. Carbonate Sedimentation and Enviornments, Shark Bay, Western Australia. American Association of Petroleum Geologist, 38-84

Meyers, P.A., Ishiwatari, R., 1993. Lacustrine organic geochemistry—an overview of indicators of organic matter sources and diagenesis in lake sediments. Organic Geochemistry, 20(7): 867-900.

Oehlert, A.M., Swart, P.K., 2014. Interpreting carbonate and organic carbon isotope covariance in the sedimentary record. Nature Communications, 5: 4672.

Playford, P.E., 1990. Geology of the Shark Bay area, Western Australia. Research in Shark Bay, Report of the France–Australe Bicentenary Expedition Committee. Western Australian Museum, Perth: 13-31.

Price, R.M., Skrzypek, G., Grierson, P.F., Swart, P.K., Fourqurean, J.W., 2012. The use of stable isotopes of oxygen and hydrogen to identify water sources in two hypersaline estuaries with different hydrologic regimes. Marine and Freshwater Research, 63(11): 952-966.

Robin, R., Stokes, R., 1959. Electrolyte solutions. London: Butterworths.

Rumolo, P., Barra, M., Gherardi, S., Marsella, E., Sprovieri, M., 2011. Stable isotopes and C/N ratios in marine sediments as a tool for discriminating anthropogenic impact. Journal of Environmental Monitoring, 13(12): 3399-3408.

Sharp, Z., 2007. Stable Isotope Geochemistry. Pearson Prentice Hall, Upper Saddle River, 344 pp.

Steneck, R.S., Miller, T.E., Reid, R.P., Macintyre, I.G., 1998. Ecological controls on stromatolite development in a modern reef environment: A test of the ecological refuge paradigm. Carbonates And Evaporites, 13(1): 48-65.

Suosaari, E. et al., 2016a. New multi-scale perspectives on the stromatolites of Shark Bay, Western Australia. Scientific reports, 6: 20557.

Suosaari, E.P. et al., 2016b. Environmental Pressures Influencing Living Stromatolites In Hamelin Pool, Shark Bay, Western Australia. Palaios, 31(10): 483-496.

Swart, P., Oehlert, A., Mackenzie, G., Eberli, G., Reijmer, J., 2014. The fertilization of the Bahamas by Saharan dust: A trigger for carbonate precipitation? Geology, 42(8): 671-674.

Swart, P.K., 1991a. Factors affecting the oxygen isotopic composition of the Black Sea, Black Sea Oceanography. Springer, pp. 75-88.

Swart, P.K., 1991b. The oxygen and hydrogen isotopic composition of the Black Sea. Deep-Sea Research, 38: s761-s772.

Swart, P.K., 1991c. The oxygen and hydrogen isotopic composition of the Black Sea. Deep Sea Research Part A. Oceanographic Research Papers, 38: S761-S772.

Swart , P.K. et al., 2003. Data Report: Carbonate Mineralogy of Sites Drilled during Leg 182 In: Feary, D.A., Hine, A.C., Malone, M.J. (Eds.), Proceedings of the Ocean Drilling Program Scientific Results. Ocean Drilling Program, College Station.

Swart, P.K., Kramer, P.A., 1998. Geology of mud islands in Florida Bay. In: Vacher, H.L., Quinn, T. (Eds.), *The Hydrology of Carbonate Islands*. Elsevier, pp. 249-274.

Tucker, M.E., 2003. Sedimentary rocks in the field. John Wiley & Sons.

Appendix

Tables

$\phi<-1$	**$-1>\phi>0$**
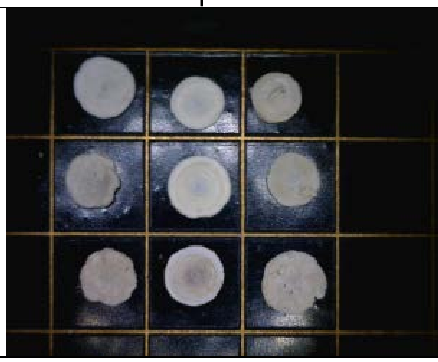	
Marginopora vertebralis	Gastropods
	
Fragum eragatum	*Marginopora vertebralis*
	
Micrite/Precipitate	*Surpulid* Tubes
	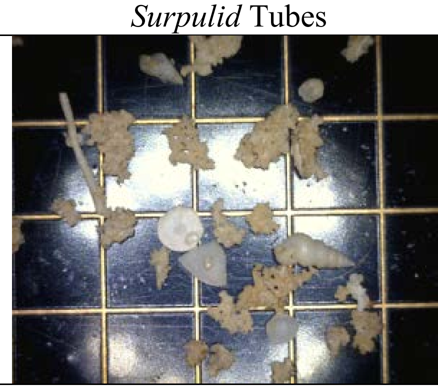
Mixed	Mixed

Table 7-1 Sediment composition for size fractions $\phi<-1$ and $-1>\phi>0$, each grid is 1cm.

0> ϕ >1	
	
Micrite/Precipitate	*Penerpplis planatus*
	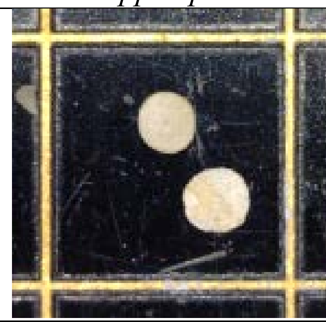
Spirolina sp.	*Marginopora vertebralis*
	
Acetabularia sp. Stalks	Mixed
1> ϕ >2	
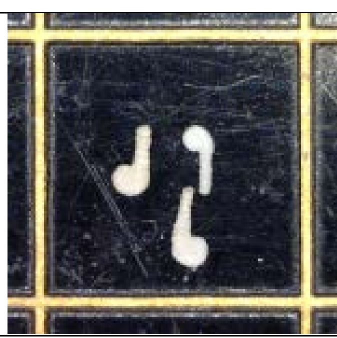	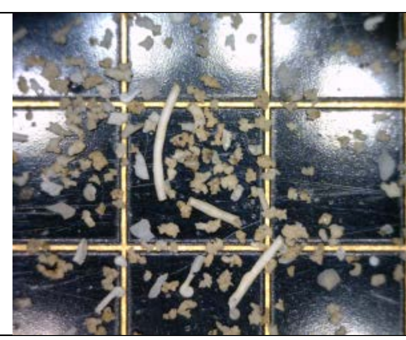
Sprolina sp.	Mixed

Table 7-2. Sediment composition for size fractions 0>PHI>1and 1>PHI>2, each grid is 1cm.

2> ϕ >3	**3> ϕ >4**
	
Debris/Juvenile	Debris/Juvenile
	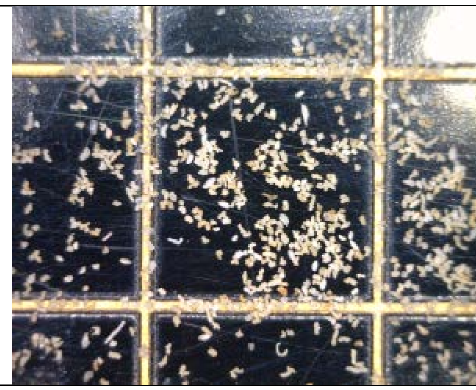
Debris/Juvenile	Debris/Juvenile

Table 7-3. Sediment composition for size fractions 2> ϕ >3and 3> ϕ >4, each grid is 1cm.

Code	Aprx H	Long	Lat	Code	Aprx H	Long	Lat	Code	Aprx H	Long	Lat	Code	Aprx H	Long	Lat
WSPA_001	surface	114.0607	-26.0031	WSPA_031	deep	114.1457	-26.1864	WSPA_063	deep	114.0602	-26.0950	WSPA_093	surface	114.1890	-26.0554
WSPA_002	surface	114.1801	-26.3831	WSPA_032	deep	114.2158	-26.2652	WSPA_064	surface	114.0320	-26.3499	WSPA_094	surface	114.2185	-26.2675
WSPA_003	surface	114.1801	-26.3831	WSPA_034	surface	114.1868	-26.2760	WSPA_065	surface	114.0324	-26.2592	WSPA_095	deep	114.1291	-25.9946
WSPA_004	surface	114.1801	-26.3831	WSPA_035	deep	114.1890	-26.3483	WSPA_066	surface	114.1897	-26.2436	WSPA_097	deep	114.1320	-26.1401
WSPA_005	surface	114.2275	-26.3283	WSPA_036	surface	114.1314	-26.4152	WSPA_067	deep	114.1325	-26.2408	WSPA_098	surface	114.0345	-26.3909
WSPA_006	surface	114.2271	-26.3276	WSPA_037	surface	114.2158	-26.2652	WSPA_068	deep	114.1328	-26.2951	WSPA_099	surface	114.1324	-26.0971
WSPA_007	surface	114.2269	-26.3272	WSPA_038	deep	114.1314	-26.4152	WSPA_069	deep	114.0320	-26.3499	WSPA_100	surface	114.1320	-26.1401
WSPA_008	surface	114.2263	-26.3268	WSPA_039	surface	114.1924	-26.2653	WSPA_070	surface	114.0976	-26.3217	WSPA_101	surface	114.1314	-26.0018
WSPA_009	surface	114.2275	-26.3271	WSPA_040	surface	114.1369	-26.3302	WSPA_071	surface	114.1328	-26.2951	WSPA_102	deep	114.0345	-26.3909
WSPA_010	surface	114.2321	-26.3199	WSPA_041	deep	114.1897	-26.2436	WSPA_072	surface	113.9925	-26.1559	WSPA_104	surface	114.2002	-26.0807
WSPA_011	surface	114.2322	-26.3035	WSPA_042	deep	114.0273	-26.3067	WSPA_073	surface	113.9441	-26.0487	WSPA_105	deep	114.1316	-26.0510
WSPA_012	deep	114.0854	-26.4398	WSPA_043	deep	113.9324	-26.0131	WSPA_074	deep	113.9195	-26.0413	WSPA_106	deep	114.1497	-26.0926
WSPA_013	surface	114.1890	-26.3483	WSPA_044	surface	114.0631	-26.2931	WSPA_075	surface	113.9368	-26.0918	WSPA_108	surface	114.2156	-26.2654
WSPA_014	deep	114.1453	-26.3827	WSPA_045	surface	114.0629	-26.1390	WSPA_076	surface	113.9195	-26.0413	WSPA_109	deep	114.1314	-26.0018
WSPA_015	surface	114.1453	-26.3827	WSPA_046	deep	113.9875	-26.2909	WSPA_077	surface	113.9864	-26.1356	WSPA_110	deep	114.1324	-26.0971
WSPA_016	surface	114.1331	-26.3979	WSPA_047	deep	113.9557	-26.1592	WSPA_078	deep	113.9287	-26.0438	WSPA_111	surface	114.1291	-25.9946
WSPA_018	deep	114.0640	-26.4006	WSPA_048	surface	114.1325	-26.2408	WSPA_079	surface	114.0607	-26.0031	WSPA_112	deep	114.1895	-26.0956
WSPA_019	deep	114.0625	-26.0483	WSPA_049	surface	113.9872	-26.2349	WSPA_080	deep	113.9859	-26.0014	WSPA_113	deep	114.2156	-26.2654
WSPA_020	surface	114.0640	-26.4006	WSPA_050	surface	113.9875	-26.2909	WSPA_081	surface	114.0602	-26.0950	WSPA_114	surface	114.1497	-26.0926
WSPA_021	deep	114.1341	-26.4152	WSPA_051	deep	114.1890	-26.2946	WSPA_082	deep	113.9368	-26.0918	WSPA_115	surface	114.1316	-26.0510
WSPA_022	surface	114.1457	-26.1864	WSPA_052	surface	113.9287	-26.0438	WSPA_083	deep	113.9925	-26.1559	WSPA_116	surface	114.1895	-26.0956
WSPA_023	deep	114.1369	-26.3302	WSPA_053	deep	113.9872	-26.2349	WSPA_085	deep	114.0629	-26.1390	WSPA_117	deep	114.1890	-26.0554
WSPA_024	surface	114.1329	-26.3519	WSPA_054	surface	114.0625	-26.0483	WSPA_086	deep	113.9441	-26.0487	WSPA_118	surface	113.9418	-26.1502
WSPA_025	surface	113.9324	-26.0131	WSPA_055	deep	114.0643	-26.3501	WSPA_087	deep	113.9864	-26.1356	WSPA_119	deep	114.2002	-26.0807
WSPA_026	deep	114.1331	-26.3979	WSPA_056	deep	114.0324	-26.2592	WSPA_088	deep	114.0629	-26.1884	WSPA_121	surface	114.1885	-26.0182
WSPA_027	surface	114.1890	-26.2946	WSPA_058	surface	113.9869	-26.1815	WSPA_089	surface	113.9859	-26.0014	WSPA_203	surface	113.9863	-26.0445
WSPA_028	surface	114.0632	-26.2386	WSPA_060	deep	114.0631	-26.2931	WSPA_090	surface	113.9557	-26.1592	WSPA_211	deep	113.9867	-26.0887
WSPA_029	surface	114.1341	-26.4152	WSPA_061	deep	114.0976	-26.3217	WSPA_091	surface	114.0629	-26.1884	WSPA_213	deep	113.9863	-26.0445
WSPA_030	surface	114.0854	-26.4398	WSPA_062	surface	114.0273	-26.3067	WSPA_092	deep	114.1885	-26.0182	WSPA_215	surface	113.9867	-26.0887

Table 7-4. Listed are the codes, coordinates and approximate heights for waters sampling sites.

Code	Sal	$\delta^{18}O$‰	$\delta^{2}H$‰	Code	Sal	$\delta^{18}O$‰	$\delta^{2}H$‰	Code	Sal	$\delta^{18}O$‰	$\delta^{2}H$‰	Code	Sal	$\delta^{18}O$‰	$\delta^{2}H$‰
WSPA_001		4.49	25.67	WSPA_031	58.20	4.31	24.10	WSPA_064	59.30	3.92	23.00	WSPA_094	58.00	3.82	22.15
WSPA_002	61.00	4.43	25.96	WSPA_032	60.50	4.98	26.10	WSPA_065	59.90	4.04	23.75	WSPA_095	55.80	3.59	20.90
WSPA_003	61.00	5.27	23.31	WSPA_034	59.10	3.90	23.35	WSPA_066	58.40	3.82	22.59	WSPA_097	55.80	3.52	21.17
WSPA_004	61.00	4.11	23.37	WSPA_035	59.10	3.83	22.96	WSPA_067	58.40	3.82	23.61	WSPA_098	54.90	3.16	14.32
WSPA_005	61.00	4.09	24.29	WSPA_036	59.80	5.22	26.73	WSPA_068	58.20	3.79	22.61	WSPA_099	55.40	3.63	21.50
WSPA_006	59.90	4.13	24.55	WSPA_037	59.70	4.04	23.17	WSPA_069	58.20	3.84	23.58	WSPA_100	56.50	3.88	22.39
WSPA_007	59.90	3.98	24.68	WSPA_038	59.70	3.97	22.95	WSPA_070	59.30	3.90	23.57	WSPA_101	56.20	3.80	21.38
WSPA_008	59.80	4.12	23.36	WSPA_039	59.80	4.25	24.88	WSPA_071	61.10	4.07	24.00	WSPA_102	57.90	3.72	22.00
WSPA_009	59.80	4.00	24.36	WSPA_040	59.70	4.03	23.84	WSPA_072	59.80	4.28	24.75	WSPA_104	58.80	4.00	22.84
WSPA_010	59.90	3.96	23.11	WSPA_041	58.90	3.82	22.62	WSPA_073	59.50	4.17	23.63	WSPA_105	57.00	3.57	20.88
WSPA_011	59.90	3.79	21.51	WSPA_042	59.90	4.08	24.08	WSPA_074	59.50	3.97	23.99	WSPA_106	57.00	3.55	21.09
WSPA_012	59.40	3.94	23.20	WSPA_043	60.00	4.14	24.67	WSPA_075	57.40	4.22	24.49	WSPA_108	56.00	3.79	22.02
WSPA_013	59.40	3.91	22.99	WSPA_044	59.00	3.87	23.57	WSPA_076	58.50	3.94	22.63	WSPA_109	58.70	3.88	23.21
WSPA_014	61.30	4.10	22.90	WSPA_045	59.30	3.94	23.53	WSPA_077	53.90	3.33	20.18	WSPA_110	58.10	3.56	21.89
WSPA_015	61.40	3.90	19.61	WSPA_046	60.00	4.08	23.86	WSPA_078	58.10	3.70	22.48	WSPA_111	58.30	3.79	22.30
WSPA_016	59.40	3.97	22.35	WSPA_047	59.90	4.07	23.42	WSPA_079	58.10	4.33	23.47	WSPA_112	58.90	3.76	22.77
WSPA_018	59.80	3.83	21.04	WSPA_048	58.50	4.12	23.78	WSPA_080	59.30	3.78	22.88	WSPA_113	58.80	3.83	22.66
WSPA_019	59.60	3.86	23.24	WSPA_049	61.60	4.39	24.79	WSPA_081	59.50	3.72	20.78	WSPA_114	55.10	3.53	20.87
WSPA_020	59.20	3.84	23.38	WSPA_050	59.10	4.06	23.21	WSPA_082	40.50	3.52	20.56	WSPA_115	55.10	3.51	20.52
WSPA_021	59.50	3.95	23.01	WSPA_051	59.10	4.16	24.08	WSPA_083	57.40	3.85	21.81	WSPA_116	57.70	3.56	21.83
WSPA_022	59.70	4.06	24.14	WSPA_052	59.80	3.61	19.74	WSPA_085	59.00	4.10	23.92	WSPA_117	58.20	3.81	22.47
WSPA_023	59.70	4.95	24.75	WSPA_053	60.50	4.11	24.09	WSPA_086	56.50	3.91	22.73	WSPA_118	54.00	3.80	21.26
WSPA_024	59.90	3.99	23.79	WSPA_054	60.40	4.24	24.95	WSPA_087	57.50	3.73	22.47	WSPA_119	54.30	3.34	19.93
WSPA_025	59.90	4.05	23.89	WSPA_055	59.00	3.89	23.38	WSPA_088	57.50	3.68	21.91	WSPA_121	54.60	3.64	21.43
WSPA_026	58.80	3.81	23.15	WSPA_056	59.00	3.90	22.48	WSPA_089	59.10	4.08	23.85	WSPA_203	56.40	3.55	21.88
WSPA_027	58.60	4.35	23.69	WSPA_058	60.00	4.32	24.71	WSPA_090	52.90	3.30	19.33	WSPA_211	56.30	3.95	21.90
WSPA_028	58.60	4.67	26.68	WSPA_060	59.70	4.22	24.66	WSPA_091	58.40	3.90	21.97	WSPA_213	54.10	3.34	19.24
WSPA_029	59.90	4.43	25.69	WSPA_061	58.50	3.76	22.00	WSPA_092	61.00	4.15	24.20	WSPA_215	54.20	3.46	20.38
WSPA_030	61.00	4.07	19.22	WSPA_062	58.70	4.01	22.74	WSPA_093	58.70	3.89	23.35				
Total Mean	**58.44**	**3.95**	**22.86**												
Total Min	**40.50**	**3.16**	**14.32**												
Max	**61.60**	**5.27**	**26.73**												
n	**114**	**115**	**115**												

Table 7-5 Salinity and water isotope values for basinal waters of Hamelin Pool.

Code	Grams	Int Ph	Alk	Code	Grams	Int Ph	Alk	Code	Grams	Int Ph	Alk	Code	Grams	Int Ph	Alk
WSPA_004	7.16	7.90	3.21	WSPA_035	7.14	7.82	2.99	WSPA_066	7.27	7.79	2.96	WSPA_097	7.17	7.82	2.93
WSPA_005	6.98	7.74	3.15	WSPA_036	7.04	7.58	3.17	WSPA_067	7.39	7.93	3.14	WSPA_098	7.11	7.83	2.93
WSPA_006	6.99	7.76	3.13	WSPA_037	6.96	7.84	3.21	WSPA_068	6.87	7.78	3.17	WSPA_099	7.34	7.87	2.91
WSPA_007	6.97	7.72	3.17	WSPA_038	7.03	7.93	3.17	WSPA_069	6.93	7.96	3.21	WSPA_100	7.04	7.83	2.95
WSPA_008	7.04	7.91	3.25	WSPA_039	7.14	7.82	3.09	WSPA_070	7.33	7.95	3.11	WSPA_101	7.07	7.89	3.06
WSPA_009	7.09	7.88	3.20	WSPA_040	7.35	7.99	3.15	WSPA_071	7.03	7.97	3.15	WSPA_102	7.12	7.91	3.07
WSPA_010	6.97	7.88	3.22	WSPA_041	7.34	7.92	3.16	WSPA_072	7.15	7.69	4.09	WSPA_104	7.07	7.85	2.87
WSPA_011	7.10	7.90	3.23	WSPA_042	6.70	7.80	3.02	WSPA_073	7.27	7.86	3.17	WSPA_105	7.27	7.67	3.08
WSPA_012	6.95	7.82	3.15	WSPA_043	7.15	7.96	3.18	WSPA_074	7.23	7.93	3.14	WSPA_106	7.41	7.91	2.41
WSPA_013	6.99	7.85	3.16	WSPA_044	7.28	7.96	3.20	WSPA_075	7.21	7.79	3.08	WSPA_108	7.07	7.83	2.97
WSPA_014	7.06	7.95	3.23	WSPA_045	7.14	7.84	3.15	WSPA_076	7.02	7.95	3.05	WSPA_109	7.15	7.92	3.08
WSPA_015	7.14	7.92	3.12	WSPA_046	7.05	8.10	3.18	WSPA_077	7.11	7.87	2.94	WSPA_110	7.01	6.99	2.73
WSPA_016	7.01	7.79	2.91	WSPA_047	7.49	8.10	3.21	WSPA_078	7.43	8.36	3.22	WSPA_111	7.03	7.72	2.40
WSPA_018	7.12	7.84	3.19	WSPA_048	7.03	7.77	3.15	WSPA_079	7.30	7.49	3.37	WSPA_112	7.14	7.89	3.15
WSPA_019	6.98	7.83	3.21	WSPA_049	6.99	7.93	3.05	WSPA_080	7.15	7.90	3.09	WSPA_113	7.02	7.84	3.07
WSPA_020	7.19	7.63	3.15	WSPA_050	7.03	7.89	3.08	WSPA_081	7.05	7.96	3.18	WSPA_114	7.13	7.91	2.95
WSPA_021	7.11	7.95	3.15	WSPA_051	7.07	7.89	3.07	WSPA_082	7.26	7.94	3.00	WSPA_115	7.49	7.88	2.92
WSPA_022	7.27	7.93	3.26	WSPA_052	7.09	7.81	3.20	WSPA_083	7.37	7.84	2.99	WSPA_116	7.13	7.68	3.13
WSPA_023	7.15	7.38	3.61	WSPA_053	7.28	7.77	3.06	WSPA_085	7.07	7.92	3.03	WSPA_117	7.39	7.74	2.68
WSPA_024	7.05	7.91	3.20	WSPA_054	7.24	7.85	3.08	WSPA_086	7.37	7.90	3.02	WSPA_118	7.27	7.45	3.09
WSPA_025	7.25	7.77	3.15	WSPA_055	7.28	7.93	3.13	WSPA_087	7.34	7.78	2.74	WSPA_119	7.04	7.90	2.86
WSPA_026	7.05	7.70	3.16	WSPA_056	7.20	7.79	3.08	WSPA_088	7.21	7.94	2.49	WSPA_121	7.14	7.84	2.91
WSPA_027	7.05	7.77	3.42	WSPA_058	7.26	7.62	2.93	WSPA_089	7.05	7.90	3.03	WSPA_203	7.32	7.83	3.07
WSPA_028	7.01	7.70	2.81	WSPA_060	7.06	7.90	3.12	WSPA_090	7.10	7.90	2.85	WSPA_211	7.16	7.76	3.47
WSPA_029	7.00	6.81	2.52	WSPA_061	7.23	7.96	3.03	WSPA_091	7.20	7.68	2.29	WSPA_213	7.10	7.92	2.94
WSPA_030	7.00	7.80	2.99	WSPA_062	7.01	7.89	2.91	WSPA_092	7.25	7.92	3.18	WSPA_215	7.02	7.86	2.87
WSPA_031	7.07	7.84	3.30	WSPA_063	7.18	7.70	3.32	WSPA_093	7.05	7.92	3.00				
WSPA_032	7.05	7.77	3.44	WSPA_064	7.50	7.88	3.16	WSPA_094	7.45	7.29	3.14				
WSPA_034	7.16	7.32	2.95	WSPA_065	7.14	7.95	3.02	WSPA_095	7.11	7.91	2.99				
Total Mean	**7.14**	**7.82**	**3.07**												
Total Min	**6.70**	**6.81**	**2.29**												
Max	**7.50**	**8.36**	**4.09**												
n	**113**	**113**	**113**												

Table 7-6 Initial pH the amount of grams of water measured and alkalinity results for Hamelin Pool basinal waters.

Code	Cl mM	Ca315mM	Ca422mM	FemM	KmM	MgmM	NamM	SmM	SrmM	Code	Cl mM	Ca315mM	Ca422	FemM	KmM	MgmM	NamM	SmM	SrmM
WSPA_004	978.81	18.40	17.64	616.89	17.46	91.05	811.27	51.14	0.16	WSPA_035	930.51	17.64	15.47	1088.81	17.58	84.36	771.23	49.37	0.15
WSPA_005	948.30	17.70	16.51	761.37	17.35	87.77	785.98	49.40	0.15	WSPA_036	1076.73	20.06	19.23	1112.51	19.54	97.25	892.43	56.23	0.17
WSPA_006	934.46	17.65	16.58	848.62	16.79	87.59	774.51	49.14	0.15	WSPA_037	1002.77	19.17	17.18	687.59	18.90	90.42	831.13	52.86	0.16
WSPA_007	922.59	17.41	16.15	654.85	16.69	84.99	764.67	48.07	0.15	WSPA_038	1163.63	21.79	19.43	523.77	22.45	96.23	964.45	62.57	0.18
WSPA_008	911.22	17.28	15.61	749.82	16.49	84.88	755.24	48.00	0.14	WSPA_039	1065.21	20.19	19.37	862.97	19.56	95.34	882.88	55.04	0.17
WSPA_009	967.76	18.37	16.70	949.44	18.08	87.84	802.11	51.47	0.16	WSPA_040	888.48	16.99	14.88	676.64	16.57	82.31	736.40	47.31	0.14
WSPA_010	1061.16	19.63	18.65	798.80	19.58	94.37	879.52	55.06	0.17	WSPA_041	1391.48	26.54	22.91	952.79	27.68	106.13	1153.30	74.26	0.22
WSPA_011	932.73	17.66	16.53	494.70	16.84	87.68	773.07	48.68	0.15	WSPA_042	921.18	17.00	16.05	661.69	16.60	84.96	763.50	47.48	0.15
WSPA_012	943.61	17.86	16.87	626.66	16.93	88.60	782.09	48.82	0.15	WSPA_043	998.70	19.01	16.81	435.51	18.79	89.58	827.75	53.21	0.16
WSPA_013	913.08	17.32	15.98	490.96	16.34	85.47	756.78	47.69	0.15	WSPA_044	973.13	18.14	16.51	777.17	18.00	87.19	806.56	51.80	0.15
WSPA_014	823.60	15.75	13.59	588.50	15.58	76.78	682.63	44.11	0.13	WSPA_045	886.80	16.89	14.97	670.42	16.33	82.29	735.00	47.08	0.14
WSPA_015	935.23	17.79	15.35	629.03	18.18	82.78	775.15	50.02	0.15	WSPA_046	890.98	16.97	15.18	468.85	16.55	82.38	738.47	46.36	0.14
WSPA_016	1118.52	21.28	20.89	774.25	20.41	99.70	927.07	57.19	0.19	WSPA_047	882.27	16.87	15.04	570.10	16.35	82.58	731.25	46.29	0.14
WSPA_018	1039.96	19.11	18.36	857.32	18.84	92.43	861.95	53.00	0.17	WSPA_048	911.38	17.36	15.91	570.57	16.72	85.47	755.37	48.70	0.15
WSPA_019	961.83	18.08	17.18	813.56	17.33	89.96	797.19	49.88	0.16	WSPA_049	841.38	16.06	13.85	831.46	15.73	77.28	697.36	44.29	0.13
WSPA_020	921.41	17.35	16.14	653.55	16.44	86.82	763.69	47.71	0.15	WSPA_050	808.91	15.44	13.19	327.16	15.39	75.54	670.45	42.86	0.13
WSPA_021	886.27	16.86	14.88	475.90	16.29	82.37	734.57	46.41	0.14	WSPA_051	804.77	15.37	13.05	490.85	15.36	75.56	667.02	43.16	0.13
WSPA_022	981.83	18.46	16.43	619.96	18.89	86.46	813.77	52.52	0.15	WSPA_052	924.03	17.51	15.98	756.92	17.11	85.71	765.86	47.92	0.15
WSPA_023	976.99	18.66	16.29	722.02	18.68	86.48	809.76	52.50	0.15	WSPA_053	958.73	17.95	16.63	920.64	17.51	87.48	794.62	50.03	0.15
WSPA_024	1010.06	18.93	18.15	765.06	18.25	92.30	837.17	52.65	0.16	WSPA_054	1036.11	19.58	17.80	361.02	19.21	92.41	858.75	54.99	0.16
WSPA_025	906.37	17.20	15.75	623.06	16.51	84.93	751.23	47.65	0.14	WSPA_055	862.70	16.57	14.67	424.86	16.03	79.70	715.03	44.81	0.14
WSPA_026	921.96	17.43	16.28	773.63	16.48	86.48	764.15	48.24	0.15	WSPA_056	873.70	16.49	14.67	681.38	16.22	79.91	724.15	46.10	0.14
WSPA_027	969.13	18.39	16.70	749.96	17.87	88.33	803.25	50.93	0.15	WSPA_058	1043.27	19.88	18.07	579.41	19.57	92.26	864.70	55.43	0.16
WSPA_028	1207.91	22.11	21.34	841.94	22.23	103.15	1001.15	60.96	0.19	WSPA_060	561.37	10.74	9.47	390.48	10.15	59.13	465.28	29.33	0.09
WSPA_029	1193.64	22.14	21.54	699.19	21.90	104.05	989.32	62.23	0.19	WSPA_061	1063.67	19.73	17.89	693.71	20.12	92.64	881.60	56.94	0.17
WSPA_030	1061.51	19.81	19.19	688.72	19.11	95.71	879.81	54.51	0.17	WSPA_062	955.71	17.71	15.78	614.86	18.16	83.75	792.12	50.12	0.15
WSPA_031	1014.01	19.07	18.55	620.11	18.32	93.55	840.44	53.02	0.17	WSPA_063	893.09	16.88	15.51	426.96	15.97	83.77	740.22	46.56	0.14
WSPA_032	1065.12	19.77	19.07	803.89	19.39	95.29	882.80	54.54	0.17	WSPA_064	871.39	16.59	14.88	692.33	15.98	82.23	722.24	45.81	0.14
WSPA_034	859.71	16.37	14.43	426.44	15.93	80.73	712.55	45.97	0.14										

Table 7-7 The results from the ICP-OES analysis. Results have been converted to mM. 1/2

Code	Cl mM	Ca315mM	Ca422mM	FemM	KmM	MgmM	NamM	SmM	SrmM	Code	Cl mM	Ca315mM	Ca422	FemM	KmM	MgmM	NamM	SmM	SrmM
WSPA_065	936.18	17.71	15.75	489.47	17.50	85.45	775.93	49.83	0.15	WSPA_094	777.75	14.96	12.61	335.73	14.91	73.82	644.63	41.93	0.12
WSPA_066	866.82	16.53	14.28	579.95	16.26	79.47	718.45	46.49	0.13	WSPA_095	770.10	14.64	12.51	483.96	14.87	72.84	638.28	40.14	0.12
WSPA_067	907.86	17.39	14.95	615.92	17.10	82.44	752.46	48.47	0.14	WSPA_097	753.33	14.39	12.20	484.05	14.42	71.83	624.39	40.44	0.12
WSPA_068	915.35	17.16	16.08	520.15	16.50	84.95	758.67	47.36	0.15	WSPA_098	754.84	14.38	12.32	546.01	14.34	71.93	625.63	39.74	0.12
WSPA_069	888.44	16.94	15.66	546.89	16.02	84.66	736.36	46.69	0.14	WSPA_099	738.93	14.23	12.10	392.24	14.10	71.15	612.45	39.59	0.12
WSPA_070	850.17	16.29	14.34	955.58	15.69	79.60	704.65	44.96	0.14	WSPA_100	771.58	14.82	12.63	302.13	14.71	73.55	639.51	41.18	0.12
WSPA_071	901.74	17.10	15.34	687.18	16.65	83.24	747.39	47.30	0.14	WSPA_101	774.88	14.80	12.57	544.86	14.70	73.70	642.25	41.15	0.12
WSPA_072	871.05	16.67	14.22	566.36	16.30	79.69	721.95	46.50	0.14	WSPA_102	837.46	15.86	13.96	594.84	15.55	77.56	694.11	44.84	0.13
WSPA_073	913.18	17.52	15.24	688.88	17.19	82.54	756.87	48.40	0.14	WSPA_104	1031.62	19.66	16.91	441.76	20.00	88.97	855.04	54.94	0.16
WSPA_074	847.70	16.11	13.93	461.07	15.82	78.08	702.60	45.47	0.13	WSPA_105	1010.25	19.09	17.94	693.61	18.54	91.68	837.33	52.72	0.16
WSPA_075	949.95	18.12	15.44	363.95	18.50	84.42	787.35	52.04	0.15	WSPA_106	927.60	17.13	15.25	687.44	17.52	82.72	768.82	47.89	0.14
WSPA_076	810.26	15.47	13.20	444.97	15.47	75.96	671.56	43.72	0.13	WSPA_108	757.69	14.54	12.31	411.31	14.84	72.39	628.00	40.31	0.12
WSPA_077	739.95	14.22	12.22	319.96	14.01	71.06	613.29	39.45	0.12	WSPA_109	806.81	15.01	12.62	524.39	15.23	73.65	668.71	41.51	0.12
WSPA_078	853.28	16.15	14.52	596.55	15.78	80.66	707.23	44.32	0.14	WSPA_110	875.32	16.45	14.75	958.23	16.26	80.95	725.49	46.08	0.14
WSPA_079	825.79	15.68	13.56	542.96	15.49	77.24	684.44	43.96	0.13	WSPA_111	848.21	16.13	13.90	438.00	15.83	78.92	703.02	45.02	0.13
WSPA_080	881.40	16.62	14.55	839.25	16.43	81.21	730.53	47.06	0.14	WSPA_112	938.47	17.63	15.37	588.72	17.68	84.02	777.83	49.53	0.15
WSPA_081	922.77	17.79	15.28	597.35	17.56	83.79	764.82	49.65	0.15	WSPA_113	905.46	17.36	15.17	517.17	17.24	82.99	750.47	48.37	0.14
WSPA_082	773.32	14.80	12.74	520.87	14.81	73.79	640.95	41.38	0.12	WSPA_114	744.31	14.24	12.22	449.26	14.30	71.86	616.90	39.57	0.12
WSPA_083	1102.80	21.43	18.39	750.09	21.81	91.89	914.03	60.43	0.17	WSPA_115	764.74	14.56	12.39	513.04	14.58	72.72	633.84	41.20	0.12
WSPA_085	831.33	15.45	13.15	467.77	15.34	75.19	689.03	43.55	0.13	WSPA_116	900.44	16.72	15.60	921.85	16.11	83.83	746.31	46.28	0.14
WSPA_086	1169.01	21.85	18.48	638.88	22.65	93.16	968.91	62.43	0.18	WSPA_117	890.28	16.70	15.24	512.02	16.38	82.57	737.89	46.35	0.14
WSPA_087	850.64	16.11	14.12	629.05	15.67	79.18	705.04	45.06	0.13	WSPA_118	803.78	15.81	13.79	469.49	15.30	76.33	666.20	42.46	0.13
WSPA_088	849.98	16.24	14.17	653.87	15.82	78.34	704.48	45.54	0.13	WSPA_119	757.54	14.40	12.41	330.36	14.53	73.14	627.87	40.52	0.12
WSPA_089	804.60	15.39	13.15	630.37	15.27	75.84	666.88	43.15	0.13	WSPA_121	1085.68	20.21	17.25	634.41	21.01	89.56	899.84	57.29	0.17
WSPA_090	717.63	13.84	11.72	177.06	13.84	69.87	594.79	38.73	0.12	WSPA_203	793.59	15.15	13.18	479.48	15.08	75.95	657.75	41.72	0.13
WSPA_091	915.23	17.46	15.36	441.79	17.24	82.50	758.57	49.46	0.14	WSPA_211	1547.86	31.06	25.10	1179.42	32.57	114.22	1282.91	86.78	0.25
WSPA_092	903.59	17.26	14.91	685.38	17.28	82.03	748.92	48.73	0.14	WSPA_213	748.10	14.34	12.23	331.17	14.34	71.78	620.05	39.78	0.12
WSPA_093	808.84	15.05	12.65	427.61	15.02	74.29	670.39	42.20	0.12	WSPA_215	766.54	14.04	11.95	613.09	13.77	71.14	635.33	39.44	0.12
Total Mean	**916.31**	**17.36**	**15.50**	**615.81**	**17.12**	**83.53**	**759.46**	**48.38**	**0.15**										
Total Min	**561.37**	**13.84**	**10.74**	**9.47**	**13.84**	**10.15**	**59.13**	**38.73**	**0.12**										
Total Max	**1547.86**	**31.06**	**25.10**	**1179.42**	**32.57**	**114.22**	**1282.91**	**86.78**	**0.25**										
n	**113**	**113**	**113**	**113**	**113**	**113**	**113**	**113**	**113**										

Table 7-8 Is a continuation of Table 5b with the averages and ranges highlighted below. 2/2

Code	Sr/Ca	Mg/Ca	Ca/Cl	Mg/Cl	Ωcalcite	Ωarag	Code	Sr/Ca	Mg/Ca	Ca/Cl	Mg/Cl	Ωcalcite	Ωarag
WSPA_004	8.70	4.95	18.80	93.03	2.82	1.93	WSPA_035	8.26	4.78	18.96	90.66	2.80	1.91
WSPA_005	8.49	4.96	18.66	92.56	2.19	1.50	WSPA_036	8.61	4.85	18.63	90.32	3.94	2.69
WSPA_006	8.53	4.96	18.89	93.73	0.23	0.16	WSPA_037	8.35	4.72	19.11	90.17	3.47	2.37
WSPA_007	8.46	4.88	18.87	92.12	2.95	2.01	WSPA_038	8.26	4.42	18.73	82.70	3.66	2.51
WSPA_008	8.35	4.91	18.96	93.16	3.16	2.16	WSPA_039	8.59	4.72	18.95	89.51	3.25	2.22
WSPA_009	8.49	4.78	18.98	90.76	3.50	2.39	WSPA_040	8.19	4.85	19.12	92.64	3.05	2.09
WSPA_010	8.72	4.81	18.50	88.93	1.87	1.28	WSPA_041	8.21	4.00	19.07	76.27	1.95	1.33
WSPA_011	8.54	4.96	18.94	94.01	3.18	2.18	WSPA_042	8.60	5.00	18.46	92.23	3.45	2.36
WSPA_012	8.59	4.96	18.93	93.90	3.80	2.60	WSPA_043	8.32	4.71	19.03	89.69	2.26	1.55
WSPA_013	8.48	4.94	18.96	93.60	3.99	2.73	WSPA_044	8.48	4.81	18.65	89.59	4.36	2.98
WSPA_014	8.31	4.87	19.12	93.22	3.34	2.28	WSPA_045	8.20	4.87	19.05	92.80	10.19	6.97
WSPA_015	8.23	4.65	19.02	88.51	3.29	2.25	WSPA_046	8.33	4.86	19.04	92.46	5.98	4.09
WSPA_016	9.11	4.69	19.02	89.14	3.21	2.19	WSPA_047	8.30	4.89	19.13	93.60	4.41	3.02
WSPA_018	8.79	4.84	18.37	88.88	3.81	2.60	WSPA_048	8.47	4.92	19.05	93.78	4.27	2.92
WSPA_019	8.66	4.97	18.80	93.53	2.24	1.53	WSPA_049	8.14	4.81	19.09	91.85	3.71	2.54
WSPA_020	8.54	5.00	18.83	94.23	3.97	2.72	WSPA_050	8.23	4.89	19.09	93.38	6.06	4.15
WSPA_021	8.25	4.89	19.02	92.94	2.80	1.92	WSPA_051	8.31	4.92	19.10	93.89	4.47	3.06
WSPA_022	8.39	4.68	18.80	88.06	2.86	1.96	WSPA_052	8.38	4.90	18.95	92.76	0.37	0.25
WSPA_023	8.23	4.64	19.10	88.52	2.36	1.62	WSPA_053	8.45	4.87	18.72	91.25	4.15	2.84
WSPA_024	8.69	4.87	18.75	91.38	2.01	1.37	WSPA_054	8.38	4.72	18.89	89.19	2.90	1.98
WSPA_025	8.39	4.94	18.97	93.70	2.28	1.56	WSPA_055	8.16	4.81	19.20	92.39	4.27	2.92
WSPA_026	8.57	4.96	18.91	93.80	3.35	2.29	WSPA_056	8.33	4.85	18.87	91.46	4.15	2.84
WSPA_027	8.40	4.80	18.97	91.14	2.84	1.95	WSPA_058	8.29	4.64	19.05	88.44	4.10	2.80
WSPA_028	8.77	4.67	18.30	85.40	2.54	1.74	WSPA_060	8.38	5.50	19.14	105.34	3.34	2.28
WSPA_029	8.64	4.70	18.55	87.17	2.48	1.70	WSPA_061	8.43	4.69	18.55	87.09	0.90	0.62
WSPA_030	8.74	4.83	18.66	90.16	2.67	1.83	WSPA_062	8.29	4.73	18.54	87.64	4.28	2.93
WSPA_031	8.69	4.90	18.81	92.26	4.42	3.03	WSPA_063	8.47	4.96	18.90	93.80	2.47	1.69
WSPA_032	8.69	4.82	18.56	89.46	2.76	1.89	WSPA_064	8.33	4.96	19.04	94.37	4.14	2.83
WSPA_034	8.35	4.93	19.04	93.91	3.22	2.20							

Table 7-9 Trace Metal Ratios and saturation state results from Hamelin Pool basinal.

Code	Sr/Ca	Mg/Ca	Ca/Cl	Mg/Cl	Ωcalcite	Ωarag	Code	Sr/Ca	Mg/Ca	Ca/Cl	Mg/Cl	Ωcalcite	Ωarag
WSPA_065	8.30	4.82	18.92	91.28	2.78	1.91	WSPA_094	8.18	4.94	19.23	94.91	3.89	2.66
WSPA_066	8.16	4.81	19.07	91.67	3.46	2.37	WSPA_095	8.24	4.98	19.01	94.59	3.51	2.40
WSPA_067	8.21	4.74	19.15	90.80	3.46	2.37	WSPA_097	8.20	4.99	19.10	95.35	3.91	2.68
WSPA_068	8.54	4.95	18.74	92.81	4.66	3.19	WSPA_098	8.28	5.00	19.05	95.30	4.37	2.99
WSPA_069	8.39	5.00	19.06	95.29	1.37	0.94	WSPA_099	8.26	5.00	19.26	96.28	3.90	2.67
WSPA_070	8.34	4.89	19.16	93.63	3.09	2.12	WSPA_100	8.27	4.96	19.20	95.32	3.17	2.17
WSPA_071	8.34	4.87	18.96	92.31	4.41	3.02	WSPA_101	8.24	4.98	19.10	95.12	3.23	2.21
WSPA_072	8.16	4.78	19.14	91.48	3.64	2.49	WSPA_102	8.34	4.89	18.93	92.61	4.03	2.75
WSPA_073	8.18	4.71	19.18	90.39	3.75	2.56	WSPA_104	8.19	4.52	19.06	86.24	3.66	2.50
WSPA_074	8.33	4.85	19.01	92.11	3.79	2.59	WSPA_105	8.54	4.80	18.90	90.75	3.00	2.06
WSPA_075	8.18	4.66	19.08	88.86	1.65	1.13	WSPA_106	8.39	4.83	18.47	89.18	3.50	2.39
WSPA_076	8.30	4.91	19.09	93.75	3.20	2.19	WSPA_108	8.21	4.98	19.18	95.54	3.47	2.37
WSPA_077	8.29	5.00	19.21	96.03	3.77	2.58	WSPA_109	8.25	4.91	18.61	91.28	3.11	2.12
WSPA_078	8.44	5.00	18.92	94.53	1.89	1.29	WSPA_110	8.31	4.92	18.80	92.48	3.30	2.26
WSPA_079	8.32	4.93	18.99	93.54	1.36	0.93	WSPA_111	8.29	4.89	19.01	93.05	2.96	2.02
WSPA_080	8.22	4.89	18.86	92.14	3.06	2.09	WSPA_112	8.26	4.77	18.79	89.53	3.59	2.45
WSPA_081	8.21	4.71	19.28	90.81	3.22	2.20	WSPA_113	8.23	4.78	19.17	91.66	3.47	2.37
WSPA_082	8.26	4.99	19.14	95.41	3.97	2.72	WSPA_114	8.28	5.05	19.13	96.55	3.35	2.29
WSPA_083	7.97	4.29	19.43	83.32	3.98	2.72	WSPA_115	8.27	4.99	19.04	95.09	3.56	2.43
WSPA_085	8.26	4.87	18.58	90.44	1.59	1.09	WSPA_116	8.60	5.01	18.57	93.10	3.82	2.61
WSPA_086	8.12	4.26	18.69	79.69	3.25	2.22	WSPA_117	8.38	4.94	18.76	92.75	3.13	2.14
WSPA_087	8.33	4.91	18.94	93.08	4.52	3.09	WSPA_118	8.31	4.83	19.67	94.97	2.93	2.00
WSPA_088	8.24	4.82	19.10	92.16	2.86	1.96	WSPA_119	8.28	5.08	19.01	96.55	2.78	1.90
WSPA_089	8.34	4.93	19.13	94.25	3.53	2.41	WSPA_121	8.21	4.43	18.62	82.49	3.35	2.29
WSPA_090	8.32	5.05	19.28	97.36	3.13	2.14	WSPA_203	8.33	5.01	19.09	95.71	3.07	2.10
WSPA_091	8.17	4.72	19.08	90.14	4.01	2.74	WSPA_211	8.08	3.68	20.06	73.79	3.63	2.48
WSPA_092	8.20	4.75	19.11	90.78	3.45	2.36	WSPA_213	8.33	5.01	19.16	95.95	3.73	2.55
WSPA_093	8.22	4.94	18.61	91.85	2.84	1.94	WSPA_215	8.28	5.07	18.32	92.81	0.91	0.62
Total Mean	8.36	4.84	18.95	91.68	3.31	2.27							
Total Min	7.97	3.68	18.30	73.79	0.23	0.16							
Total Max	9.11	5.50	20.06	105.34	10.19	6.97							
n	113.00	113.00	113.00	113.00	113.00	113.00							

Table 7-10 Continuation of table 12 trace metal ratios and saturation state results from Hamelin Pool basinal waters. 2/2

Code	Long	Lat	> φ-1 wt%	φ-1 - φ0 wt%	φ0 - φ1 wt%	φ1 - φ2 wt%	φ2 - φ3 wt%	φ3 - φ4 wt%	< φ4 wt%
140317_T1_14	114.1675	-26.2473	18.20	18.90	24.87	22.53	12.17	2.95	0.38
140317_T1_7	114.1941	-26.2437	46.73	21.88	16.12	6.12	6.29	2.49	0.36
140317_T2_10	114.2278	-26.3021	46.63	10.53	12.36	17.84	9.97	2.67	0.00
140317_T2_2	114.1898	-26.2996	29.47	19.03	23.59	18.87	7.62	1.28	0.15
140317_T2_5	113.9728	-26.3019	35.80	4.50	8.94	42.60	7.73	0.38	0.05
140317_T2_8	114.2147	-26.3023	56.23	15.85	14.16	9.39	3.80	0.45	0.12
140318_T1_3	114.1810	-26.1799	53.00	19.79	0.00	17.17	7.69	2.09	0.26
140318_T3_3	114.2102	-26.2683	25.61	15.33	23.77	21.53	11.88	1.88	0.00
140318_T3_4	114.2092	-26.2693	29.21	17.10	18.78	18.53	12.54	3.02	0.82
140319_T1_5	114.0366	-26.3896	65.24	7.66	4.11	7.48	10.95	4.56	0.00
140319_T1_9	114.0348	-26.3910	5.11	15.99	30.80	43.50	4.46	0.14	0.00
140319_T2_5	114.0218	-26.3793	4.41	23.01	36.61	31.55	4.30	0.12	0.00
140321_T1_1	113.9948	-26.1764	21.88	23.66	15.31	19.25	12.39	5.63	1.88
140321_T1_3	113.9831	-26.1804	72.22	16.67	2.78	2.78	2.78	2.78	0.00
140321_T1_6	113.9618	-26.1845	40.36	18.46	19.79	15.93	4.33	1.01	0.12
140321_T1_8	113.9543	-26.1839	50.43	13.45	19.70	13.54	2.51	0.32	0.06
140322_T1_1	114.0081	-26.2327	17.84	20.03	23.02	21.63	12.45	4.33	0.69
140322_T1_14	113.9737	-26.2332	55.61	10.13	8.41	15.30	9.58	0.97	0.00
140322_T1_2	114.0043	-26.2304	19.98	39.73	39.44	0.76	0.10	0.00	0.00
140322_T1_20	113.9685	-26.2462	24.52	29.41	35.45	6.90	1.86	1.02	0.84
140322_T1_22	113.9656	-26.2470	33.69	9.61	7.86	20.07	24.22	4.34	0.22
140322_T1_6	114.0004	-26.2238	32.73	13.99	28.22	18.51	5.74	0.72	0.09
140322_T1_8	113.9930	-26.2119	26.53	12.81	16.86	17.58	16.00	8.67	1.55
140322_T2_6	113.9819	-26.2725	11.89	3.11	28.72	54.75	1.54	0.00	0.00
140324_T1_10b	113.9759	-26.2817	22.40	6.06	16.22	40.65	14.49	0.12	0.06
140324_T1_14	113.9701	-26.2824	30.51	8.51	16.09	33.43	10.45	0.90	0.12
140324_T1_2	113.9898	-26.2836	49.80	18.26	17.69	9.05	4.89	0.08	0.24
140324_T1_7	113.9815	-26.2833	20.01	15.93	37.69	19.42	6.26	0.67	0.03
140324_T1_8	113.9805	-26.2829	40.49	36.61	15.84	5.10	1.67	0.29	0.00
140324_T1_9	114.1907	-26.2448	27.32	16.12	24.12	21.45	9.84	1.11	0.04
140324_T1_start	113.9919	-26.2835	51.05	5.99	7.49	14.97	16.69	3.74	0.07
140324_T2_5	113.9926	-26.3009	24.08	5.85	11.73	41.03	15.90	1.25	0.16
140324_T3_1	114.0024	-26.3203	40.37	16.17	9.38	14.16	12.39	5.09	2.43

Table 7-11 The weight percent results from the dry sieving of Hamelin Pool sediments. 1/5.

Code	Long	Lat	> φ-1wt%	φ-1 - φ0wt%	φ0 - φ1wt%	φ1 - φ2wt%	φ2 - φ3wt%	φ3 - φ4wt%	< φ4wt%
140324_t3_2_spaven	113.9901	-26.3237	49.78	10.89	8.65	13.24	13.39	3.66	0.39
140324_T3_5a	113.9853	-26.3245	82.31	6.73	3.77	5.15	1.74	0.21	0.09
140324_t5_2 boolodah	114.1599	-26.3250	63.60	8.09	14.71	10.29	2.94	0.37	0.00
140324_t5_6 booldah	114.1686	-26.3336	41.56	9.60	16.22	23.58	8.61	0.40	0.03
140325_T1_1	114.1996	-26.3020	22.89	13.15	22.55	26.60	13.22	1.46	0.14
140325_T1_11	114.2243	-26.3181	52.55	14.48	13.20	12.44	6.35	0.88	0.11
140325_T1_12	114.2199	-26.3229	14.68	9.81	20.60	32.36	20.07	2.48	0.00
140325_T1_3	114.2188	-26.3233	36.77	23.71	16.85	15.10	6.45	0.99	0.14
140325_T1_6	114.2110	-26.3073	31.85	34.72	23.50	7.81	1.79	0.29	0.04
140325_T2_1	114.2156	-26.3283	8.70	4.11	12.66	51.58	22.63	0.16	0.16
140325_T2_4	114.2123	-26.3245	37.53	14.80	15.12	19.09	12.97	0.50	0.00
140325_T2_8	114.1918	-26.3220	24.60	18.51	29.19	19.62	7.35	0.72	0.00
140329_T1_Start	114.0745	-26.4135	42.50	15.46	11.80	14.81	10.65	4.28	0.50
140330 SedTrapMe	114.2158	-26.2652	33.04	21.29	19.52	15.69	8.08	2.11	0.29
140330_T1_03	114.1557	-26.3562	28.19	21.96	18.62	17.78	9.13	3.45	0.88
140330_T1_4	114.1590	-26.3593	20.31	18.00	19.78	22.56	12.43	5.62	1.30
140330_T1_Start	114.1414	-26.3453	23.78	38.38	17.30	8.65	5.41	4.32	2.16
140331_T1_1	113.9428	-26.0006	0.17	2.67	12.15	49.52	34.82	0.67	0.00
140331_T1_3	113.9231	-25.9927	8.55	2.83	3.58	11.18	67.22	6.63	0.00
140331_T1_5	113.9132	-25.9890	9.94	7.36	26.25	36.76	19.16	0.52	0.00
140331_T1_8	113.9088	-25.9958	70.10	2.05	1.95	16.59	8.60	0.51	0.20
140331_T1_Start	113.9462	-26.0026	7.55	17.08	31.22	21.35	16.68	5.79	0.34
140331_T2_Start	113.9099	-26.0044	11.83	7.54	12.07	42.66	19.05	5.45	1.40
140331_T4_01	113.9134	-26.0325	10.72	2.97	10.90	43.92	30.99	0.49	0.00
140331_T5_8	113.9265	-26.0618	5.41	5.02	14.59	53.60	13.52	4.98	2.87
140401_01	114.1705	-26.0146	1.04	1.37	5.28	63.75	28.49	0.08	0.00
140401_02	114.1759	-26.0150	4.83	2.97	9.87	53.26	27.85	1.16	0.07
140401_04	114.1870	-26.0100	87.21	2.12	1.94	4.87	3.17	0.57	0.13
140401_04b	114.1870	-26.0100	7.24	2.21	6.18	17.88	65.34	1.13	0.02
140401_07	114.1338	-26.0126	15.05	4.50	44.79	21.36	12.15	2.11	0.04
140401_07B	114.1338	-26.0126	4.93	11.17	64.55	15.87	2.91	0.56	0.00
140401_08	114.2004	-26.0327	37.59	12.32	18.32	24.69	6.27	0.73	0.07

Table 7-12 The weight percent results from the dry sieving of Hamelin Pool sediments. 2/5

Code	Long	Lat	> φ-1wt%	φ-1 - φ0wt%	φ0 - φ1wt%	φ1 - φ2wt%	φ2 - φ3wt%	φ3 - φ4wt%	< φ4wt%
140401_12	114.1914	-26.0436	5.11	3.05	9.79	10.12	25.85	44.08	2.00
140401_15	114.1758	-26.0565	14.20	16.22	21.84	23.00	16.70	6.64	1.40
140401_16 hutch	114.2024	-26.0520	32.87	16.84	17.85	24.83	7.53	0.07	0.00
140401_36	114.2126	-26.0482	18.83	14.49	33.36	24.54	6.50	2.06	0.22
140406_Black Line	114.2146	-26.0657	15.59	4.61	9.66	12.75	33.52	22.35	1.52
140406_Hutch_05	114.2235	-26.0631	2.78	0.89	3.19	29.79	62.34	1.01	0.00
140406_Hutch_34	114.1846	-26.1449	28.72	8.47	19.59	38.67	4.53	0.02	0.00
140407_05_FP	114.1371	-26.3855	19.48	25.00	14.98	14.19	15.32	9.12	1.91
140407_05_NIL	114.1226	-26.4213	37.85	14.68	17.59	18.41	10.13	1.34	0.00
140407_Flag_02	114.1481	-26.4043	46.32	17.45	17.01	13.73	4.96	0.53	0.00
140407_Flag_03	114.1457	-26.3993	52.03	18.07	10.63	10.57	7.32	1.31	0.06
140407_Flag_06	114.1355	-26.3679	44.66	10.59	12.50	17.15	13.26	1.83	0.00
140407_Flag_07	114.1492	-26.3741	43.93	16.25	14.38	14.62	8.28	2.30	0.24
140407_Flag_14	114.2098	-26.3268	28.85	24.08	23.13	20.38	3.09	0.47	0.00
140407_Nil_02	114.1170	-26.4041	34.37	21.34	15.19	17.91	9.11	1.84	0.24
140408_Carbla_02	114.2307	-26.2975	7.49	18.61	53.02	17.83	2.89	0.13	0.03
140408_Flag_12	114.1978	-26.3192	35.19	20.20	23.71	13.21	6.27	1.33	0.09
140410_Nanga_04	113.9307	-26.0714	36.97	15.16	21.55	21.19	4.69	0.43	0.00
140410_Nanga_34	113.9150	-26.1078	39.49	27.57	19.45	10.05	3.37	0.06	0.00
140414_Carbla_16b	114.1887	-26.2565	43.20	17.88	15.85	14.83	7.17	1.02	0.04
GTH 12	114.1818	-26.1469	10.25	1.55	5.90	73.88	8.30	0.11	0.00
HP13_43_10	114.1014	-26.4414	0.90	0.49	1.55	9.70	86.56	0.80	0.00
HP13_43_15	144.1031	-26.4396	49.89	13.45	13.68	12.41	7.93	2.41	0.23
HP13_43_2	114.0965	-26.4529	6.05	7.61	9.16	15.39	29.34	24.03	8.41
HP13_43_5	114.0964	-26.4497	8.01	2.27	4.79	15.77	38.55	29.27	1.32
HP13_43_6	114.0964	-26.4488	6.66	1.75	2.20	8.07	54.18	26.58	0.56
HP13_77_12	114.2357	-26.0847	33.39	28.55	21.65	11.90	3.25	0.87	0.40
HP13_F003	113.9817	-26.3532	15.02	26.39	45.84	9.93	2.03	0.78	0.00
HP13_F010	113.9120	-25.9858	5.15	5.15	5.87	10.66	69.29	3.88	0.00
HP13_F012	113.9058	-25.9931	0.05	0.00	0.40	61.25	37.94	0.35	0.00
HP13_J002	114.1903	-26.1197	81.96	0.31	2.45	4.59	10.70	0.00	0.00
HP13_P000	114.0317	-26.2592	52.51	26.94	10.05	5.94	4.11	0.46	0.00

Table 7-13 The weight percent results from the dry sieving of Hamelin Pool sediments. 3/5

Code	Long	Lat	> φ-1wt%	φ-1 - φ0wt%	φ0 - φ1wt%	φ1 - φ2wt%	φ2 - φ3wt%	φ3 - φ4wt%	< φ4wt%
HP13_P002	113.9861	-26.0014	2.18	4.04	7.95	6.67	22.88	49.42	6.86
HP13_P003	113.9865	-26.0451	20.56	11.34	15.34	19.95	21.29	8.73	2.79
HP13_P004	113.9867	-26.0891	10.02	17.72	28.23	24.30	15.24	3.93	0.56
HP13_P005	113.9868	-26.1356	17.59	16.29	18.68	22.69	13.90	5.43	5.43
HP13_P006	113.9869	-26.1815	36.63	22.74	11.37	12.00	11.37	4.63	1.26
HP13_P007	113.9873	-26.2349	26.60	12.17	18.33	23.56	17.24	2.11	0.00
HP13_P008	113.9875	-26.2915	21.70	29.66	15.34	16.36	9.66	6.02	1.25
HP13_P009	114.0607	-26.0031	2.19	9.27	30.83	45.38	12.33	0.00	0.00
HP13_P010	114.0625	-26.0483	19.89	17.95	21.42	24.25	14.55	1.94	0.00
HP13_P011	114.0603	-26.0950	52.85	13.31	11.89	9.55	7.32	4.27	0.81
HP13_P012	114.0629	-26.1390	8.50	11.81	17.36	24.02	32.89	5.10	0.32
HP13_P013	114.0631	-26.1884	59.82	24.11	9.82	5.80	0.45	0.00	0.00
HP13_P014	114.0633	-26.2387	20.26	26.91	19.73	17.84	10.43	4.31	0.53
HP13_P015	114.0636	-26.2926	17.15	25.28	14.74	15.05	15.35	8.93	3.51
HP13_P016	114.0640	-26.3501	61.47	15.41	6.83	6.48	6.13	2.63	1.05
HP13_P017	114.0640	-26.4006	32.23	11.65	9.42	17.44	19.34	9.17	0.74
HP13_P018	114.0625	-26.0483	0.82	5.06	33.71	36.16	17.19	5.88	1.19
HP13_P019	114.1316	-26.0510	35.05	14.06	14.01	17.25	15.31	3.73	0.59
HP13_P021	114.1320	-26.1399	25.45	13.43	28.44	23.96	7.86	0.79	0.08
HP13_P022	114.1322	-26.1902	38.87	24.61	19.62	11.24	4.34	1.25	0.07
HP13_P023	114.1324	-26.2405	19.73	18.27	25.53	21.72	11.83	2.81	0.12
HP13_P024	114.1327	-26.2953	29.35	22.97	19.08	14.73	8.53	4.42	0.92
HP13_P025	114.1329	-26.3519	93.64	5.45	0.00	0.00	0.00	0.00	0.91
HP13_P026	114.1331	-26.3979	30.06	16.01	13.42	18.92	15.38	5.57	0.63
HP13_P028	114.1890	-26.0554	55.53	8.61	7.65	7.42	9.13	10.47	1.19
HP13_P029	114.1890	-26.0950	32.88	14.48	25.51	17.65	8.02	1.45	0.00
HP13_P030	114.1897	-26.2432	16.24	17.38	32.23	23.93	9.52	0.70	0.00
HP13_P031	114.1890	-26.2953	33.41	19.21	23.25	18.23	5.46	0.44	0.00
HP13_P032	114.1890	-26.3483	75.72	9.83	4.28	5.20	4.05	0.81	0.12

Table 7-14 The weight percent results from the dry sieving of Hamelin Pool Sediments. 4/5

Code	Long	Lat	> φ-1wt%	φ-1 - φ0wt%	φ0 - φ1wt%	φ1 - φ2wt%	φ2 - φ3wt%	φ3 - φ4wt%	< φ4wt%
HP13_P033	114.0318	-26.2592	23.36	23.96	19.49	19.12	10.34	3.20	0.52
HP13_S44_4	114.1113	-26.4337	8.54	15.12	37.23	35.32	3.57	0.21	0.00
HP13_S45_1	114.1172	-26.4313	25.90	16.06	16.47	24.20	17.37	0.00	0.00
HP13_S45_2	114.1170	-26.4303	24.53	13.63	33.59	24.89	3.32	0.00	0.04
HP13_S45_4	114.1151	-26.4282	4.46	2.16	5.66	15.22	72.06	0.43	0.00
HP13_S45_4.1	114.1202	-26.4297	10.23	6.79	10.46	20.02	33.59	14.91	4.00
HP13_ST11_01	114.1642	-26.0892	23.87	23.34	18.57	20.95	10.08	3.18	0.00
HP13_ST11_02	114.1796	-26.0857	32.86	22.89	15.61	13.26	8.57	5.75	1.06
HP13_ST11_03	114.1901	-26.0833	0.13	4.78	21.60	50.20	23.02	0.27	0.00
HP13_ST11_04	114.1961	-26.0820	15.90	10.99	40.81	25.43	6.84	0.04	0.00
HP13_ST11_05	114.2024	-26.0805	8.40	4.01	8.68	35.30	43.23	0.38	0.00
HP13_ST11_06	114.2102	-26.0788	5.96	1.47	3.70	46.26	41.02	1.59	0.00
HP13_ST11_07	114.2148	-26.0777	38.76	1.61	3.61	8.16	26.45	20.38	1.03
HP13_ST11_08	114.2206	-26.0764	47.60	2.31	7.89	15.06	15.06	11.60	0.49
HP13_ST11_09	114.2259	-26.0752	71.83	4.94	6.25	4.94	5.30	6.75	0.00
HP13_ST11_10	114.2299	-26.0743	67.21	6.70	8.77	9.41	6.56	1.35	0.00
HP13_ST11_11	114.2308	-26.0741	60.64	4.23	4.94	14.94	12.82	2.37	0.06
HP13_ST11_12	114.2311	-26.0741	48.68	3.13	8.58	17.36	19.99	2.26	0.00
Light	114.1341	-26.4152	28.87	9.47	22.12	28.06	11.02	0.46	0.00
P34	113.9324	-26.0131	8.23	1.66	3.50	4.99	21.45	56.30	3.85
P35	113.9481	-26.0482	35.43	7.56	11.34	14.57	16.53	11.76	2.80

Table 7-15 The weight percent results from the dry sieving of Hamelin Pool sediments. 5/5

Code	Long	Lat	% Arag	% HMC	$\delta^{13}C$‰	$\delta^{18}O$‰	Code	Long	Lat	% Arag	% HMC	$\delta^{13}C$‰	$\delta^{18}O$‰
140330 SedTrapMe	114.2158	-26.2652	0.95	0.05	5.01	3.53	HP13_P027	114.1890	-26.0193	0.87	0.14	3.61	2.56
HP13_43_10	114.1014	-26.4414	0.86	0.15	5.33	3.39	HP13_P028	114.1890	-26.0554	0.91	0.10	3.94	3.31
HP13_43_15	114.1031	-26.4396	0.83	0.18	5.46	3.49	HP13_P029	114.1890	-26.0950	0.69	0.33	3.64	2.87
HP13_43_2	114.0965	-26.4529	0.90	0.11	5.66	3.67	HP13_P030	114.1897	-26.2432	0.74	0.28	4.99	3.51
HP13_43_6	114.0964	-26.4488	0.93	0.07	5.31	3.51	HP13_P031	114.1890	-26.2953	0.91	0.09	5.23	3.39
HP13_F003	113.9817	-26.3532	0.88	0.13	5.80	3.52	HP13_P032	114.1890	-26.3483	0.90	0.11	5.00	3.60
HP13_F010	113.9120	-25.9858	0.78	0.24	4.66	2.81	HP13_P033	114.0318	-26.2592	0.80	0.21	4.18	3.37
HP13_F011	113.9075	-25.9904	0.77	0.24	5.01	3.06	HP13_S45_2	114.1170	-26.4303	0.96	0.04	5.26	3.59
HP13_F012	113.9058	-25.9931	0.91	0.09	5.00	2.99	HP13_S45_4	114.1151	-26.4282	0.79	0.22	5.15	3.40
HP13_J002	114.1903	-26.1197	0.92	0.08	3.96	3.17	HP13_ST1_CM	113.9194	-26.0475	0.97	0.03	4.50	3.20
HP13_P001	114.2334	-26.3065	0.87	0.14	4.52	3.17	HP13_ST1_ME	113.9287	-26.0439	0.44	0.60	3.37	3.02
HP13_P002	113.9861	-26.0014	0.52	0.50	3.05	2.23	HP13_ST10_ME	114.1457	-26.1864	0.94	0.06	4.71	3.54
HP13_P003	113.9865	-26.0451	0.81	0.20	3.49	3.06	HP13_ST11_02	114.1796	-26.0857	0.78	0.23	4.41	3.10
HP13_P004	113.9867	-26.0891	0.77	0.20	4.12	3.02	HP13_ST11_03	114.1901	-26.0833	0.58	0.44	3.76	2.83
HP13_P005	113.9868	-26.1356	0.80	0.21	3.80	2.72	HP13_ST11_04	114.1961	-26.0820	0.90	0.10	4.35	3.13
HP13_P006	113.9869	-26.1815	0.63	0.39	4.14	2.88	HP13_ST11_05	114.2024	-26.0805	0.86	0.15	4.34	3.11
HP13_P007	113.9873	-26.2349	0.88	0.13	4.35	3.34	HP13_ST11_06	114.2102	-26.0788	0.92	0.09	4.29	3.12
HP13_P008	113.9875	-26.2915	0.83	0.18	4.47	3.14	HP13_ST11_07	114.2148	-26.0777	0.84	0.17	3.86	3.16
HP13_P009	114.0607	-26.0031	0.67	0.35	3.11	2.17	HP13_ST11_08	114.2206	-26.0764	0.84	0.17	4.08	3.21
HP13_P010	114.0625	-26.0483	0.76	0.25	3.42	2.94	HP13_ST11_09	114.2259	-26.0752	0.93	0.07	4.31	3.35
HP13_P011	114.0603	-26.0950	0.92	0.09	4.01	3.10	HP13_ST11_10	114.2299	-26.0743	0.92	0.08	3.48	4.07
HP13_P013	114.0631	-26.1884	0.89	0.11	4.36	3.40	HP13_ST11_11	114.2308	-26.0741	0.89	0.11	4.06	3.17
HP13_P014	114.0633	-26.2387	0.85	0.12	4.62	3.20	HP13_ST11_12	114.2311	-26.0741	0.85	0.16	4.35	3.13
HP13_P015	114.0636	-26.2926	0.83	0.18	4.24	2.95	HP13_ST11_CM	114.2000	-26.0807	0.88	0.13	4.36	3.16
HP13_P016	114.0640	-26.3501	0.62	0.40	3.75	3.08	HP13_ST11_ME	114.1462	-26.0933	0.79	0.23	4.71	3.60
HP13_P017	114.0640	-26.4006	0.98	0.03	4.97	3.56	HP13_ST3_01	114.0225	-26.2082	0.84	0.17	4.54	3.42
HP13_P018	114.0625	-26.0483	0.35	0.68	3.34	2.54	HP13_ST3_CM	113.9925	-26.2156	0.89	0.12	4.06	3.26
HP13_P019	114.1316	-26.0510	0.91	0.10	3.76	3.17	HP13_ST4_ME	114.0044	-26.3416	0.95	0.05	4.92	3.74
HP13_P020	114.1318	-26.0968	0.88	0.13	4.10	3.47	HP13_ST5_ME	114.0639	-26.4049	0.91	0.09	4.97	3.64
HP13_P021	114.1320	-26.1399	0.85	0.16	4.45	3.08	HP13_ST6_ME	114.0854	-26.4398	0.91	0.09	5.19	3.73
HP13_P022	114.1322	-26.1902	0.87	0.14	4.75	3.34	HP13_ST7a_ME	114.1453	-26.3827	0.92	0.09	4.53	3.82
HP13_P024	114.1327	-26.2953	0.83	0.18	4.87	3.40	HP13_ST8_ME	114.1369	-26.3302	0.71	0.30	4.28	3.47
HP13_P025	114.1329	-26.3519	0.49	0.54	3.68	2.75	HP13_ST9a_ME	114.5753	-26.2650	0.92	0.08	5.62	3.33
HP13_P026	114.1331	-26.3979	0.90	0.11	4.46	3.71							
Mean			0.83	0.18	4.40	3.23							
Max			0.98	0.68	5.80	4.07							
Min			0.35	0.03	3.05	2.17							
n			67.00	67.00	67.00	67.00							

Table 7-16 Mineralogic and inorganic stable istopes data of 2013 Hamelin Pool sediements.

Code	Long	Lat	% Arag	% HMC	Code	Long	Lat	% Arag	% HMC
140317_21	114.2278	-26.3021	0.92	0.08	140322_T2_10	113.9986	-26.2733	0.84	0.17
140317_T1_14	114.1675	-26.2473	0.88	0.13	140322_T2_3	113.9715	-26.2731	0.96	0.04
140317_T1_15	114.1898	-26.2996	0.77	0.24	140322_T2_6	113.9819	-26.2725	0.96	0.05
140317_T1_19	114.2147	-26.3023	0.81	0.20	140324_t1_1	113.9900	-26.2835	0.92	0.08
140317_T1_7	114.1941	-26.2437	0.95	0.05	140324_T1_10b	113.9759	-26.2817	0.96	0.04
140318_T1_13	114.1572	-26.1811	0.92	0.08	140324_T1_14	113.9701	-26.2824	0.96	0.04
140318_T1_2	114.1854	-26.1798	0.94	0.07	140324_T1_2	113.9898	-26.2836	0.92	0.09
140318_T1_3	114.1810	-26.1799	0.87	0.14	140324_T1_3	113.9875	-26.2835	0.93	0.07
140318_T1_5	114.1767	-26.1797	0.93	0.07	140324_T1_7	113.9815	-26.2833	0.90	0.11
140319_T1_1	114.0513	-26.3705	0.80	0.21	140324_T1_9	113.9799	-26.2831	0.95	0.05
140319_T1_4	114.0388	-26.3867	0.95	0.05	140324_T1_start	113.9919	-26.2835	0.92	0.09
140319_T1_5	114.0366	-26.3896	0.96	0.04	140324_T2_4	113.9860	-26.3010	0.96	0.04
140319_T1_6	114.0360	-26.3898	0.96	0.04	140324_T2_5	113.9926	-26.3009	0.95	0.05
140319_T1_9	114.0348	-26.3910	0.96	0.04	140324_T2_6	113.9998	-26.3013	0.77	0.25
140319_T2_4	114.0162	-26.3713	0.94	0.06	140324_T3_1	114.0024	-26.3203	0.83	0.18
140319_T2_5	114.0218	-26.3793	0.91	0.09	140324_t3_2_spaven	113.9901	-26.3237	0.94	0.06
140321_T1_12a	113.9440	-26.1848	0.95	0.05	140324_T3_2b	113.9901	-26.3237	0.93	0.07
140321_T1_3	113.9831	-26.1804	0.74	0.27	140324_T3_5a	113.9853	-26.3245	0.96	0.04
140321_T1_4	113.9748	-26.1817	0.83	0.18	140324_t5_1 booldah	114.1578	-26.3245	0.83	0.18
140321_T1_6	113.9618	-26.1845	0.93	0.08	140324_T5_2	114.1599	-26.3250	0.93	0.07
140321_T1_7	113.9593	-26.1839	0.95	0.05	140324_T5_6	114.1686	-26.3336	0.94	0.07
140321_T1_8	113.9543	-26.1839	0.96	0.05	140324_t5_start booldah	114.1545	-26.3236	0.74	0.27
140322_T1_1	114.0081	-26.2327	0.83	0.18	140324-t1-13	113.9718	-26.2814	0.97	0.03
140322_T1_16	113.9728	-26.2412	0.98	0.03	140324-t3-4	113.9861	-26.3242	0.95	0.05
140322_T1_17	113.9710	-26.2445	0.85	0.16	140324-t4-3	114.0021	-26.3524	0.89	0.12
140322_T1_2	114.0043	-26.2304	0.94	0.06	140324-t5-2	114.1599	-26.3250	0.93	0.07
140322_T1_22	113.9656	-26.2470	0.94	0.06	140324-t5-6	114.1686	-26.3336	0.94	0.07
140322_T1_3	114.0041	-26.2289	0.91	0.10	140325 gth 12	114.1818	-26.1469	0.94	0.06
140322_T1_6	114.0004	-26.2238	0.95	0.05	140325_T1_1	114.1996	-26.3020	0.74	0.27

Table 7-17 Mineralogic results from the 2014 Hamelin Pool Sedimetns. 1/3

Code	Long	Lat	% Arag	% HMC	Code	Long	Lat	% Arag	% HMC
140325_t1_10	114.2201	-26.3156	0.75	0.27	140401_01	114.1705	-26.0146	0.46	0.49
140325_T1_11	114.2243	-26.3181	0.87	0.14	140401_03	114.1801	-26.0130	0.72	0.30
140325_T1_12	114.2199	-26.3229	0.95	0.05	140401_04b	114.1870	-26.0100	0.90	0.10
140325_T1_3	114.2188	-26.3233	0.61	0.42	140401_06	114.1856	-26.0103	0.90	0.11
140325_t1_4	114.2091	-26.3051	0.80	0.21	140401_07	114.1338	-26.0126	0.87	0.14
140325_T1_6	114.2110	-26.3073	0.93	0.07	140401_08	114.2004	-26.0327	0.80	0.21
140325_T2_1	114.2156	-26.3283	0.93	0.08	140401_12	114.1914	-26.0436	0.51	0.52
140325_t2_3	114.2133	-26.3252	0.95	0.05	140401_14□	114.1832	-26.0526	0.81	0.20
140325_T2_4	114.2123	-26.3245	0.95	0.05	140401_15	114.1758	-26.0565	0.84	0.17
140325_t2_5	114.2104	-26.3212	0.90	0.10	140401_16 hutch	114.2024	-26.0520	0.86	0.15
140325_T2_8	114.1918	-26.3220	0.90	0.11	140401_18	114.2126	-26.0482	0.89	0.11
140325_t2_9	114.1831	-26.3263	0.94	0.07	140401_19	114.2171	-26.0475	0.68	0.34
140325_T3_15	114.1843	-26.3435	0.87	0.14	140401_3b	114.1801	-26.1297	0.80	0.21
140329_T1_Start	114.0745	-26.4135	0.93	0.08	140406 GT2 hutch	114.1657	-26.1145	0.89	0.11
140330 head 42	114.1366	-26.2017	0.89	0.12	140406_01	114.2289	-26.0739	1.00	0.00
140330 SedTrapMe	114.2158	-26.2652	0.82	0.19	140406_09	114.2158	-26.0603	0.89	0.11
140330_T1_03	114.1557	-26.3562	0.90	0.10	140406_10	114.2137	-26.0626	0.91	0.10
140330_t1_1	114.1484	-26.3504	0.80	0.21	140406_12	114.2183	-26.0723	0.91	0.10
140330_t1_2	114.1520	-26.3532	0.89	0.12	140406_13	114.2100	-26.0794	0.83	0.18
140330_T1_4	114.1590	-26.3593	0.94	0.06	140406_14	114.1989	-26.0877	0.88	0.13
140330_t1_5	114.1629	-26.3626	0.84	0.17	140406_18	114.1936	-26.0912	0.87	0.13
140330_T1_Start	114.1414	-26.3453	0.82	0.20	140406_21 hutch	114.1807	-26.1014	0.91	0.10
140331_T1_1	113.9428	-26.0006	0.93	0.08	140406_22	114.1858	-26.1066	0.86	0.15
140331_T1_3	113.9231	-25.9927	0.85	0.15	140406_23 hutch	114.1923	-26.1090	0.90	0.11
140331_T1_5	113.9132	-25.9890	0.87	0.14	140406_25	114.2025	-26.1131	0.88	0.13
140331_T1_8	113.9088	-25.9958	0.88	0.13	140406_27	114.2143	-26.1189	0.97	0.03
140331_T1_Start	113.9462	-26.0026	0.53	0.49	140406_31 htuch	114.1722	-26.1383	0.86	0.15
140331_T2_Start	113.9099	-26.0044	0.45	0.58	140406_5 hutch	114.2235	-26.0631	0.89	0.11
140331_T4_01	113.9134	-26.0325	1.00	0.00	140406_Black Line	114.2146	-26.0657	0.82	0.19
140331_T5_8	113.9265	-26.0618	0.62	0.41	140406_t1_hutch_me	114.1553	-26.1292	0.86	0.15
140401 (B) Hutch 19	114.2171	-26.0475	0.80	0.21	140407 flag 01	114.1495	-26.4066	0.91	0.09

Table 7-18 Mineralogic results from the 2014 Hamelin Pool sedimetns. 2/3

Code	Long	Lat	% Arag	% HMC
140407_02	114.1481	-26.4043	0.90	0.11
140407_04 nilemah	114.1209	-26.4098	0.96	0.05
140407_05_FP	114.1371	-26.3855	0.84	0.17
140407_05_NIL	114.1226	-26.4213	0.91	0.10
140407_06	114.1355	-26.3679	0.91	0.10
140407_08 Flag	114.1576	-26.3740	0.88	0.13
140407_12 Nill	114.1296	-26.4171	0.93	0.08
140407_14	114.2096	-26.3593	0.93	0.07
140407_3	114.1457	-26.3993	0.93	0.08
140407_Flag_07	114.1492	-26.3741	0.87	0.13
140407_Nil_07	114.1226	-26.4213	0.88	0.13
140408_02	114.2307	-26.2975	0.95	0.05
140408_09	114.2032	-26.3229	0.89	0.11
140408_18	114.2214	-26.3161	0.81	0.20
140408_25	114.2266	-26.3024	0.82	0.19
140410_05	113.9260	-26.0726	0.88	0.13
140410_06	113.9248	-26.0701	0.95	0.05
140410_09	113.9170	-26.0743	0.95	0.05
140410_14_Nanga	113.9150	-26.1078	0.95	0.05
140410_34	113.9150	-26.1078	0.92	0.09
140414_20	114.2090	-26.2569	0.97	0.03
GT 13	114.1780	-26.1447	0.98	0.03
GTH 12	114.1818	-26.1469	0.94	0.06
GTH 16	114.1607	-26.1300	0.85	0.16
GTH_17	114.1588	-26.1289	0.78	0.23
P34	113.9324	-26.0131	0.62	0.40
P36 HP March '14	113.9368	-26.0918	0.78	0.23
Total Mean			0.88	0.13
Total Min			0.45	0.00
Total Max			1.00	0.58
Total n			147.00	147.00

Table 7-19 Mineralogic results from the 2014 Hamelin Pool sedimetns. 3/3

Code	$\delta^{13}C$‰	$\delta^{13}O$‰	Code	$\delta^{13}C$‰	$\delta^{13}O$‰	Code	$\delta^{13}C$‰	$\delta^{13}O$‰
140317_21	5.00	3.16	140324_T1_14	5.32	3.36	140330_t1_2	4.87	3.55
140317_T1_14	5.02	2.53	140324_T1_3	4.55	3.29	140330_T1_4	5.30	3.46
140317_T1_15	5.35	2.79	140324_T1_7	5.47	3.24	140330_t1_5	4.73	3.91
140317_T1_19	5.09	2.58	140324_T1_start	4.78	3.13	140330_T1_Start	4.65	3.13
140317_T1_7	4.95	3.49	140324_T2_4	4.43	3.80	140331_T1_1	2.82	2.74
140318_T1_13	4.59	3.11	140324_T2_6	4.66	3.46	140401_03	3.78	2.98
140318_T1_2	4.35	2.92	140324_t3_2_spaven	4.62	3.61	140401_19	4.28	2.55
140318_T1_3	4.57	2.95	140324_T3_2b	4.62	3.61	140401_3b	3.46	2.51
140318_T1_5	4.70	2.81	140324_T3_5a	4.70	3.81	140406_01	3.79	4.05
140318_T1_7	4.35	3.00	140324_T5_2	4.26	3.31	140406_12	4.07	2.23
140318_T3_3	5.27	2.87	140324_T5_6	4.81	3.41	140406_13	3.76	3.28
140319_T1_1	3.86	2.94	140324-t1-13	5.41	3.61	140406_18	3.57	2.84
140319_T1_4	5.12	2.76	140324-t3-4	4.99	3.72	140406_22	4.07	3.31
140319_T1_5	5.22	2.74	140324-t4-3	4.92	3.73	140406_27	4.34	3.50
140319_T1_6	5.01	3.13	140324-t5-2	4.26	3.31	140406_Black Line	4.02	3.27
140319_T1_9	6.06	3.52	140324-t5-6	4.81	3.41	140406_t1_hutch	4.68	3.47
140319_T2_4	5.39	2.52	140325 gth 12	4.94	2.74	140407_02	4.45	3.77
140319_T2_5	6.18	2.67	140325_T1_1	5.43	3.01	140407_05_FP	4.79	3.19
140321_T1_1	4.79	3.10	140325_t1_10	5.48	3.27	140407_06	5.05	3.17
140321_T1_12a	5.21	3.22	140325_T1_11	5.57	3.16	140407_14	5.88	2.90
140321_T1_3	4.43	2.89	140325_T1_12	5.51	3.03	140407_3	4.83	2.72
140321_T1_4	4.55	3.11	140325_T1_3	5.54	2.81	140408_02	4.84	3.29
140321_T1_6	5.01	3.32	140325_t1_4	5.50	3.39	140408_09	5.43	3.06
140321_T1_7	4.92	3.25	140325_T1_6	5.72	2.98	140408_18	5.35	3.16
140321_T1_8	5.21	3.37	140325_T2_1	5.71	3.05	140408_25	5.15	3.92
140322_T1_1	4.66	3.13	140325_t2_3	5.88	3.00	140410_05	4.11	3.56
140322_T1_16	5.22	3.37	140325_T2_4	5.09	3.25	140410_06	3.63	3.80
140322_T1_17	5.61	3.26	140325_t2_5	5.51	3.23	140410_09	4.09	3.56
140322_T1_2	5.01	3.15	140325_T2_8	5.32	2.98	140410_34	4.58	3.65
140322_T1_22	5.17	3.12	140325_t2_9	5.60	3.07	140414_20	4.52	4.02
140322_T1_3	4.43	2.31	140325_T3_15	5.55	2.83	GT 13	4.63	2.62
140322_T1_6	4.81	3.52	140329_T1_Start	5.30	3.45	GTH 12	4.07	2.23
140322_T2_10	5.01	3.05	140330 head 42	4.75	3.20	GTH 16	5.09	2.50
140322_T2_3	5.26	3.04	140330_T1_03	5.55	3.17	GTH_17	4.64	2.84
140322_T2_6	5.66	3.10	140330_t1_1	4.50	3.30			
Total Mean	4.86	3.17						
Total Min	2.82	2.23						
Total Max	6.18	4.05						
n	104.00	104.00						

Table 7-20 Reuslts from the inorganic stable isotopes of the 2014 Hamelin Pool sediments.

Code	Latitude	Longitude	δ^{15}Norg	δ^{13}Corg	% Inso	%C wt	%N wt	C:N	Code	Latitude	Longitude	δ^{15}Norg	δ^{13}Corg	% Inso	%C wt	%N wt	C:N
140407_07	114.1226	-26.4213	1.42	-15.50	4.64	0.00	0.00	0.00	140330_t1_start	114.1414	-26.3336	0.42	-14.93	8.73	0.09	0.01	9.24
140407_06	114.1233	-26.4176	0.73	-13.23	58.03	1.21	0.08	18.67	140325_T3_15	114.1843	-26.3250	0.69	-13.83	0.69	0.01	0.00	9.33
140407_12	114.1296	-26.4171	0.77	-13.29	1.63	0.01	0.00	7.29	140324_t5_6	114.1686	-26.3245	0.80	-16.40	3.59	0.06	0.01	10.57
140407_12	114.1296	-26.4171	0.74	-13.44	3.92	0.03	0.00	8.70	140324_t5_2	114.1599	-26.3245	1.29	-17.05	2.08	0.01	0.00	8.87
Dark	114.1314	-26.4152	-0.08	-14.83	4.79	0.07	0.01	9.53	140324_t5_1	114.1578	-26.3245	6.97	-14.37	6.20	0.22	0.04	7.26
140329_t1_start	114.0745	-26.4135	0.23	-13.88	2.81	0.58	0.06	11.12	140324_t3_5	113.9853	-26.3242	0.71	-13.97	1.19	0.02	0.00	9.92
140407_02	114.1481	-26.4043	0.28	-13.82	2.66	0.50	0.05	10.94	140325_t2_4	114.2123	-26.3237	0.07	-13.81	1.93	0.06	0.01	11.15
140407_3	114.1457	-26.3993	0.11	-14.15	2.45	0.55	0.07	9.42	140324_t3_4	113.9867	-26.3237	0.63	-12.79	2.44	0.12	0.01	13.86
140407_03	114.1457	-26.3993	2.12	-13.31	7.97	0.11	0.02	5.96	140324_t3_2	113.9901	-26.3236	-1.05	-13.50	3.01	0.02	0.00	9.72
140407_04	114.1421	-26.3930	-1.36	-17.49	2.44	0.01	0.00	8.17	140324_t3_2	113.9901	-26.3229	0.61	-16.01	1.88	0.24	0.03	9.45
140407_04	114.1421	-26.3930	0.02	-14.20	23.95	0.55	0.06	11.13	140324_t5_start	114.1545	-26.3229	-0.17	-17.58	8.96	0.34	0.03	12.56
140319_T1_6	114.0360	-26.3898	0.24	-12.37	13.89	0.18	0.02	9.48	140408_09	114.2032	-26.3220	0.96	-15.58	1.70	0.65	0.07	10.31
140319_T1_5	114.0366	-26.3896	1.24	-12.42	9.10	0.76	0.09	10.18	140325_t1_12	114.2199	-26.3212	0.40	-13.83	2.20	0.41	0.05	10.14
140319_T1_4	114.0388	-26.3867	0.54	-12.15	1.33	0.29	0.03	11.91	140325_t2_8	114.1918	-26.3203	0.85	-13.06	6.36	0.47	0.04	12.96
140407_05	114.1371	-26.3855	0.46	-12.83	12.47	2.33	0.24	11.54	140325_t2_5	114.2104	-26.3181	0.79	-14.00	3.29	0.18	0.02	9.13
140407_05 LIL	114.1371	-26.3855	-0.22	-12.96	1.87	0.04	0.00	11.33	140324_t3_1	114.0024	-26.3181	1.08	-15.70	1.57	0.22	0.03	8.42
140319_T2_5	114.0218	-26.3793	1.74	-16.91	22.47	0.35	0.03	13.00	140325_t2_3	114.2243	-26.3161	1.01	-8.59	4.08	0.51	0.04	14.80
140407_08	114.1576	-26.3740	0.62	-15.82	1.67	0.02	0.00	8.85	140325_t1_11	114.2243	-26.3156	0.36	-15.98	3.84	0.12	0.02	8.33
140319_t2_4b	114.0162	-26.3713	0.66	-14.06	40.88	0.25	0.03	8.90	140408_18	114.2214	-26.3156	0.57	-15.63	1.99	0.44	0.05	10.50
140319_t2_4a	114.0162	-26.3679	0.39	-15.52	2.37	0.46	0.05	11.25	140325_t2_1	114.2201	-26.3073	0.66	-14.93	1.55	0.36	0.04	10.33
140319_T1_1	114.0513	-26.3658	-1.30	-17.58	3.76	0.01	0.00	7.00	140325_t1_10	114.2201	-26.3024	0.71	-15.72	1.98	0.31	0.04	10.41
140407_06	114.1355	-26.3626	0.17	-13.33	6.40	1.09	0.11	11.20	140325_t1_6	114.2110	-26.3023	-0.92	-16.04	1.15	0.25	0.03	9.99
140330_t1_6	114.1664	-26.3593	0.07	-14.59	4.56	0.70	0.07	11.31	140325_t1_3	114.2069	-26.3021	0.76	-14.80	4.41	0.77	0.09	10.03
140330_t1_5	114.1629	-26.3593	-0.16	-13.39	2.00	0.04	0.00	11.30	140408_25	114.2266	-26.3020	0.49	-14.55	2.48	0.30	0.04	9.38
140330_t1_4	114.1590	-26.3562	-0.43	-15.89	3.46	0.01	0.00	8.75	140317_19	114.2147	-26.3020	0.85	-15.87	2.14	0.41	0.05	10.45
140407_14	114.2096	-26.3532	0.06	-14.95	5.11	0.97	0.10	11.89	140317_21	114.2278	-26.3017	0.52	-15.79	10.19	0.11	0.01	10.31
140330_t1_3	114.1557	-26.3524	1.27	-14.90	7.23	0.09	0.01	8.92	140325_t1_1	114.1996	-26.3013	0.19	-16.35	11.69	0.07	0.01	7.26
140330_t1_2	114.1520	-26.3504	0.68	-14.14	5.08	1.03	0.11	11.28	140325_t1_4	114.1996	-26.3010	0.63	-12.74	10.59	0.65	0.06	13.43
140324_t4_3	114.0021	-26.3453	0.61	-13.95	7.04	1.19	0.12	11.21	140324_t2_2	113.9771	-26.3006	0.17	-15.35	12.40	0.33	0.03	11.21
140330_t1_1	114.1484	-26.3435	1.82	-16.09	1.07	0.23	0.03	9.54	140324_t2_6	113.9998	-26.2985	-0.14	-14.98	14.95	0.08	0.01	8.50

Table 7-21 Organic δ^{14}N and δ^{13}C isotopic values, carbon to nitrogen percentage and C:N ratio results of the organic matter from the 2014 Hamelin Pool sediments. 1/3

Code	Latitude	Longitude	δ^{15}Norg	δ^{13}Corg	% Inso	%C wt	%N wt	C:N	Code	Latitude	Longitude	δ^{15}Norg	δ^{13}Corg	% Inso	%C wt	%N wt	C:N
140324_t2_4	113.9860	-26.2975	1.27	-21.88	5.03	0.66	0.05	15.02	140322_T1_6	114.0004	-26.1845	-1.14	-15.61	6.94	0.35	0.04	10.07
140324_t2_5	113.9896	-26.2836	1.07	-13.87	8.81	0.00	0.01	0.00	140330_42head	114.1366	-26.1839	-4.28	-15.92	1.55	0.18	0.02	9.71
21	114.0221	-26.2835							140321_T1_12a	113.9440	-26.1839	-1.30	-13.82	2.97	0.62	0.06	11.14
140408_02	114.2307	-26.2835	1.54	-15.42	6.18	0.20	0.02	11.15	140321_t1_6	113.9618	-26.1839	-0.83	-16.13	2.05	0.17	0.02	10.02
140324_t1_2	113.9898	-26.2833	-0.11	-14.62	2.75	0.04	0.00	8.81	140321_T1_8	113.9543	-26.1817	-0.48	-13.74	13.25	2.06	0.23	10.38
140324_t1_3	113.9875	-26.2833	0.63	-14.73	47.70	0.32	0.05	7.11	140321_T1_7	113.9593	-26.1811	6.96	-18.09	1.63	0.23	0.03	10.22
140324_t1_start	113.9919	-26.2831	0.05	-17.17	2.16	0.02	0.00	8.40	140321_T1_4	113.9748	-26.1804	0.04	-14.14	21.14	3.54	0.42	9.92
140324_t1_7 FP	113.9815	-26.2829	0.39	-17.61	1.60	0.02	0.00	11.17	140321_T1_4b	113.9748	-26.1799	0.22	-15.70	2.64	0.33	0.03	11.01
140324_t1_7 FP	113.9815	-26.2824	0.03	-13.88	23.20	0.19	0.02	9.45	140318_t1_13	114.1572	-26.1798	1.63	-18.53	2.71	0.37	0.06	6.98
140324_t1_9	113.9799	-26.2817	0.31	-13.89	39.97	0.73	0.08	10.62	140321_T1_3	113.9831	-26.1797	-0.32	-17.89	3.84	0.37	0.04	10.46
140324_t1_8	113.9805	-26.2814	2.99	-11.69	32.40	0.19	0.02	11.67	140318_t1_3	114.1810	-26.1796	0.32	-17.63	2.35	0.20	0.02	9.55
140324_t1_14	113.9701	-26.2814	-0.10	-17.48	20.94	0.11	0.01	9.00	140318_t1_2	114.1854	-26.1764	2.00	-13.54	5.09	0.43	0.02	24.67
140324_t1_10b	113.9759	-26.2733	0.54	-15.62	14.62	0.28	0.04	9.43	140318_t1_5	114.1767	-26.1447	1.82	-16.89	5.97	0.15	0.02	7.63
140324_t1_13	113.9718	-26.2731	2.91	-16.03	42.99	0.19	0.03	8.75	140318_t1_7	114.1729	-26.1383	0.89	-13.34	1.87	0.02	0.00	10.92
140324_t1_13	113.9718	-26.2725	0.06	-15.58	1.99	0.40	0.05	9.93	140321_T1_1	113.9948	-26.1300	1.07	-18.13	1.84	0.30	0.04	8.56
140322_T2_10	113.9986	-26.2725	1.92	-17.82	21.02	0.26	0.04	8.10	GT 13	114.1780	-26.1297	3.15	-16.57	4.79	1.50	0.35	4.99
140322_T2_3	113.9715	-26.2683	-0.43	-16.54	2.94	0.34	0.04	11.09	140406_31	114.1722	-26.1297	0.35	-17.85	3.85	0.22	0.04	6.62
140322_T2_9	113.9958	-26.2569	0.15	-14.54	1.55	0.29	0.05	6.85	GTH 16	114.1607	-26.1289	4.99	-16.14	3.92	1.11	0.11	12.30
140322_T2_6	113.9819	-26.2565	1.71	-15.33	1.87	0.04	0.00	13.42	140401_3b	114.1801	-26.1189	0.33	-15.48	1.79	0.26	0.04	8.34
140318_T3_3	114.2102	-26.2473	0.09	-16.44	3.15	0.67	0.08	9.99	140401_3	114.1801	-26.1145	0.93	-16.34	2.18	0.04	0.00	10.13
140414_20	114.2090	-26.2445	1.29	-15.33	11.22	0.54	0.07	9.70	GTH_17	114.1588	-26.1131	-0.50	-17.60	-0.31	0.00	0.00	8.75
140414_16	114.1887	-26.2437	-0.19	-17.38	1.16	0.29	0.03	11.82	140406_27	114.2143	-26.1099	0.95	-16.12	3.55	0.11	0.01	11.23
140317_T1_14	114.1675	-26.2412	1.10	-15.13	2.71	0.18	0.03	8.34	140406_GT2	114.1657	-26.1078	2.31	-14.13	2.75	0.32	0.04	8.81
140322_T1_17	113.9710	-26.2327	-1.46	-14.80	3.41	0.25	0.03	9.35	140406_25	114.2025	-26.1066	1.11	-17.44	1.75	0.30	0.04	9.49
140317_7	114.1941	-26.2304	6.02	-17.72	3.93	1.96	0.22	10.52	140406_GT1	114.1421	-26.1014	0.56	-16.29	3.14	0.08	0.01	11.21
140322_T1_16	113.9728	-26.2304	0.16	-16.59	3.34	0.37	0.05	9.23	140410_34	113.9150	-26.0918	0.88	-12.85	1.91	0.12	0.01	12.98
140322_T1_1	114.0081	-26.2289	2.19	-16.87	3.22	0.37	0.05	9.25	140406_22	114.1858	-26.0912	0.65	-15.29	8.08	0.54	0.04	14.94
140322_T1_2b	114.0043	-26.2238	0.85	-16.51	1.91	0.34	0.04	9.48	140406_21	114.1807	-26.0877	0.26	-17.98	2.21	0.02	0.00	8.50
140322_T1_2	114.0043	-26.2017	2.33	-17.32	4.17	0.36	0.04	9.81	P36	113.9368	-26.0794	0.39	-15.82	3.22	0.11	0.01	9.20
140322_T1_3	114.0041	-26.1848	6.01	-15.74	5.67	0.15	0.02	10.11	140406_18	114.1936	-26.0769	1.42	-15.50	28.89	0.00	0.00	0.00

Table 7-22 Organic δ^{14}N and δ^{13}C isotopic values, carbon to nitrogen percentage and C:N ratio results of the organic matter from the 2014 Hamelin Pool sediments. 2/3

Code	Latitude	Longitude	δ^{15}Norg	δ^{13}Corg	% Inso	%C wt	%N wt	C:N
140406_14	114.1989	-26.0743	9.06	-16.81	26.82	0.20	0.03	6.64
140406_13	114.2100	-26.0739	0.90	-16.82	2.84	0.66	0.07	11.67
140410_14	113.9104	-26.0739	2.59	-13.47	1.04	0.17	0.03	7.09
140410_9	113.9170	-26.0726	1.09	-16.34	24.66	0.29	0.03	9.92
140406_t1_hutch	114.2289	-26.0723	2.65	-14.83	3.76	0.17	0.03	7.82
140406_01	114.2289	-26.0701	0.66	-16.41	17.25	0.22	0.03	8.85
140410_05	113.9260	-26.0650	0.42	-16.28	6.90	0.02	0.00	7.93
140406_12	114.2183	-26.0631	-0.97	-15.42	14.56	0.06	0.01	8.36
140410_06	113.9248	-26.0626	0.50	-16.06	3.13	0.02	0.00	8.28
140331_T5_15	113.9104	-26.0618	-2.22	-13.16	4.27	0.00	0.00	0.00
140406_5	114.2235	-26.0603	1.26	-17.04	7.51	0.09	0.01	9.11
140406_10	114.2137	-26.0565	-0.33	-14.20	3.94	0.08	0.01	10.13
140331_t5_8	113.9265	-26.0526	0.62	-15.66	1.96	0.03	0.00	9.15
140406_09	114.2158	-26.0520	0.92	-16.51	3.41	0.05	0.01	10.71
140401_15	114.1758	-26.0482	1.36	-17.55	6.81	0.21	0.03	9.09
140401_14	114.1832	-26.0482	0.58	-13.07	3.51	0.02	0.00	9.48
140401_16	114.2024	-26.0475	0.25	-15.90	16.58	0.14	0.02	9.80
140401_18	114.2126	-26.0346	0.96	-16.55	1.01	0.01	0.00	8.71
140401_01_18	114.2126	-26.0327	1.28	-15.96	7.00	0.08	0.01	8.10
140401_19	114.2171	-26.0325	-0.26	-15.68	46.94	0.68	0.08	9.88
140401_10	114.1992	-26.0278	-0.69	-18.19	6.11	0.02	0.00	6.53
140401_08	114.2004	-26.0131	-0.15	-15.65	11.12	0.23	0.02	10.92
140331_t4_1	113.9134	-26.0126	0.08	-13.83	8.18	0.17	0.02	10.21
140331_t4_me	113.9200	-26.0103	0.84	-17.06	6.29	0.04	0.00	10.17
P34	113.9324	-26.0044	0.24	-14.58	30.10	0.52	0.06	10.68
140401_07	114.1338	-26.0006	0.64	-18.62	38.66	0.06	0.01	8.75
140401_06	114.1856	-25.9970	0.91	-17.31	7.19	0.11	0.01	10.23
140331_t2_start	113.9099	-25.9958	0.82	-14.25	40.40	0.29	0.02	16.57
140331_t1_1	113.9428	-25.9927	0.83	-16.41	50.73	0.99	0.11	10.34
140331_t1_start	113.9076	-25.9890	-2.22	-13.16	24.52	0.00	0.00	0.00
Total Average			0.77	-15.38	8.74	0.34	0.04	9.72
Total Min			-4.28	-21.88	-0.31	0.00	0.00	0.00
Total Max			9.06	-8.59	58.03	3.54	0.42	24.67
n			149	149	149	149	149	149

Table 7-23 Organic δ^{14}N and δ^{13}C isotopic values, carbon to nitrogen percentage and C:N ratio results of the organic matter from the 2014 Hamelin Pool sediments. 3/3